Entanglement Characteristics of Dipole Coupled Two-level Atoms

A Thesis Submitted for the Degree of

DOCTOR OF PHILOSOPHY

In

PHYSICS

By

SHAIK AHMED

School of Physics

University of Hyderabad

Hyderabad 500 046, India

December 2016

Dedicated to.....

My Family

DECLARATION

I, **Shaik Ahmed**, hereby declare that this thesis entitled "**Entanglement Characteristics of Dipole Coupled Two-level Atoms**" submitted by me under the guidance and supervision of Prof. P. Anantha Lakshmi is a bonafide research work which is also free from plagiarism. I also declare that it has not been submitted previously in part or in full to this University or any other University or Institution for the award of any degree or diploma. I hereby agree that my thesis can be deposited in Shodganga/INFLIBNET.

A report on plagiarism statistics from the University Librarian is enclosed.

(Shaik Ahmed)

Place: Hyderabad

Date:

CERTIFICATE

This is to certify that the thesis entitled "**Entanglement Characteristics of Dipole Coupled Two-Level Atoms"** submitted by **Shaik Ahmed** bearing registration number 08PHPH09 in the partial fulfillment of the requirements for award of Doctor of Philosophy in the School of Physics is a bonafide work carried out by him under my supervision and guidance.

This thesis is free from plagiarism and has not been submitted previously in part or in full to this or any other University or Institution for award of any degree or diploma.

Part of this thesis has been:

A. Published in the following publications:
   1. Physical Science International Journal vol 4, issue 4, 591 (2014).
   2. Pramana - J. Phys. 83, issue 2, 167 (2014).

and

B. Presented in the following conferences:
   1. 3rd *DAE-BRNS Symposium on Atomic, Molecular and Optical Physics* held at IISER Kolkata, December 14-17, 2012.
   2. National Laser Symposium (NLS-21), 6-9 February 2013, organized by BARC-Mumbai, Mumbai.

Further, the student has passed following courses towards fulfillment of coursework requirement for Ph.D.

Course code	Name	Credits	Pass/Fail
PY900	Advanced Quantum Mechanics	4	Pass
PY901	Advanced Statistical Mechanics	4	Pass
PY902	Advanced Electromagnetic Theory	4	Pass
PY903	Advanced Classical Mechanics	4	Pass

Supervisor Dean

ACKNOWLEDGEMENTS

Being grateful to each and every one who supported me throughout this journey, first and foremost, I would like to thank my supervisor Prof. P. Anantha Lakshmi for her continuous guidance, instigation and encouragement throughout my Ph.D programme. Her vision of Physics inspired me to grasp things in a new way.

I would like to thank Dr. Ashoka Udayagiri, Prof. Suneel Singh and Prof. D. Narayana Rao for their valuable suggestions during the doctoral committee meetings. I would like to unreservedly thank Prof. Prasanta K. Panigrahi for his help, support and guidance. It has been a privilege to work with such a special person.

I convey my sincere thanks to Prof. Bindu A. Bambah, Dean, School of Physics and former Deans Prof. R. Singh**,** Prof. S. Chaturvedi**,** Prof. S.P. Tewari and other faculty members for their co-operation in providing facilities in the School.

I would like to thank my best friends G. Rama Krishna Prasad, D. Sanjeev and Dr. Azeem for helping me to get through difficult times and for all the emotional support. I would like thank my friends Dr. Monisha, Dr. I. V. Shankar, Dr. Aalu, Dr. Saikiran, Anil Mettu, Luhluh, Uma, Dr. Suman kalyan, Chari gaaru Ram who made my life joyful and memorable on this campus.

I would like to thank T. Abraham, Deepika and other non-teaching staff for their help and support at various stages when needed. I acknowledge the UGC, Govt. of India for providing me with the necessary fellowship to pursue research at University of Hyderabad.

I would like to specially thank my parents. Without their encouragement, help and support, I would not be the person I am today. Many heartfelt thanks to my sister. Lastly, and most importantly, I would like to thank my wife Azra, for all her love and never-ending support. A simple thanks to my family members is not enough and I dedicate this thesis to them.

.....Ahmed

Contents

List of Figures

List of Abbreviations

DD	Dipole-dipole interaction
RWA	Rotating Wave Approximation
EDA	Electric-Dipole Approximation
ESB	Entanglement Sudden Birth
ESD	Entanglement Sudden Death
CONC	Concurrence
QD	Quantum Discord
QMI	Quantum Mutual Information

List of Symbols

ρ ..... Density operator
$\mathcal{L}$ ..... Liouvilliean operator
Ω_{ij} ..... Dipole-dipole coupling strength
Γ_{ij} ..... Cooperative decay
Ω_0 ..... Rabi field strength
$\tilde{\Omega}$ ..... Modified Rabi field strength
Δ_1 ..... Detuning of the atom 1
Δ_2 ..... Detuning of the atom 2
Δ ..... Total detuning of the atomic system
S^+ ..... Raising operator
S^- ..... Lowering operator
S_z ..... Energy operator
ω ..... Atomic transition frequency
I ..... Intensity
g^2 ..... Second order correlation function
θ ..... Observation angle
k ..... Wave number
Z ..... Partition function
k_B ..... Boltzmann constant
T ..... Temperature

Chapter 1

Introduction

1.1 Introduction

Microscopic systems consisting of a collection of atoms tend to exhibit a rich variety of cooperative effects [1–9], which arise due to the interaction between individual atoms, mediated by the environment. For example, when an atomic ensemble, confined in a region of space smaller than an optical wavelength, is irradiated with a single mode radiation field, each atom in the ensemble interacts with the external radiation field as well as with the radiation emitted from all the other atoms. In this case, the intensity of radiation emitted by this collection of atoms shows markedly different behaviour from that arising due to emission from independent atoms. These cooperative effects, which arise mainly due to the dipole-dipole interaction between the atoms, lead to interesting modification in the behaviour of the system, starting from formation of Dicke states, collective emission from the group of atoms which can show either subradiant or superradiant behaviour, depending on the strength of the interaction, geometry of the physical system, Rabi field strengths and the decay rates from different channels. In recent times, several interesting

manifestations of the cooperative effects among atoms are being studied, from the view point of practical application in the fields of quantum information, quantum engineering of states for quantum computing, cryptography etc. A complete understanding of the behaviour of such a system necessitates a microscopic formulation of the different interactions between the atoms and the environment in which they are present.

When treating a system of many atoms, the net force experienced by any single atom is computed as a collective sum of interactive forces with all the other atoms. Coherent addition of all these inter-atomic interactions gives rise to, what is known as, the cooperative phenomena. Therefore, the model for collective microscopic behaviour of the entire system can be built in terms of a basic building block involving interaction between a pair of atoms. One of the most common interactions of this kind is the dipole-dipole (D-D) interaction.

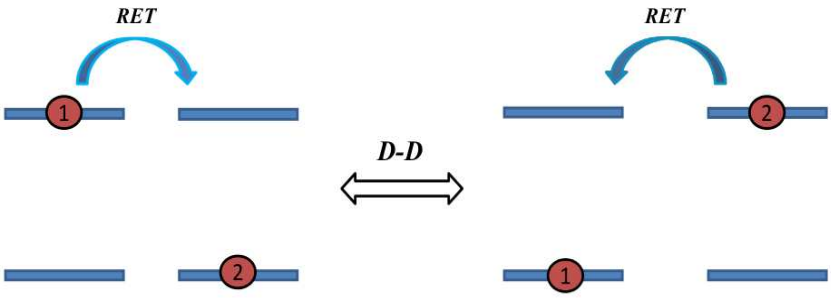

Figure 1-1: Origin of dipole-dipole interaction

Whenever an atom, in its excited state, comes very close (within a wavelength) to another atom in its ground state, energy is transferred to the second atom non-radiatively. This non-radiative energy exchange reverses the role of

the individual atoms participating in this interaction, viz., the second atom becomes the excited atom and the first one goes to its ground state. This phenomenon reverses after a while, with the second atom transferring energy to the first one. This kind of energy exchange leads to an interaction between the participating atoms. The nature of this interaction is equivalent to the one derived from the dipole term of the classical electromagnetic interaction, and hence termed 'dipole-dipole interaction' (see figure 1-1).

The static form of long-range interaction between two dipoles $\vec{\mu_1}$ and $\vec{\mu_2}$ separated by a distance r is given by

$$\Omega_{st} = \frac{1}{4\pi\epsilon_0}\left[\frac{(\widehat{\mu_1}.\widehat{\mu_2})r^2 - 3(\widehat{\mu_1}.\mathbf{r})(\widehat{\mu_2}.\mathbf{r})}{r^5}\right] \tag{1.1}$$

where $\widehat{\mu_1}$, $\widehat{\mu_2}$ are the unit vectors along the two dipole moments, $r = |\mathbf{r}|$ and ϵ_0 is the vacuum permittivity.

Unlike the typical van der Waal's interaction, one can see that the D-D interaction has two characteristic features, i.e., long range since it decays as $\Omega_{st} \propto 1/r^3$, and anisotropic since it depends on the relative angles between the dipoles [10]. For all identical dipoles aligning in the direction of electric or magnetic field, the interaction simplifies to

$$\Omega_{st} = \frac{1}{4\pi\epsilon_0}\left[\frac{1 - 3\cos^2\theta}{r^3}\right], \tag{1.2}$$

where θ is the angle between the dipole moment $\vec{\mu}$ and the inter atomic axis. For parallel dipoles polarized in a direction perpendicular to the inter atomic axis, i.e. for $\theta = \pi/2$, the interaction is repulsive, whereas the interaction is attractive for $\theta = 0$.

The D-D interaction at smaller inter atomic distances gives rise to a variety of phenomena, which have generated considerable interest in the past. Some of the early reports in this direction include new resonance fluorescence peaks that arise due to D-D interactions [11], suppression of existing fluorescence peaks [12], modification of transition rates and level shifts, thus giving rise to significant changes in the multiple jump dynamics [13] and a host of others. In the context of quantum information, entanglement between the atom pair arising due to dipole-dipole interaction [14], and their subsequent evolution [15] is another widely studied aspect. Dipole-dipole interaction between Rydberg atoms, which are stronger due to their large dipole moments [16], application of this to quantum computation schemes [17], have also generated a lot of interest. Due to the strong and long-range D-D interactions, Rydberg atoms offer efficient tools for quantum engineering [18]. This is due to the fact that, resonant condition can be achieved experimentally in these Rydberg atoms, by tuning the levels with microwave or external electric fields. The D-D interaction between the atoms creates an energy shift, depending on the inter-atomic distance, which in turn controls the excitation of the neighbouring atoms around a previously excited atom [17, 22]. In effect, the shift created by the D-D interaction allows a single Rydberg excitation in a large atomic sample, inhibiting all other excitations. This is generally referred to as 'dipole blockade'. The dipole blockade regime for two atoms has been recently measured experimentally, in the collective excitation of a pair of individually trapped atoms [20, 21]. Such a result opens up a way to controlling the behaviour of a few-atom sample.

There exist several other physical systems, which have the same dynamics as that of two two-level atoms, such as modes in ring cavities, quantum

dots, excitons in plasmonic waveguides etc. All of them show similar coupling mechanism, where a resonant energy transfer between any two entities takes place. Hence, they can be solved with the general mathematical formalism shown in this work and are most likely to show similar behaviour, under appropriate conditions. Finally, with the great experimental control obtained, a many atomic sample may be employed as quantum simulator to answer some challenging open questions of quantum optics/quantum information. Despite the large amount of work that already exists in literature, it is not an understatement to claim that a clear understanding of the D-D interaction effects is far from complete.

In order to understand these cooperative effects in a sizeable system of many atoms, it is necessary to have a microscopic formulation of the interaction between the atoms and the radiation field. A first step in this direction would be to understand the dynamics of a two atom system interacting with a single mode radiation field, wherein the cooperative effects among the atoms become important. Though the system of two atoms interacting with a single mode radiation field is well studied, we present an overview of the system of two atoms interacting with a radiation field, for maintaining continuity with the later work that is reported in this thesis. After gaining understanding of the behaviour of the two atom system, the next step would be to extend it to include a third atom, which would bring the study closer to a real system. Though a fully quantum mechanical picture describes the energy exchange phenomena more effectively, such an approach becomes cumbersome as the size of the system increases. With this in mind, we present a detailed study using the semi classical approach, wherein the atoms are treated quantum mechanically and the field is treated as a classical variable.

In case of the many body problem, systems with three correlated atoms often show qualitatively different features as compared to its two-atom counterpart. For example, it has been shown that the dipole blockade can be broken by adding a third Rydberg atom [22]. Furthermore, it has been predicted that systems of more than two D-D interacting atoms exhibit conical intersections [23, 24], which are relevant for photo-chemical processes. As a three-body problem, this leads to various effects such as formation of Effimov states [25] and/or correlation between those atoms that are not directly interacting with each other, mediated by the intermediate atom, are some of the few phenomena that make the study of these systems worthwhile.

As a first step in this direction, we extended our study to a set of three atoms, in which pairwise interaction between atoms is considered. The excitement to study dynamics of D-D interaction among three atoms stems from the fact that, in addition to the already stated interesting features that are exhibited by the three atom systems, this phenomenon can further be exploited for several applications. For instance, Deutsch and co-workers, in the context of quantum information, have exploited the motion of a particle in a double well to trap alkali atoms in a 1D lattice [26]. They have employed a photon mediated collision, resulting in an effective D-D interaction, which provided a handle to control an ensemble of uncoupled atomic systems. They demonstrated that controlling the strength of the optical field provides a direct control on the strength of the D-D interaction. This is perhaps one of the many ways of experimentally realizing the schemes that are studied in the present work.

In this thesis, a system of three atoms, all of them interacting with the same single mode radiation field, are considered. Inclusion of a third atom

opens up multiple ways of arranging them. However, here we consider two of the simplest and important configurations - a linear chain where all the three atoms are on a single line and a closed configuration, where all three are on the vertices of an equilateral triangle. It is to be noted that any other arrangement would be a simple variation of these two. In our model, for the linear arrangement, the interaction between two farthest atoms is neglected whereas in the closed loop arrangement, all three atoms are assumed to interact with each other with equal strength. Because the atom-atom coupling manifests in different ways in both these configurations, the results for the two configurations are markedly different.

Many realistic composite systems are open and sensitive to the surrounding environment, which usually has the effect to eventually destroy the quantum features of the system. For example, entanglement is one of the most striking features of quantum mechanics [11, 12] and is very sensitive to the system-reservoir interaction, even when this interaction is weak [28]. Due to this fact, it was thought that entanglement could exist only in systems with small number of particles, and that too, at very low temperatures. However, recent experimental observations indicated that entanglement also exists in systems containing a large number of particles, at finite temperatures [29]. In this sense, the use of an entanglement witness has helped to demonstrate the existence of entangled states in thermal systems even at high temperatures [30], through the measurement of certain thermodynamic observables, such as the magnetization, magnetic susceptibility, specific heat etc. Some of these studies in real physical systems include a detailed analysis in spin chains described by Heisenberg models [31], atom-cavity systems [32] and also in simple molecular models [33]. In view of the many potential applications, the measurements

of thermodynamic quantities may provide in the context of quantum information theory, it is of interest to study the thermal entanglement measures in a prototype model. This is the motivation in this thesis, for considering a three atom system, both in a linear chain as well as in a loop configuration, to study the temperature dependent entanglement measures, viz., the bipartite concurrence and quantum discord.

Yet another manifestation of the D-D interaction is that the resulting correlations between the atoms would strongly influence the optical properties of the atomic system. For example, Dicke [1] predicted that the decay time of an ensemble of N correlated atoms is proportional to $\frac{1}{N\gamma}$ and the mean radiated intensity, which is distributed anisotropically, is proportional to the square of the number of atoms N^2, as opposed to a common exponential decay and isotropic emission of the radiation (proportional to N), observed for the case of uncorrelated atoms. This kind of enhanced radiation is known as superradiance and is one of the best examples of cooperative effects due to D-D interactions among the atoms. Here, the D-D interaction between the atoms plays the role of a phase synchronizing factor, leading to the enhancement of spontaneous emission, the exact nature of which depends on the spatial distribution of atoms or the sample geometry [34, 35]. By controlling the dipole coupling strength, properties of radiation emitted from such a system can be drastically altered, ranging from superradiant transitions to the generation of the Fock state of light [36].

Further, it is of particular interest to explore how the super and subradiant behaviour gets affected for a collection of atoms, when the states are entangled in different ways. For three particles, from the perspective of teleportation, the entangled states can be classified into two categories, the GHZ-states [37] and

the W-states [38]. These states have found lot of practical importance in the field of quantum information processing [39], teleportation [40, 41] as well as in super dense coding [42]. Recently, Wiegner et al. [43] have investigated the super and subradiant characteristics of an N-atom system prepared in generalized W-states of the form $\frac{1}{\sqrt{n}}|n-1,1>$, with one atom in the ground state and (n-1) atoms in the excited states. In this thesis, we investigate the super and subradiant characteristics of the radiation emitted from a system of three two-level atoms, in the GHZ-states as well as in W-states. We observe that the radiative properties of these states are quite different from the properties of a separable state. Finally, in this work, we show how the nature of entangled state dictates its radiative characteristics, leading to super and/or subradiant behaviour. This will open up pathways for optical probing of entangled states and may also throw light on the nature of entanglement.

1.2 Organization of the thesis

The organization of the thesis is as follows:

In chapter 2, the interaction of a pair of two-level atoms interacting with a single mode radiation field and interacting with each other through the dipole-dipole interaction is reviewed. In the first section, the model and the mathematical formulation of the problem are presented, for the sake of completeness. Master equation method [44] for the evolution of the density operator, in the semi-classical approximation, that is employed in this study is discussed. The resulting density matrix equations, after the usual rotating wave approximation, are solved numerically for an extensive parameter regime. In the next section, transient behaviour of the system is investigated. In particular, the

role of D-D interaction and Rabi field strength on different level populations and atomic coherences of the system is examined both for identical as well as non-identical atoms. The feature of D-D interaction between atoms acting as dipole blockade is studied. Next, we study the effect of D-D interaction on the steady state characteristics of the system. We present some of our numerical results highlighting the influence of the interplay between the Rabi frequency and the D-D interaction strength on the steady state level populations, atomic coherences, two photon absorption etc., both for identical as well as non-identical atoms. The anomalous behaviour of the two photon resonance, for the case of non-identical atoms is reported. The two photon resonance is found to increase with an increase in the applied Rabi field strength. In the last section, we study the effect of D-D interaction on the steady state entanglement characteristics of the two atom system. From a detailed analysis of the two-atom excited state population and the concurrence, a qualitative connection between the dipole blockade and the entanglement is made. In summary, in Chapter 2, some of the previous results are reproduced, to maintain continuity of the discussion, followed by the new results that were obtained in the current study.

In chapter 3, we extend our work to three coupled two-level atoms, all interacting with the same monochromatic radiation field. In the first section, we present the model of the system of three two-level atoms, as an equivalent eight level system, and study the same using the density matrix formalism. In the next section, we present our results for the steady state characteristics of three identical atoms coupled through the D-D interaction. We have studied two possible scenarios in which the three atoms can be present and observed that the results for both these show different behaviour. Attempts have been

made to explain the differences in behaviour of the system for these two cases. In the last section, studies on the entanglement characteristics of the system, both in line and loop configurations, are presented. In particular, the bipartite and tripartite negativities as a function of D-D interaction and Rabi field strength are discussed. We observe that there is an optimal value of Rabi field strength for which the tripartite negativity is maximum and this optimal value increases as a function of the dipole coupling strength. Entanglement sudden death feature is observed both in line and loop configurations. Our study reveals that the entanglement between the end atoms persists even though they are not connected directly through the D-D interaction.

In chapter 4, a study of temperature dependent quantum correlations, for all possible bipartite subsystems of the three coupled atoms, in both line and loop configurations, is presented. In particular, we investigate the effects of temperature, atomic transition frequency and D-D coupling strength, on the entanglement characteristics and the quantum correlations of three coupled two-level atoms. In both the line and loop configurations, it is seen that bipartite quantum correlations increase with an increase in the ratio of dipole coupling strength to atomic transition frequency and decrease as the ratio of temperature to atomic transition frequency is increased. From the results presented in this chapter, it is observed that quantum correlation switches can be constructed by properly tuning the temperature and dipole coupling strengths. Further, when the atoms are arranged in loop configuration, certain interesting and counter-intuitive features are observed, which are in agreement with the earlier reported studies on similar systems.

In chapter 5, we examine a system of three two-level atoms prepared in well characterised entangled states, namely GHZ- and W-states, for a wide

range of dipole coupling strengths and observation angles. For both the geometrical configurations of atoms, the super and subradiant characteristics of the radiation emitted from different W- and GHZ- states are presented. It is shown that the nature of the entanglement present in the atomic system is seen to modify the super/subrradiant behaviour. From the study presented, it is inferred that the quantum statistical properties of the emitted radiation show distinctly different characteristics for the GHZ and W-states, making it possible for optical probing of entangled states. Further, this study reveals that, in loop configuration, the strong D-D interaction leads to directional emission of radiation from atoms prepared in symmetric W-state.

Finally, chapter 6 summarizes the results presented in the thesis and suggestions are made on some possible future directions.

References

[1] R. H. Dicke, Phys. Rev. **93**, 99 (1954).

[2] U. Fano, Rev. Mod. Phys. **55**, 855 (1983).

[3] G. S. Agarwal, A. C. Brown, L. M. Narducci and G. Vetri, Phys. Rev. A **15**, 1613 (1977); I. R. Senitzky, Phys. Rev. Lett. **40**, 1334 (1978).

[4] H. S. Freedhoff, Phys. Rev. A **19**, 1132 (1979).

[5] Z. Ficek, R. Tanaś and S. Kielich, Optica Acta **33**, 1149 (1986).

[6] M. J. Stephen, J. Chem. Phys. **40**, 669 (1964).

[7] R. H. Lehmberg, Phys. Rev. A **2**, 889 (1970).

[8] P. W. Milonni and P. L. Knight, Phys. Rev. A **10**, 1096 (1974).

[9] M. S. Iqbal, S. Mahmood, M. S. K. Razmi and M. S. Zubairy, J. Opt. Soc. America B **5**, 1312 (1988).

[10] T. J. Carroll, K. Claringbould, A. Goodsell, M. J. Lim and M. W. Noel, Phys. Rev. Lett. **93**, 153001 (2004); S. Ravets, H. Labuhn, D. Barredo, T. Lahaye and A. Browaeys, Phys. Rev. A **92**, 020701(R) (2015).

[11] G. S. Agarwal, L. M. Narducci and E. Apostolidis, Opt. Comm. **36**, 285 (1981).

[12] Q. V. Lawande, B. N. Jagatap and S. V. Lawande, Phys. Rev. A **42**, 4343 (1990).

[13] M. S. Kim, F. A. M. de Oliveira and P. L. Knight, Opt. Comm. **70**, 473 (1989).

[14] J. von Zanthier, T. Bastin and G. S. Agarwal, Phys. Rev. A **74**, 061802 (2006).

[15] J. Gillet, G. S. Agarwal and T. Bastin, Phys. Rev. A **81**, 013837 (2010).

[16] T. Wilk, A. Gaëtan, C. Evellin, J. Wolters, Y. Miroshnychenko, P. Grangier and A. Browaeys, Phys. Rev. Lett. **104**, 010502 (2010); Z. J. Zhang, Opt. Comm. **261**, 199 (2006); Q. Y. Cai and Y. G. Tan, Phys. Rev. A **73**, 032305 (2006).

[17] D. Jaksch, J. I. Cirac, P. Zoller, S. L. Rolston, R. Côté and M. D. Lukin, Phys. Rev. Lett. **85**, 2208 (2000).

[18] M. Saffman, T. G. Walker and K. Molmer, Rev. Mod. Phys. **82**, 2313 (2010).

[19] M. D. Lukin, M. Fleischhauer, R. Côté, L. M. Duan, D. Jaksch, J. I. Cirac, and P. Zoller, Phys. Rev. Lett. **87**, 037901 (2001).

[20] A. Gaëtan, Y. Miroshnychenko, T. Wilk, A. Chotia, M. Viteau, D. Comparat, P. Pillet, A. Browaeys and P. Grangier, Nat. Phys. **5**, 115 (2009).

[21] L. Isenhower, E. Urban, X. L. Zhang, A. T. Gill, T. Henage, T. A. Johnson, T. G. Walker and M. Saffman, Phys. Rev. Lett. **104**, 010503 (2010).

[22] T. Pohl and P. R. Berman, Phys. Rev. Lett. **102**, 013004 (2009).

[23] S. Wüster, A. Eisfeld and J. M. Rost, Phys. Rev. Lett. **106**, 153002 (2011).

[24] D. R. Yarkony, Rev. Mod. Phys. **68**, 985 (1996); Electronic Structure, Dynamics and Spectroscopy, Vol. 15, edited by W. Domcke, D. R. Yarkony, and H. Köppel (World Scientific, 2004).

[25] V. Efimov, Phys. Lett. B **33**, 563 (1970).

[26] G. K. Brennen, I. H. Deutsch and P. S. Jessen, Phys. Rev. A **61**, 062309 (2000); P. S. Jessen, D. L. Haycock, G. Klose, G. A. Smith, I. H. Deutsch and G. K. Brennen, Quant. Inform. Comput. **1**, 20 (2001).

[27] E. Schrödinger, Naturwissenschaften **23**, 807; ibid 823; ibid 844 (1935).

[28] T. Yu and J. H. Eberly, Science **323**, 598 (2009).

[29] L. Amico, R. Fazio, A. Osterloh and V. Vedral, Rev. Mod. Phys. **80**, 517 (2008); D. Markham, J. Anders, V. Vedral, M. Murao and A. Miyake, Eur. Phys. Lett. **81**, 40006 (2008); K. C. Lee et al. Science **334**, 1253 (2011).

[30] T. G. Rappoport, L. Ghivelder, J. C. Fernandes, R. B. Guimarães and M. A. Continentino, Phys. Rev. B **75**, 054422 (2007); A. Tribedi and I. Bose, Phys. Rev. A **74**, 012314 (2006); H. Singh, T. Chakraborty, P. K. Panigrahi and C. Mitra, Quant. Inf Proc. **14**, 951 (2015).

[31] S. S. Gong and S. Gang, Phys. Rev. A **80**, 012323 (2009).

[32] H. Wang, S. Liu and H. Jizhou, Phys. Rev. E **79**, 041113 (2009).

[33] A. K. Pal and I. Bose, J. Phys.: Condens. Matter **22**, 016004 (2010).

[34] M. Gross and S. Haroche, Phys. Rep. **93**, 301 (1982).

[35] L. I. Menshikov, Phys. Usp. **42**, 107 (1999).

[36] M. Greiner, O. Mandel, T. Esslinger, T. W. Hansch and E. Bloch, Nature (London) **415**, 39 (2002); M. Greiner, O. Mandel, T. W. Hansch and E. Bloch, Nature (London) **419**, 51 (2002).

[37] D. M. Greenberger, M. A. Horne and A. Zeilinger, *Quantum theory and conceptions of the Universe* (Springer, Netherlands), 69 (1989).

[38] W. D*ür*, G. Vidal and J. I. Cirac, Phys. Rev. A **62**, 062314 (2000).

[39] J. Joo, Y. J. Park, S. Oh and J. Kim J, New J. Phys. **5**, 136 (2003).

[40] C. H. Bennett, G. Brassard, C. Crepeau, R. Jozsa, A. Peres and W. K. Wootters, Phys. Rev. Lett. **70**, 1895 (1993).

[41] D. D. Bhaktavatsala Rao, S. Ghosh and P. K. Panigrahi, Phys. Rev. A **78**, 042328 (2008).

[42] A. Karlsson and M. Bourennane, Phys. Rev. A **58**, 4394 (1998).

[43] R. Wiegner, J. von-Zanthier and G. S. Agarwal, Phy. Rev. A **84**, 023805 (2011).

[44] G. S. Agarwal, *Quantum Optics*, Springer Tracts in Modern physics, Vol 70, sec 6 ed Höhler G et al, New York: Springer-Verlag (1974).

Chapter 2

Studies on system of two two-level atoms interacting with radiation field

Within the many areas of Quantum Optics, one of the simplest non trivial problems involving the atom-field interaction is the coupling of a two-level atom with a single mode of the radiation field [1,2]. A two-level atom approximation is valid if the two energy levels in an atomic system are resonant or nearly resonant with the applied field, while all other levels are off resonant. Under certain realistic circumstances, it is possible to reduce this problem to a simple form which can be solved exactly. In the dipole approximation, when the the size of the atom is much smaller than the optical wavelength, the atom-field interaction problem is mathematically equivalent to a spin-half particle interacting with an external magnetic field [3]. The basic dynamical equations governing the evolution of two-level atom variables, are practically same as those appropriate to spins. An understanding of this simple model of the atom-field interaction enables one to consider more complicated problems

involving an ensemble of atoms interacting with the field. One of the most important examples of such a problem is the interaction of two two-level atoms with a monochromatic radiation field, some aspects of which will be discussed in this chapter.

In this chapter, we begin with the theoretical formulation of the system of two two-level atoms mutually coupled through D-D interaction and both the atoms interacting with a single mode radiation field. Several aspects of this problem have been the subject of extensive studies [4]. For the sake of completeness we review some of the already studied aspects and present the new results we have obtained for this system. The justification for a study of this problem comes from the following considerations. The D-D interaction between two two-level atoms has given rise to a myriad of fascinating phenomena [5–7]. Especially in the field of quantum information [8–11], the D-D interaction plays an important role in the creation of maximally entangled single excitation states and the shift of the states from the single-atom energy [12]. The strong D-D interaction between two highly excited Rydberg atoms act as a Rydberg blockade [13], which can be used as a mechanism for implementing two-qubit quantum logic gates [14]. In order to achieve a robust entangled state, many researchers have made efforts to stabilize the atomic entanglement via the D-D interaction in different engineering scenarios, such as a squeezed vacuum field [15, 16], an electro-magnetic bath [17], a classical driving field [18] etc. Therefore, it is of utmost importance to have a clear understanding of the effect of D-D interaction on quantum entanglement. We address this problem in the second part of this chapter where the effects of D-D interaction on entanglement characteristics of the system are studied in detail.

Density operator

In practice we often come across situations involving statistical ensembles of states, where it is impossible to specify the state of the systems completely. A simplest example is that of a two-level atom, driven by a resonant laser field, which emits photons at random times. In order to be able to describe the system by a pure state, we need to have information on the exact emission times of all the randomly emitted photons, which is not possible. If the concrete history of the system is not known, by which we imply that the system is not in a pure state, the density matrix ρ formalism is a more convenient approach, which enables one to obtain all the physical predictions about the system. The density operator enable us to calculate the probability density of the atom being in a particular state, which is of interest to us in this study. Suppose, a system is prepared with probability P_i of being in a state $|\psi_i\rangle$, where i runs over all possible realizations of the system, then the density operator ρ of this statistical mixture is given by

$$\rho = \sum_i P_i |\psi_i\rangle\langle\psi_i|, \tag{2.1}$$

where the probability P_i lies between 0 and 1 and further $\sum_i P_i = 1$. The action of the density operator on a member of the ensemble $|\psi_i\rangle$, which can be expressed as

$$\rho|\psi_i\rangle = \sum_i P_i |\psi_i\rangle\langle\psi_i|\psi_i\rangle = P_i|\psi_i\rangle, \tag{2.2}$$

enables one to determine the probability P_i of finding the system in state $|\psi_i\rangle$. If all the members of the ensemble are in the same state, say $|\psi_k\rangle$, then the density operator reduces to $\rho = |\psi_k\rangle\langle\psi_k|$ and the system is said to be in a pure

state $|\psi_k\rangle$, with probability $P_k = 1$. From equation 2.2, the diagonal matrix elements of the density operator give the probability of finding the system in state $|\psi_i\rangle$, $\langle\psi_i|\rho|\psi_i\rangle = P_{ii}$, which are referred to as the population in the state $|\psi_i\rangle$. The off-diagonal density matrix elements are referred to as coherences.

2.1 The model

We consider two isolated two-level atoms fixed in position with a separation r, driven by a single mode resonant laser field, of frequency ω_L (wavelength λ), which is nearly resonant with the transition frequency of one of the atoms, in the region $r \ll \lambda$. Here $|\mathbf{g}_i\rangle$ and $|\mathbf{e}_i\rangle$ are respectively the ground and excited states of the i^{th} atom ($i = 1, 2$). The interaction with the field induces dipole moment in the atoms, which in turn interact with each other via photon exchange. In our model it is assumed that the external field is propagating perpendicular to the inter-atomic axis, which renders the interaction of the field with the atoms to be purely symmetric. The density operator of the two-atom system can be represented in a complete set of basis states spanned by four product states, which is usually referred to as the standard basis, the elements of which are defined as

$$\begin{aligned} |1\rangle &= |g_1\rangle \otimes |g_2\rangle \qquad |2\rangle = |e_1\rangle \otimes |g_2\rangle \\ |3\rangle &= |g_1\rangle \otimes |e_2\rangle \qquad |4\rangle = |e_1\rangle \otimes |e_2\rangle \end{aligned} \tag{2.3}$$

A schematic of this level scheme is shown in figure 2-1. However, since the D-D interaction couples the two atoms, when describing the evolution of such a system, the standard basis is usually not the most convenient basis to work

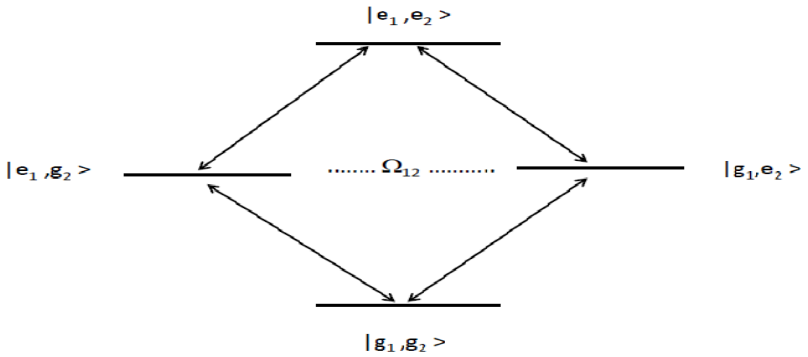

Figure 2-1: Schematic energy level diagram of two identical two-level atoms as an equivalent four-level system in product basis

with. In this case, it is more convenient to include the D-D interaction into the Hamiltonian and re-diagonalize it, giving rise to a different set of basis states, which are termed as the collective or Dicke states of the two-atom system, defined by

$$\begin{aligned} |g\rangle &= |g_1\rangle \otimes |g_2\rangle; \quad E_g = 0 \\ |s\rangle &= \frac{1}{\sqrt{2}}(|e_1\rangle \otimes |g_2\rangle + |g_1\rangle \otimes |e_2\rangle); \quad E_s = \hbar(\omega_0 + \Omega_{12}) \\ |a\rangle &= \frac{1}{\sqrt{2}}(|e_1\rangle \otimes |g_2\rangle - |g_1\rangle \otimes |e_2\rangle); \quad E_a = \hbar(\omega_0 - \Omega_{12}) \\ |e\rangle &= |e_1\rangle \otimes |e_2\rangle; \quad E_e = 2\hbar\omega_0 \end{aligned} \tag{2.4}$$

where Ω_{12} is the D-D interaction between two atoms and $\omega_0 = (\omega_1 + \omega_2)/2$, ω_1 and ω_2 are the energy level separations of atoms 1 and 2 respectively and the wave number $k = \omega_0/c$.

Unlike the standard basis states, the collective basis contains two intermediate states, $|s\rangle$ and $|a\rangle$ that are linear, symmetric and antisymmetric super positions of the product states respectively, as shown in figure 2-2. Their energies depend on the D-D interaction and these states go through a large energy

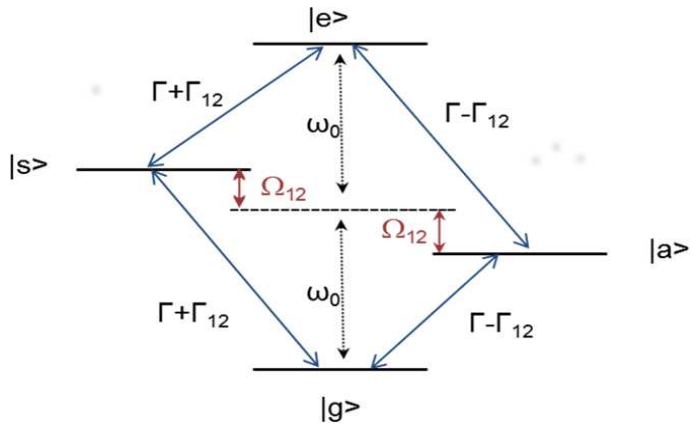

Figure 2-2: Schematic energy level diagram of two identical two-level atoms as an equivalent four-level system in collective basis

shift even for a small inter-atomic separation.

2.2 Formulation

In this section, we develop a mathematical framework to treat the atom-field interaction semi-classically where the atoms are treated quantum mechanically and the field is treated classically. In this study we assume, with no loss of generality, that the atomic dipole moments are parallel to each other and are polarized in a direction perpendicular to the inter-atomic axis, i.e., $\vec{\mu_1} = \vec{\mu_2} = \vec{\mu}$ and $\vec{\mu} \perp \vec{r}$. For the atoms in a running-wave laser field, the Rabi frequency is a complex parameter which may be written as

$$\Omega_i = \Omega_0 exp(-ik_L.r_i) \tag{2.5}$$

where $\Omega_0 = |\mu.\overrightarrow{\mathcal{E}}_L^{(+)}(r_i)|$ is the Rabi frequency, r_i is the position vector of the i^{th} atom, and k_L is the wave vector of the driving field. For the direction of propagation of the driving field perpendicular to the atomic axis, $k_L.r = 0$,

both the atoms experience the same driving field strength ($\Omega_1 = \Omega_2 = \Omega_0$). This case has been extensively studied in the literature [19,20]. When $k_L.r \neq 0$ the atoms are subject to different driving fields ($\Omega_1 \neq \Omega_2$).

Several theoretical approaches can be used to treat the system of two atoms interacting with the radiation field. One of the more preferred among these is the master equation approach [21], which enables one to treat the evolution of the atom-field system completely in terms of the atomic operators.

The master equation which governs the dynamical evolution of the density operator ρ of the two-atom system is given by

$$\frac{\partial \rho}{\partial t} = -i\sum_{i=1}^{2}\Delta_i[S_i^z,\rho] - i\sum_{i\neq j=1}^{2}\Omega_{ij}[S_i^+S_j^-,\rho] + i\frac{\Omega_0}{2}\left[(S_1^+ + S_2^+)e^{-i\omega_L t} + H.C,\rho\right] - \mathcal{L}\rho$$

where the last term $\mathcal{L}\rho = \frac{1}{2}\sum_{i,j=1}^{2}\Gamma_{ij}(\rho S_i^+S_j^- + S_i^+S_j^-\rho - 2S_j^-\rho S_i^+)$ represents the decay of the atomic system. Here, $S_i^+ = |e_i\rangle\langle g_i|$ and $S_i^- = |g_i\rangle\langle e_i|$ are the raising and lowering operators respectively, $S_i^z = \frac{1}{2}[|e_i\rangle\langle e_i| - |g_i\rangle\langle g_i|]$ is the energy operator of the i^{th} atom and ω_L is the driving field frequency and Ω_0 is the Rabi frequency. The parameters Ω_{ij} and $\Gamma_{ij}(i \neq j)$ which describe the D-D interaction and the collective damping respectively, are both functions of the inter atomic distance, given by

$$\Omega_{ij} = \frac{3\Gamma}{4}\left[-(1-\cos^2\theta)\frac{\cos(kr_{ij})}{kr_{ij}} + (1-3\cos^2\theta)\left(\frac{\sin(kr_{ij})}{(kr_{ij})^2} + \frac{\cos(kr_{ij})}{(kr_{ij})^3}\right)\right] \tag{2.6}$$

and

$$\Gamma_{ij} = \frac{3\Gamma}{2}\left[(1-\cos^2\theta)\frac{\sin(kr_{ij})}{kr_{ij}} + (1-3\cos^2\theta)\left(\frac{\cos(kr_{ij})}{(kr_{ij})^2} - \frac{\sin(kr_{ij})}{(kr_{ij})^3}\right)\right] \tag{2.7}$$

where θ is the angle between the dipole moment $\vec{\mu}$ and the inter atomic separation $\vec{r}_{ij}$. From the above equations 2.6 and 2.7, it is clearly seen that for small inter-atomic distances ($kr_{ij} \ll 1$), the collective parameters Γ_{ij} and Ω_{ij} reduce to Γ and the quasi-static D-D interaction potential respectively, the latter of which is given by $\Omega_{ij} = \frac{3\Gamma}{2(kr_{ij})^3}(1-3\cos^2\theta)$. For large inter-atomic separations ($kr_{ij} \gg 1$), the corresponding $\Omega_{ij} = \Gamma_{ij} = 0$, i.e., there is no coupling between the atoms. In this case, the master equation reduces to algebraic sum of the master equation of the single atoms.

We now remove the fast time dependence from $\rho(t)$ and the corresponding slowly varying quantities $\tilde{\rho}(t)$ are obtained (where tilde denotes a quantity in a frame rotating with the frequency of the driving field) and the terms oscillating at twice the optical frequency are neglected. This transformation is known as the rotating wave approximation (RWA). The relation between different elements of the density operator in the rotating frame and the initial frame are given by

$$\rho_{gg} = \tilde{\rho}_{gg}; \rho_{ga} = \tilde{\rho}_{ga}e^{i\omega_L t}; \rho_{gs} = \tilde{\rho}_{gs}e^{i\omega_L t}; \rho_{ge} = \tilde{\rho}_{ge}e^{2i\omega_L t}$$

$$\rho_{ag} = \tilde{\rho}_{ag}e^{-i\omega_L t}; \rho_{aa} = \tilde{\rho}_{aa}; \rho_{as} = \tilde{\rho}_{as}; \rho_{ae} = \tilde{\rho}_{ae}e^{i\omega_L t}$$

$$\rho_{sg} = \tilde{\rho}_{sg}e^{-i\omega_L t}; \rho_{sa} = \tilde{\rho}_{sa}; \rho_{ss} = \tilde{\rho}_{ss}; \rho_{se} = \tilde{\rho}_{se}e^{i\omega_L t}$$

$$\rho_{eg} = \tilde{\rho}_{eg}e^{-2i\omega_L t}; \rho_{ea} = \tilde{\rho}_{ea}e^{-i\omega_L t}; \rho_{es} = \tilde{\rho}_{es}e^{-i\omega_L t}; \rho_{ee} = \tilde{\rho}_{ee}$$

The master equation for the evolution of atomic density operator ρ, after the

RWA has been made, is given by

$$\frac{\partial\tilde{\rho}}{\partial t} = -i\sum_{i=1}^{2}\Delta_i[S_i^z,\tilde{\rho}] - i\sum_{i\neq j=1}^{2}\Omega_{ij}[S_i^+S_j^-,\tilde{\rho}] + i\frac{\Omega_0}{2}\sum_{i=1}^{2}[S_i^+ + S_i^-,\tilde{\rho}] - \mathcal{L}\tilde{\rho} \quad (2.8)$$

The equations of motion for different density matrix elements can be obtained from equation(2.8) which then can be solved both in steady state as well as in the transient regime.

2.3 Dynamical evolution of two two-level atoms

In this section, we study the interaction of two two-level atoms with each other through D-D coupling and solve the equations of motion for the system in the presence of external field. The sixteen first order differential equations of motion for the density matrix elements after RWA are obtained as follows:

$$\begin{aligned}
\partial_t\tilde{\rho}_{ee} &= i\tilde{\Omega}(\tilde{\rho}_{se}-\tilde{\rho}_{es}) - 2\Gamma\tilde{\rho}_{ee}\\
\partial_t\tilde{\rho}_{ss} &= i\tilde{\Omega}(\tilde{\rho}_{es}+\tilde{\rho}_{gs}-\tilde{\rho}_{se}-\tilde{\rho}_{sg}) + \frac{i(\Delta_2-\Delta_1)}{2}(\tilde{\rho}_{as}-\tilde{\rho}_{sa}) - (\Gamma+\Gamma_{12})(\tilde{\rho}_{ss}-\tilde{\rho}_{ee})\\
\partial_t\tilde{\rho}_{aa} &= \frac{i(\Delta_1-\Delta_2)}{2}(\tilde{\rho}_{as}-\tilde{\rho}_{sa}) - (\Gamma-\Gamma_{12})(\tilde{\rho}_{aa}-\tilde{\rho}_{ee})\\
\partial_t\tilde{\rho}_{gs} &= -i\tilde{\Omega} + \left[\frac{i(\Delta_1+\Delta_2)}{2} - \frac{(\Gamma+\Gamma_{12})}{2} + i\Omega_{12}\right]\tilde{\rho}_{gs} + \frac{i(\Delta_1-\Delta_2)}{2}\tilde{\rho}_{ga} + 2(\Gamma+\Gamma_{12})\tilde{\rho}_{se} +\\
&\quad i\tilde{\Omega}(2\tilde{\rho}_{ss}+\tilde{\rho}_{aa}+\tilde{\rho}_{ee}-\tilde{\rho}_{ge})\\
\partial_t\tilde{\rho}_{ga} &= \left[\frac{i(\Delta_1+\Delta_2)}{2} - \frac{(\Gamma-\Gamma_{12})}{2} - i\Omega_{12}\right]\tilde{\rho}_{ga} + \frac{i(\Delta_1-\Delta_2)}{2}\tilde{\rho}_{gs} - 2(\Gamma-\Gamma_{12})\tilde{\rho}_{ae} + i\tilde{\Omega}\tilde{\rho}_{sa}\\
\partial_t\tilde{\rho}_{ge} &= [i(\Delta_1+\Delta_2)-\Gamma]\,\tilde{\rho}_{ge} + i\tilde{\Omega}(\tilde{\rho}_{se}-\tilde{\rho}_{gs}) \qquad (2.9)\\
\partial_t\tilde{\rho}_{se} &= \left[\frac{i(\Delta_1+\Delta_2)}{2} - \frac{(3\Gamma+\Gamma_{12})}{2} - i\Omega_{12}\right]\tilde{\rho}_{se} + \frac{i(\Delta_2-\Delta_1)}{2}\tilde{\rho}_{ae} - i\tilde{\Omega}(\tilde{\rho}_{ss}-\tilde{\rho}_{ee}-\tilde{\rho}_{ge})\\
\partial_t\tilde{\rho}_{ae} &= \left[\frac{i(\Delta_1+\Delta_2)}{2} - \frac{(3\Gamma-\Gamma_{12})}{2} + i\Omega_{12}\right]\tilde{\rho}_{ae} + \frac{i(\Delta_2-\Delta_1)}{2}\tilde{\rho}_{se} - i\tilde{\Omega}\tilde{\rho}_{as}\\
\partial_t\tilde{\rho}_{as} &= \frac{i(\Delta_2-\Delta_1)}{2}(\tilde{\rho}_{ss}-\tilde{\rho}_{aa}) - (\Gamma-2i\Omega_{12})\tilde{\rho}_{as} - i\tilde{\Omega}(\tilde{\rho}_{ae}+\tilde{\rho}_{ag})\\
\partial_t\tilde{\rho}_{gg} &= -\partial_t\tilde{\rho}_{aa} - \partial_t\tilde{\rho}_{ss} - \partial_t\tilde{\rho}_{ee}
\end{aligned}$$

The remaining equations can be obtained from the Hermitian properties of the density matrix elements, viz.,

$$\tilde{\rho}_{ij} \;=\; \tilde{\rho}^{*}_{ji}.$$

In the above equations the atomic detuning $\Delta_i = \omega_i - \omega_L$, $i = 1, 2$, where ω_i is the frequency of i^{th} atom, ω_L is the frequency of applied field and the total two-atom detuning $\Delta = \Delta_1 + \Delta_2$. Here $\Gamma_1 = \Gamma_2 = \Gamma$ is the spontaneous decay rate of each atom and $\tilde{\Omega} = \frac{\Omega_0}{\sqrt{2}}$ is the modified Rabi frequency.

The decay from a state is referred to as super(sub)radiant, if its decay rate is larger(smaller) than the radiative decay rate Γ. A detailed inspection of the equations of motion reveals that the symmetric state is superradiant with rate $\Gamma + \Gamma_{12}$, whereas the antisymmetric state is subradiant with rate $\Gamma - \Gamma_{12}$. The slowly decaying state $|a\rangle$ can be populated through two different channels, viz., the spontaneous emission from the state $|e\rangle$ and the coherent interaction with the state $|s\rangle$. By using the completeness condition of the level populations $\tilde{\rho}_{gg} + \tilde{\rho}_{aa} + \tilde{\rho}_{ss} + \tilde{\rho}_{ee} = 1$, the 16 equations can be reduced to 15 equations, which can be cast in the form

$$\frac{\partial \Psi}{\partial t} = M\Psi + \Phi \tag{2.10}$$

where M is a 15×15 coefficient matrix and Ψ and Φ are column vectors each of length 15 which are defined in the following.

$$\Psi \;=\; [\tilde{\rho}_{ga}\ \tilde{\rho}_{gs}\ \tilde{\rho}_{ge}\ \tilde{\rho}_{ag}\ \tilde{\rho}_{aa}\ \tilde{\rho}_{as}\ \tilde{\rho}_{ae}\ \tilde{\rho}_{sg}\ \tilde{\rho}_{sa}\ \tilde{\rho}_{ss}\ \tilde{\rho}_{se}\ \tilde{\rho}_{eg}\ \tilde{\rho}_{ea}\ \tilde{\rho}_{es}\tilde{\rho}_{ee}]^{T} \tag{2.11}$$

$$\Phi \;=\; [0\ -i\tilde{\Omega}\ 0\ 0\ 0\ 0\ 0\ i\tilde{\Omega}\ 0\ 0\ 0\ 0\ 0\ 0\ 0]^{T} \tag{2.12}$$

In the equations of the density matrix elements the ' ~ ' above each of the elements corresponds to the density matrix elements in the rotating frame. From here on, for brevity of notation, the tilde ' ~ ' above each of the elements is removed, with the understanding that all the elements are defined in the rotating frame. Depending on the nature of information that is being sought, the equations can be solved either as a function of time, which will necessitate solution of 16 first order coupled differential equations, or in steady state. In the next section we present some of the results of level populations and various atomic coherences in time domain, both for identical and non-identical atoms.

2.3.1 Results and Discussion

In this section, we study the effect of D-D interaction on level populations (ρ_{ii}, for $i = g, a, s, e$) and various atomic coherences (ρ_{ij}, for $i \neq j = g, a, s, e$) in time domain both for identical and non-identical atoms. Some preliminary results for typical values of the parameters are presented. Throughout the results presented here, all the parameters, namely the atomic detunings, the Rabi frequencies, the D-D interaction strength are all normalized with respect to the population decay rate Γ.

2.3.1.1 Identical atoms

Here, we present the results for three typical values of inter-atomic separations ($r = \frac{\lambda}{10}, \frac{\lambda}{14}$ and $\frac{\lambda}{18}$) corresponding to large, moderate and small distances respectively. The D-D interaction, which scales as r^{-3}, corresponding to these three distances can be categorized as weak, moderate and strong respectively. It is of interest to study the evolution of these density matrix elements, for

certain specific choice of initial conditions on the atoms. We start with the situation of both atoms being in the ground state initially, and for moderate value of Rabi field strength $\Omega_0 = 2$ and for the total detuning $\Delta = 0$. In Figure 2-3, the blue line in each of the sub-figures shows the time evolution of the corresponding population for weak interaction ($\Omega_{12} = 2.6$), while the green line corresponds to a moderate interaction strength ($\Omega_{12} = 7.6$) and the red line pertains to a strong interaction strength ($\Omega_{12} = 16.6$).

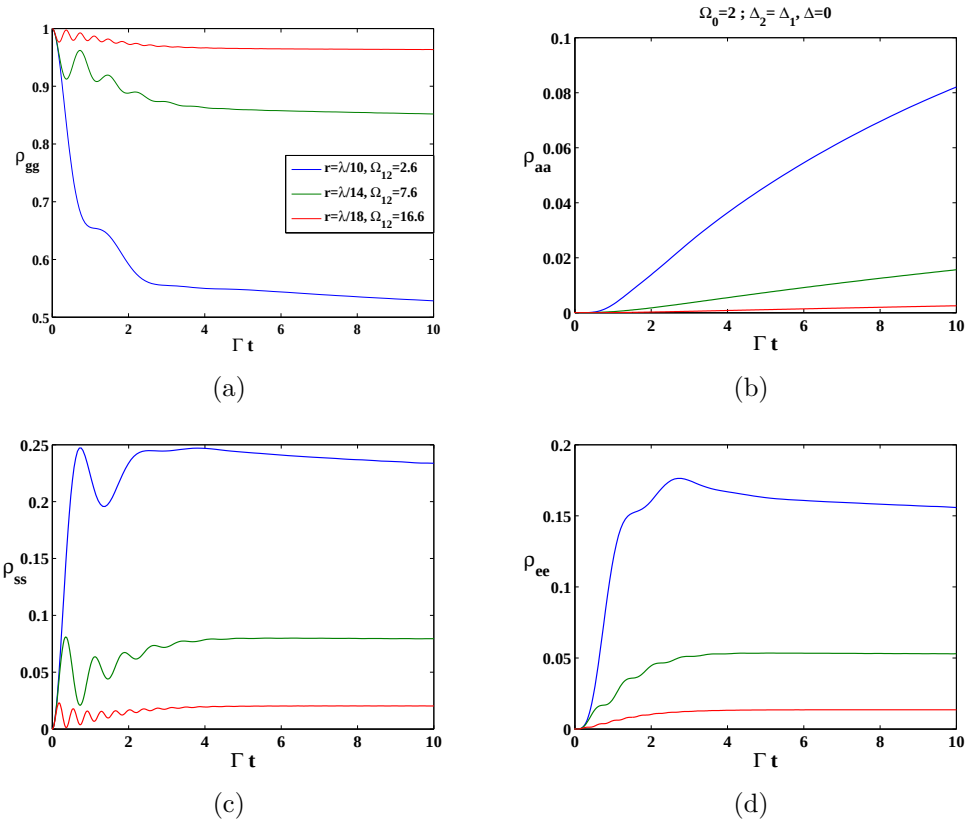

Figure 2-3: *The time evolution of level populations of two identical atoms* 2-3(a) ρ_{gg}, 2-3(b) ρ_{aa}, 2-3(c) ρ_{ss} and 2-3(d) ρ_{ee}, corresponding to inter-atomic distance $r = \frac{\lambda}{10}$ (blue line), $\frac{\lambda}{14}$ (green line) and $\frac{\lambda}{18}$ (red line) respectively.

When the atoms are far apart ($r = \frac{\lambda}{10}$), the ground state population ρ_{gg} starts from its initial value of 1 and decreases rapidly and reaches a value of

0.57 within two lifetimes and stabilizes and approaches steady state. The symmetric state population ρ_{ss} very rapidly reaches a maximum value of 0.25 and exhibits oscillatory behaviour and with further increase in time approaches steady state. As both atoms are assumed to be in the ground state initially, as expected, due to the action of the external radiation field, the population ρ_{ee} increases upto certain time and then approaches steady state. From the equations of motion of the density matrix elements, we know that the antisymmetric state $|a\rangle$ is subradiant with a decay rate of $\Gamma - \Gamma_{12}$ and further it can be populated by the spontaneous emission from the state $|e\rangle$ (since $\rho_{as} = 0$ for identical atoms). The antisymmetric state population ρ_{aa} shows a slow increase and attains a steady state value at a much larger Γt (due to its long-lived nature), as is illustrated quantitatively in figure 2-3(b).

It is obvious from the Eqs. 2.6 and 2.7 that the strength of D-D interaction and collective decay rate increase as the inter-atomic distance r decreases. For an intermediate value of inter-atomic distance $r = \frac{\lambda}{14}$ ($\Omega_{12} = 7.6$), it is observed that the ground state population ρ_{gg} exhibits oscillatory behaviour at initial times and attains a higher steady state value of 0.91, as compared to the case of weak coupling (blue line). Consequently the excited states are poorly populated. The oscillations in populations can be attributed to photon exchange interaction.

As the inter atomic distance is decreased further ($r = \frac{\lambda}{18}$), the dipole interaction becomes stronger ($\Omega_{12} = 16.6$) blocking the excitation of atoms as observed from the decreased excited state populations (fig. 2-3). The reason for the small population, is easily understood through the level shift of the symmetric and antisymmetric states, due to the D-D interaction, as shown in figure 2-2. These level shifts can have strong influence on the laser excitation of

adjacent atoms, rendering it nearly impossible to simultaneously excite both the atoms. This is a clear signature of a dipole blockade wherein the first excited atom prevents any further excitation, by shifting the resonance for its non excited neighbours, resulting in the production of singly excited collective states [22].

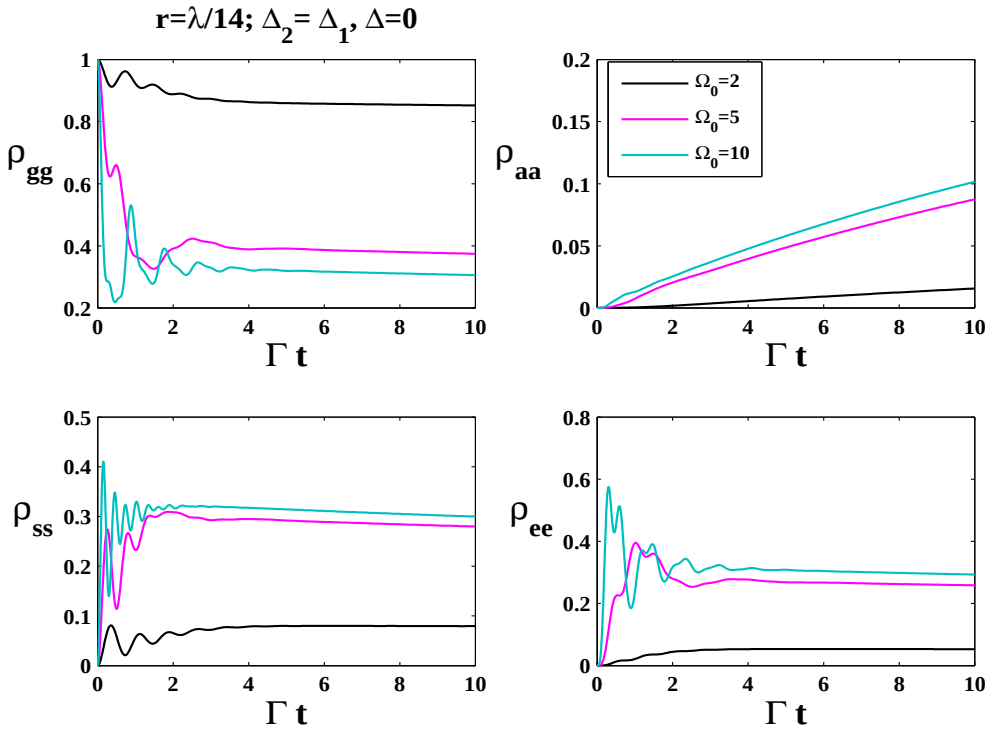

Figure 2-4: The dynamical evolution of level populations of identical atoms for different Rabi field strengths Ω_0= 2 (black line), 5 (magenta line), 10 (cyan line) when the inter-atomic distance $r = \frac{\lambda}{14}$.

To see the competition between the D-D strength and the Rabi frequency, fixing the inter-atomic distance at a particular value of $r = \frac{\lambda}{14}$, which corresponds to the moderate D-D strength of figure 2-3, we have studied the populations for different values of the Rabi field strengths. From figure 2-4, we clearly see that as the Rabi field strength is increased, the dipole blockade is lifted and the separable doubly excited state $|e\rangle$ is substantially populated.

This clearly shows how the stronger radiation field counteracts the effect of D-D interactions. In addition, the population of the antisymmetric state is relatively small for all times. This is due to the fact that the laser field couples to the symmetric state leaving the antisymmetric state nearly decoupled from the driven states.

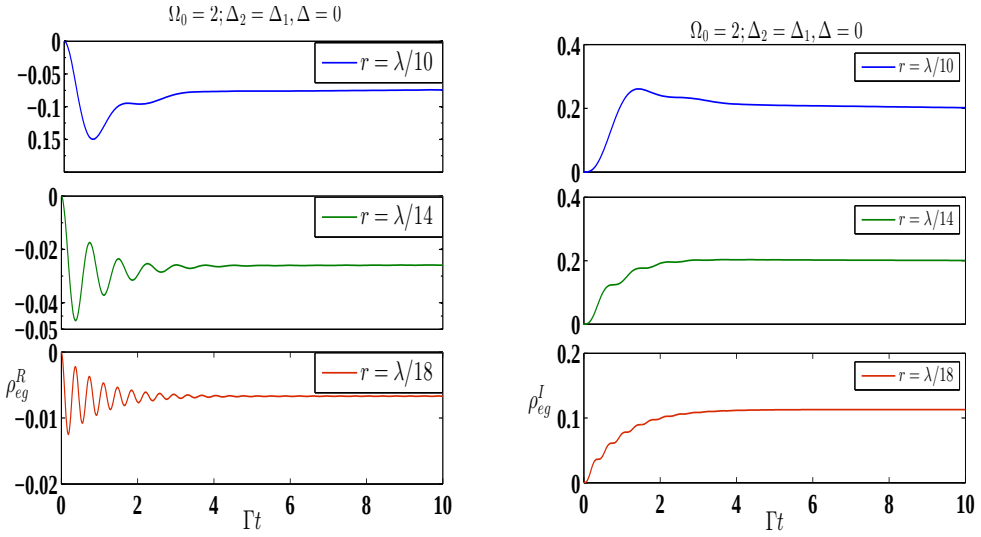

(a) (b)

Figure 2-5: *Two photon coherence ρ_{eg} for identical atoms* 2-5(a) $Re(\rho_{eg})$ and 2-5(b) $Im(\rho_{eg})$ corresponding to inter-atomic distances of $r = \frac{\lambda}{10}, \frac{\lambda}{14}$ and $\frac{\lambda}{18}$.

Next, in order to see the effect of the D-D coupling and the Rabi frequency on the atomic coherences, the real and imaginary parts of two photon coherence ρ_{eg} are plotted for identical atoms in two adjacent frames in figure 2-5. The real part of (ρ_{eg}) increases with increase in Ω_{12}. The number of oscillations increase in time with increase in Ω_{12} and the amplitude of the oscillations decreases slowly as the time progresses. On the other hand, the imaginary part of the coherence (ρ_{eg}) decreases monotonically with increase in Ω_{12}.

From the above analysis, it can be understood that the population distribution strongly depends on the D-D coupling strength. As the dipole coupling

strength is increased, the number of oscillations (before steady state is attained) are increasing in all of the populations. For a fixed Rabi field strength, an increase in the dipole coupling gives rise to inhibition of the excited state populations, showing clearly that increase in the D-D coupling is giving rise to an increase in the probability for both atoms to be trapped in their ground states. In the next section, we study these features for the case of non-identical atoms.

2.3.1.2 Non-identical atoms

For the case of non-identical atoms, we assume different energy level separation between ground and excited states of the two atoms and hence $\Delta_1 \neq \Delta_2$. We also assume that the two decay constants Γ_1 and Γ_2 are close enough, that they can be effectively considered equal, denoted by Γ. This is physically consistent, since in comparison to values of Rabi frequencies and detunings, the value of decay constants of different atoms are much closer. For example, ^{7}Li and ^{85}Rb have decay rates 5.92 MHz and 5.98 MHz respectively while their resonant wavelengths are 670 nm and 780 nm. In such case, without any loss of generality, the decay constants of both species can be replaced by an identical value of 5.9 MHz. However, when excited by a single mode radiation field, the detunings of each of these atoms would be markedly different from each other. Without a need to choose specific atomic species, we assume a situation of $\Delta_2 = \Delta_1 + 10\Gamma$, where $\Delta_1 = -5\Gamma, \Delta_2 = +5\Gamma$ such that the total detuning $\Delta = 0$.

The time evolution of the level populations of non-identical atoms for $r = \frac{\lambda}{10}$ (corresponding $\Omega_{12} = 2.6$) is shown in figure 2-6. From the figure we observe that the collective states are unequally populated. The ground

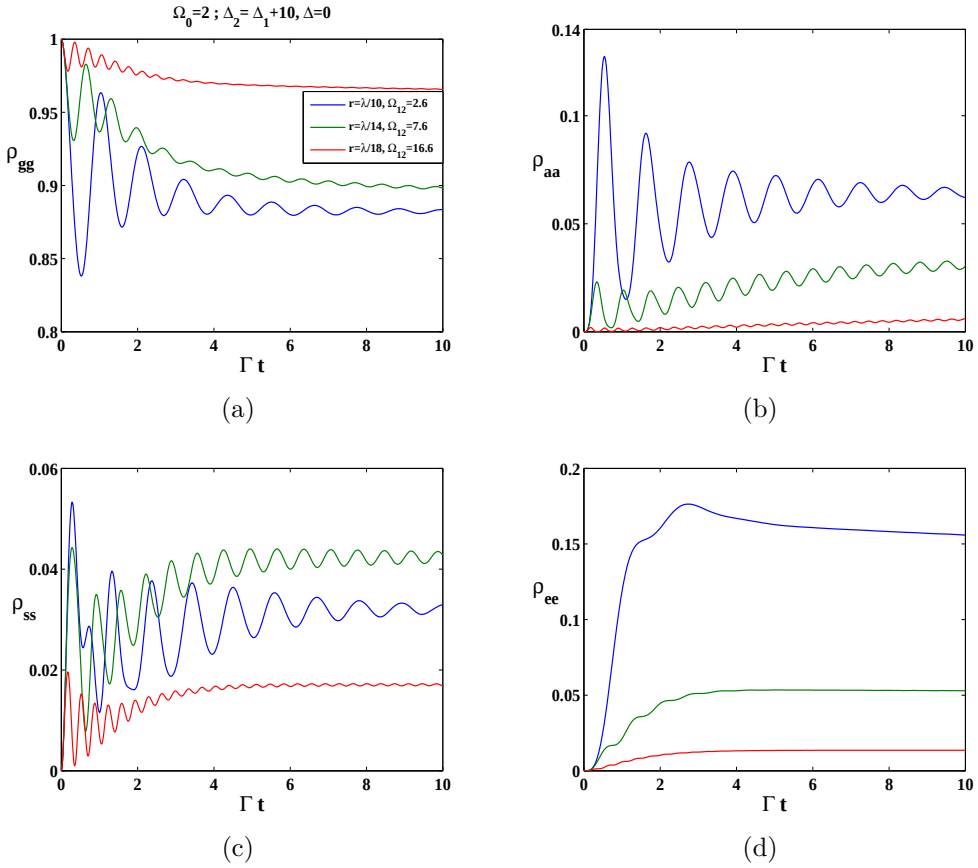

Figure 2-6: *Level populations for non-identical atoms* 2-10(a) ρ_{gg}, 2-10(b) ρ_{aa}, 2-10(c) ρ_{ss} and 2-10(d) ρ_{ee} corresponding to inter-atomic distances of $r = \frac{\lambda}{10}, \frac{\lambda}{14}$ and $\frac{\lambda}{18}$.

state population ρ_{gg}, starting from its initial value of 1, exhibits rapid oscillations, the frequency of oscillations increasing with increased D-D interaction strength. With increase in D-D coupling strength, the steady state value also increases, which is a clear manifestation of dipole blockade. As time progresses, the population ρ_{aa} reaches a steady state. Unlike the case of identical atoms, in this case, the symmetric state is poorly populated. A careful look at the equations of motion (2.9) shows that for the non-identical atoms, there is a non-vanishing coupling between the symmetric and antisymmetric states (ρ_{as}) which is absent for the identical atoms, resulting in decoupling of the

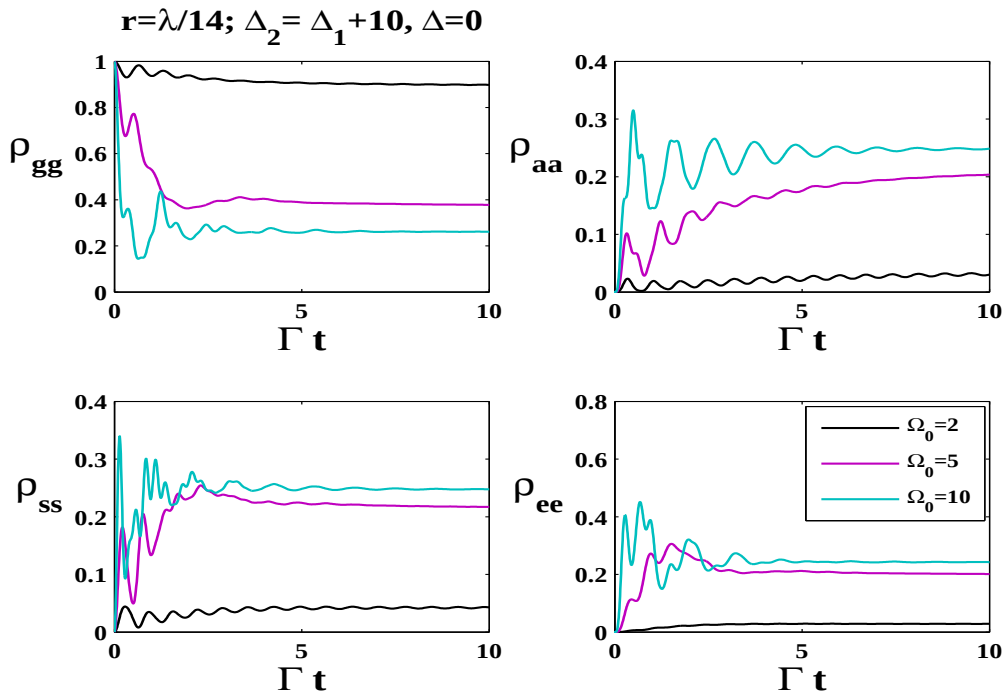

Figure 2-7: The dynamical evolution of level populations of non-identical atoms for different Rabi frequency strengths Ω_0= 2 (black line), 5 (magenta line), 10 (cyan line) when $r = \frac{\lambda}{14}$.

antisymmetric state and the triplet state. The changes in behaviour of the different populations can be largely attributed to this feature.

In the limit of small inter-atomic separation $r = \frac{\lambda}{18}$, the ground state is most populated, as a consequence of which the populations of excited states are close to zero. The number of oscillations increase with increase of Ω_{12}. However, for a strong driving field ($\Omega_0 > 2$), the effect of Ω_{12} on populations is almost insignificant and the excited states get more populated (shown in the figure 2-7). This clearly shows that there is a competing effect between the Rabi field strength and the D-D coupling. From the above analysis, one clearly sees that for a given value of D-D coupling strength, there is a cross-over value of the Rabi frequency on either side of which the system shows

markedly different behaviour.

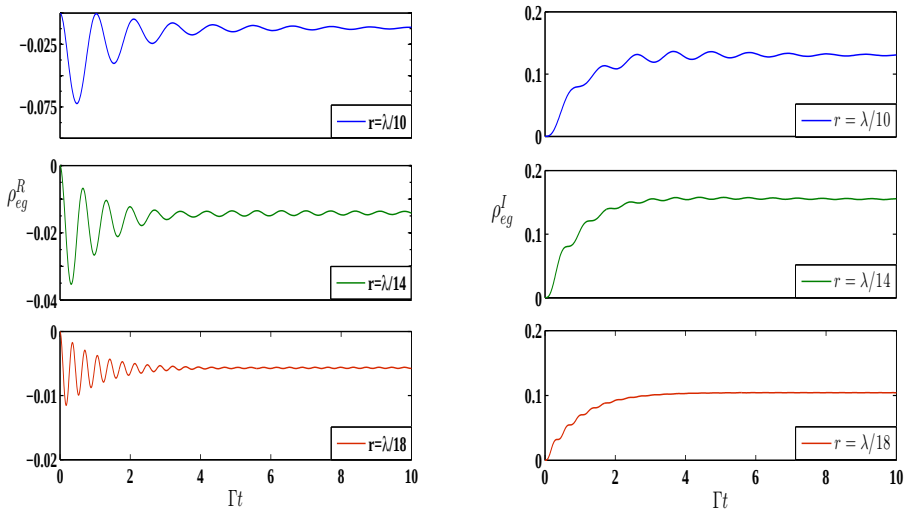

(a) (b)

Figure 2-8: *Two photon coherence ρ_{eg} for non-identical atoms* 2-8(a) $Re(\rho_{eg})$ and 2-8(b) $Im(\rho_{eg})$ corresponding to inter-atomic distances of $r = \frac{\lambda}{10}, \frac{\lambda}{14}$ and $\frac{\lambda}{18}$.

The real and imaginary parts of two photon coherence ρ_{eg} are plotted for non-identical atoms in two adjacent frames in figure 2-8. The real part of (ρ_{eg}) increases with increase in Ω_{12}. The number of oscillations increase in time with increase in Ω_{12} and the amplitude of the oscillations decreases as the time elapses. Unlike in the case of identical atoms, the imaginary(ρ_{eg}) of non-identical atoms first increases and then decreases with increase in Ω_{12}. This again demonstrates clearly the competing interplay of the Rabi field and the D-D interaction strength. In other words, fixing the dipole coupling strength, the two-photon absorption can be tuned by varying the Rabi field strength.

The above detailed analysis clearly shows that D-D coupling strongly influences the behaviour of population of both the single atom excited states as well as two-atom excited state. Further, it is seen that the modification in the

populations is quite different depending on whether the atoms are identical or otherwise. Another noteworthy feature is the decrease in the two atom excitation probability, associated with increase in the dipole coupling strength, common to both identical as well as non-identical atoms. This is due to the inhibition of simultaneous excitation of two atoms due to the D-D coupling which is also referred to as 'dipole blockade'. This feature is further studied in the next section, in the context of the steady state behaviour of the system.

2.4 Steady state analysis: Two two-level atoms

Taking the Laplace transform of the equation (2.10) in the limit $t \to \infty$, the steady state solution of the density matrix elements is obtained as

$$\Psi(t \to \infty) = \lim_{z \to 0} z\hat{\Psi}(z) = -M^{-1}\Phi \tag{2.13}$$

As the focus here is on the steady state behaviour of the two-atom system, we present numerical results of different quantities, both for identical as well as non-identical atoms, in the next section.

2.4.1 Results and Discussion

2.4.1.1 Identical atoms

For the case of identical atoms, it is found that the singlet antisymmetric state $|a\rangle$ acts as a dark state or a trapping state. This is so because the atomic coherences between this state and the rest of the triplet states are always found to be equal to zero. In this case, it is observed that the height of the central peak steadily decreases with an increase in the dipole coupling strength. Some

representative values of the parameters are chosen to demonstrate this feature in figure 2-9, in which each of the sub-figures corresponds to a different value of the inter atomic spacing which in turn defines the dipole coupling strength. For example, the steady state level populations which are plotted in figure 2-9(a)-2-9(d), show the behaviour for three values of $r = \frac{\lambda}{10}, \frac{\lambda}{14}, \frac{\lambda}{18}$.

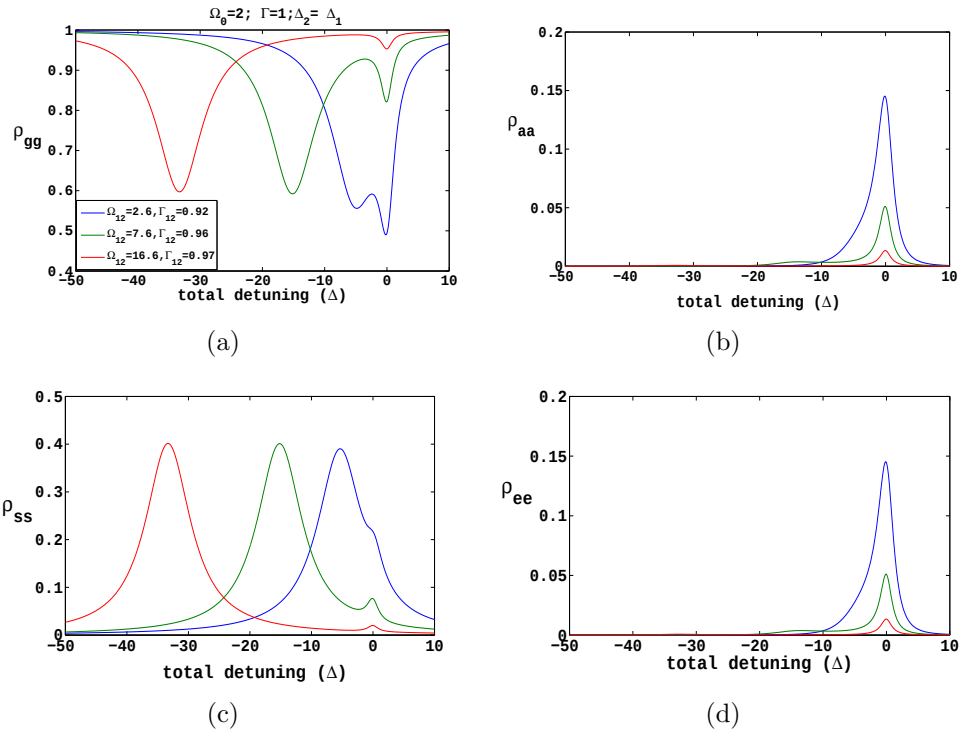

Figure 2-9: *Steady state level populations for identical atoms* 2-9(a) ρ_{gg}, 2-9(b) ρ_{aa}, 2-9(c) ρ_{ss} and 2-9(d) ρ_{ee} corresponding to inter-atomic distances of $r = \frac{\lambda}{10}, \frac{\lambda}{14}$ and $\frac{\lambda}{18}$.

For a non zero D-D interaction, the two-atom system has resonances at $\Delta = 0$ and $-2\Omega_{12}$ (here the peak position depends on the choice of detuning, for example we define detuning as $\Delta_i = \omega_L - \omega_i$, $i = 1, 2$ then the two peaks occur at $\Delta = 0$ and $2\Omega_{12}$). At $\Delta = -2\Omega_{12}$, only the ground and symmetric states [cf. Figures 2-9(a), 2-9(c)] are significantly populated. With the increase of Ω_{12} the side peaks of ρ_{gg} and ρ_{ss} are saturated. Lack of a corresponding side

peak in ρ_{ee}, shown in Figure 2-9(d), can be understood from the fact that the alternate pathways for stepwise excitation $|g\rangle \rightarrow |s\rangle \rightarrow |e\rangle$ and $|g\rangle \rightarrow |a\rangle \rightarrow |e\rangle$ are both inhibited. The central resonance peak at $\Delta = 0$ in ρ_{ee} results from a simultaneous excitation of both atoms ($|g\rangle \rightarrow |e\rangle$) which is termed as the two-photon resonance [12]. The resonances in other intermediate state populations at $\Delta = 0$ can be interpreted as arising from subsequent decay from $|e\rangle$ to these states. With increasing Ω_{12}, the value of the resonant peak at $\Delta = 0$ identically decreases for all the excited states, i.e., inhibition of two photon resonance due to the D-D interaction. A careful inspection of the behaviour of populations reveals that the step-wise excitation is more inhibited than the direct excitation.

2.4.1.2 Non-identical atoms

The steady state level populations for the case of non-identical atoms, as a function of the total detuning Δ, are presented in figure 2-10. When there is no interaction between the atoms ($\Omega_{12} = 0$), the level populations of two non-identical atoms show two peaks of equal amplitude and the peak positions are symmetric about $\Delta = 0$ (not shown in figure 2-10). In this case, the two two-level systems act as two independent two-level atoms. For $\Omega_{12} \neq 0$, there are three resonance dips in ρ_{gg} for this condition, each dip mirrored by a corresponding peak in ρ_{ss} and ρ_{aa}. The level population ρ_{ee} also shows this mirroring with two side peaks of small amplitude, indicating a step wise excitation of both the atoms, which was very strongly blocked for the case of identical atoms. As the Ω_{12} increases, the height of the right dip/peak of ρ_{gg}/ρ_{ss} decreases and the dip/peak width becomes sharper, where as the height of the left dip/peak of ρ_{gg}/ρ_{ss} is greatly increased. Moreover, the

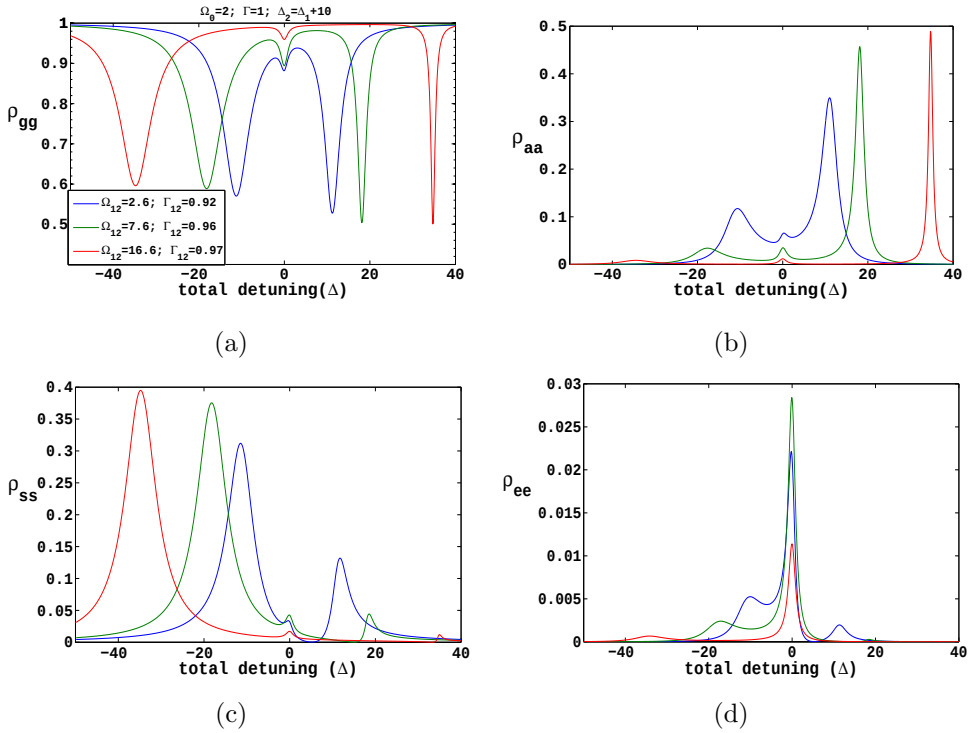

Figure 2-10: *Steady state level populations for non-identical atoms* 2-10(a) ρ_{gg}, 2-10(b) ρ_{aa}, 2-10(c) ρ_{ss} and 2-10(d) ρ_{ee} corresponding to inter-atomic distances of $r = \frac{\lambda}{10}, \frac{\lambda}{14}$ and $\frac{\lambda}{18}$

positions of side peaks/dips depend upon the eigenvalues of the Hamiltonian H. From the eigenvalue analysis (shown in figure 2-11), the positions of the side bands are given as $\Delta = 2\sqrt{|\Omega_{12}|^2 + \delta^2/4}$ and $-2\sqrt{|\Omega_{12}|^2 + \delta^2/4}$, where $\delta = \Delta_2 - \Delta_1$. The eigenvalues respectively are $\frac{\Delta}{2}, -\frac{\Delta}{2}, \pm\sqrt{|\Omega_{12}|^2 + \delta^2/4}$. The positions of the side peaks can be ascertained from the difference between the Ω_{12} dependent eigenvalues.

Unlike the behaviour exhibited in the case of identical atoms, for the non-identical atoms, one observes the presence of side bands in ρ_{ss}, ρ_{gg} as well as in ρ_{aa}. The corresponding side bands in ρ_{ee} are of small amplitude, indicating a reduced degree of inhibition of stepwise excitation in this case.

The central peak at $\Delta = 0$, which corresponds to simultaneous two-atom

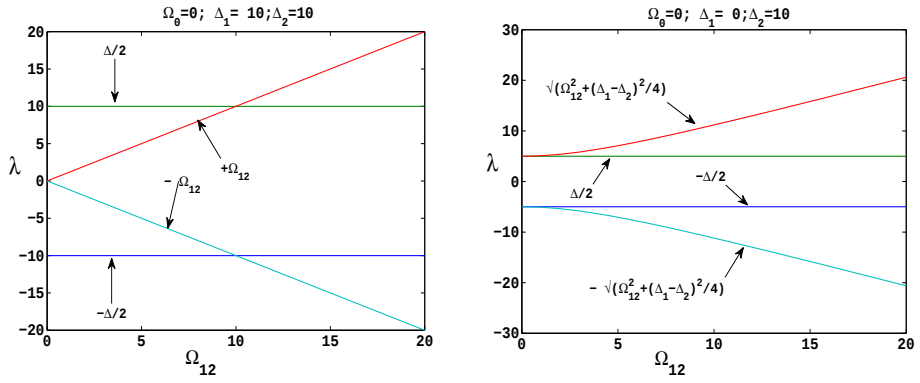

(a) (b)

Figure 2-11: *Eigenvalue spectrum for* 2-11(a) identical atoms 2-11(b) non-identical atoms.

excitation, shows very interesting behaviour. As Ω_{12} is increased, the height of the peak initially increases and further increase in Ω_{12} gives rise to a decrease in the peak height. Varada and Agarwal [12] have calculated the probability for direct two-photon resonance, for non-identical atoms, and have shown that this resonance is not present when $\Omega_{12} = 0$. It has to be noted that in our case the central peak in ρ_{ee} is a result of the combined effect of the population that can reach the state $|e\rangle$ through a stepwise excitation as well as direct excitation of the two atoms, which is obtained from a full density matrix calculation. Hence in our case, we notice the presence of the central peak even in the absence of Ω_{12}.

The reasons for the increase and subsequent decrease in the peak height, as the D-D interaction strength is continuously increased, are not obvious from the above analysis. However, looking at the eigenvalue evolution [cf. Figure 2-11], one can say that Ω_{12} causes a shift of the energies of the levels $|s\rangle$ and $|a\rangle$. A critical value of Ω_{12}, say $\Omega_{12}(c)$, exists such that, at this D-D coupling strength, the shifted energies of $|s\rangle$ and $|a\rangle$ become equal to that as seen in the

case of identical atoms. In other words, the non-identical nature of the atoms is compensated by the energy shifts due to this $\Omega_{12}(c)$. Further increase in the value of Ω_{12} beyond this critical value, will show a decrease in the central peak height of ρ_{ee}, same as the feature seen in the case of identical atoms.

In order to obtain a parametric relation for this critical value $\Omega_{12}(c)$, computations were carried out for a wide range of parameters. From a careful analysis of the data thus obtained, it is inferred that $\Omega_{12}(c)$ is given by $\frac{\Delta_2-\Delta_1}{2}$. The choice of the values of Ω_{12} in the figure is made such that this effect can be clearly demonstrated for the chosen values of the other parameters, in particular $\Delta_2 - \Delta_1 = 10\Gamma$. For example, one can clearly see the increase in the central peak height of ρ_{ee} [cf. Figure 2-10(d)], as Ω_{12} is increased from 2.6 (blue online) to 7.6 (green online) (corresponding to the range below $\Omega_{12}(c)$). The third value 16.6 (red online) is chosen to be greater than $\Omega_{12}(c)$, where the decrease in the central peak height is clearly seen.

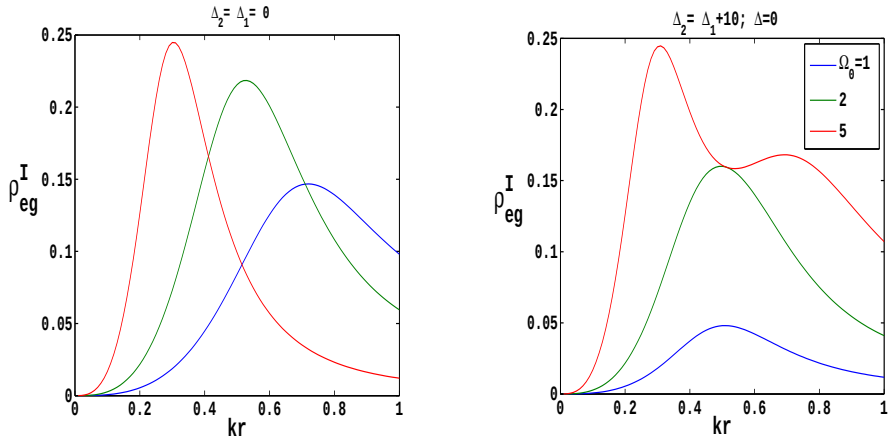

(a) (b)

Figure 2-12: *The atomic coherence Im (ρ_{eg})* on resonance for 2-12(a) identical atoms 2-12(b) non-identical atoms.

Further insight into the behaviour of this central peak can be obtained by

looking at the atomic coherence ρ_{eg}. In the next figure 2-12 the imaginary part of the atomic coherence ρ_{eg} at the line centre ($\Delta = 0$) is plotted, as a function of kr, for three values of Rabi field strength Ω_0. From the figure it is observed that the parameters Ω_0 and Ω_{12} seem to have competing effect on the behavior of the atomic coherence ρ_{eg}. The behaviour of ρ_{eg} is suggesting that there is an optimal combination of Ω_0 and Ω_{12} for which the function is attaining its maximum value. For higher values of the Rabi field strength one notices that the pattern of increase, decrease and a second increase, as evident from the two peaks in $Im(\rho_{eg})$ is similar to the behaviour exhibited by the central peak of ρ_{ee}. The small differences in the detail here can be attributed to the fact that the central peak in ρ_{ee} is a result of all the pathways of excitation put together whereas the atomic coherence ρ_{eg} is a two-photon coherence.

2.5 Steady state entanglement in two two-level atoms

Entanglement is a property of atomic ensembles, which is to exhibit correlations, that cannot be accounted for classically. Entangled state of a composite quantum system, which cannot be written as a product of the states of the individual subsystems [23], are of fundamental interest in quantum mechanics. It has been realized that the quantum entanglement can have many practical applications, ranging from quantum information processing [24], teleportation, cryptography [25], quantum computing [26] and to other tasks in quantum technology [27–30]. Two-level system, which is a prototype qubit system, is the smallest and simplest composite system that can display entanglement. It

is, therefore, the most suitable model to investigate the entanglement characteristics as well as how these properties are influenced by external field and spontaneous decay [31], which is a key point for quantum applications. In the next subsection, we investigate the entanglement characteristics of two two-level atoms interacting with a monochromatic radiation field, in the presence of D-D interaction.

2.5.1 Concurrence

For many problems in quantum information theory it is necessary to know whether a state of a quantum system is entangled or separable. To assess how much entanglement is stored in a given quantum system and how this entanglement changes with environmental effects, it is essential to have a knowledge of proper measures of entanglement. Several different measures of entanglement have been proposed to identify entanglement between two atoms. These include the entanglement of formation, the entanglement of distillation [32], relative entropy [33], negativity [34] and the concurrence [35, 36], an entanglement measure defined by Wootters, which is studied in the current work. Concurrence has been defined originally for a system of two qubits, represented in a standard basis (2.3), described by the density matrix of the form,

$$\rho_X = \begin{bmatrix} \rho_{11} & 0 & 0 & \rho_{14} \\ 0 & \rho_{22} & \rho_{23} & 0 \\ 0 & \rho_{32} & \rho_{33} & 0 \\ \rho_{41} & 0 & 0 & \rho_{44} \end{bmatrix} \tag{2.14}$$

For such a composite system, the concurrence C is defined as

$$C = max\{0, \sqrt{\lambda_1} - \sqrt{\lambda_2} - \sqrt{\lambda_3} - \sqrt{\lambda_4}\} \tag{2.15}$$

where $\{\sqrt{\lambda_i}\}, i = 1, 2, 3, 4$, are the square roots of the eigenvalues, in decreasing order, of the non-Hermitian matrix $R = \rho\tilde{\rho}$ with

$$\tilde{\rho} = \sigma_y \otimes \sigma_y \rho^* \sigma_y \otimes \sigma_y \tag{2.16}$$

where σ_y is the Pauli matrix. The range of concurrence is from 0 to 1, 0 corresponding to the unentangled (separated) atoms, while 1 refers to the maximally entangled atoms.

The matrix needed for calculation of the concurrence has the form

$$\tilde{\rho} = \begin{bmatrix} \rho_{44} & 0 & 0 & \rho_{14} \\ 0 & \rho_{33} & \rho_{23} & 0 \\ 0 & \rho_{32} & \rho_{22} & 0 \\ \rho_{41} & 0 & 0 & \rho_{11} \end{bmatrix}$$

and the square roots of the eigenvalues of the matrix R $(= \rho\tilde{\rho})$ are given by

$$\{\sqrt{\lambda_i}\} = \{\sqrt{\rho_{11}\rho_{44}} - |\rho_{14}|, \sqrt{\rho_{11}\rho_{44}} + |\rho_{14}|, \sqrt{\rho_{22}\rho_{33}} - |\rho_{23}|, \sqrt{\rho_{22}\rho_{33}} + |\rho_{23}|\}.$$

The concurrence is thus given by

$$C = max\{0, C_1, C_2\} \tag{2.17}$$

with

$$C_1 = 2(|\rho_{14}| - \sqrt{\rho_{22}\rho_{33}}); \quad C_2 = 2(|\rho_{23}| - \sqrt{\rho_{11}\rho_{44}}). \tag{2.18}$$

We have two alternative expressions for the concurrence and the convention is to choose the one which is positive. In this study, we wish to examine the steady state properties of the concurrence in the presence of D-D coupling and driving field. In this case a general state of the system is a mixed state, described by the density operator

$$\rho_{AB} = \begin{bmatrix} \rho_{gg} & \rho_{ga} & \rho_{gs} & \rho_{ge} \\ \rho_{ag} & \rho_{aa} & \rho_{as} & \rho_{ae} \\ \rho_{sg} & \rho_{sa} & \rho_{ss} & \rho_{se} \\ \rho_{eg} & \rho_{ea} & \rho_{es} & \rho_{ee} \end{bmatrix} \tag{2.19}$$

As the equations of motion for the density matrix elements (2.19) are too cumbersome for an analytical solution, due to the coupling between the populations and coherences, we study numerically the evolution of the density matrix elements, from which we compute the concurrence in the steady state, both for identical and non-identical atoms.

2.5.2 Results and Discussion

In this sub-section, we present numerical results for the concurrence of a system of two two-level atoms, for various values of kr and Ω_0 in the region of validity of dipole approximation ($kr < 1$). Three dimensional plots of the two-photon excited state population ρ_{ee} are presented in figure 2-13 and the corresponding concurrences are presented in figure 2-14. In the case of identical atoms, for a given value of Ω_0, the concurrence peaks at a specific value of kr.

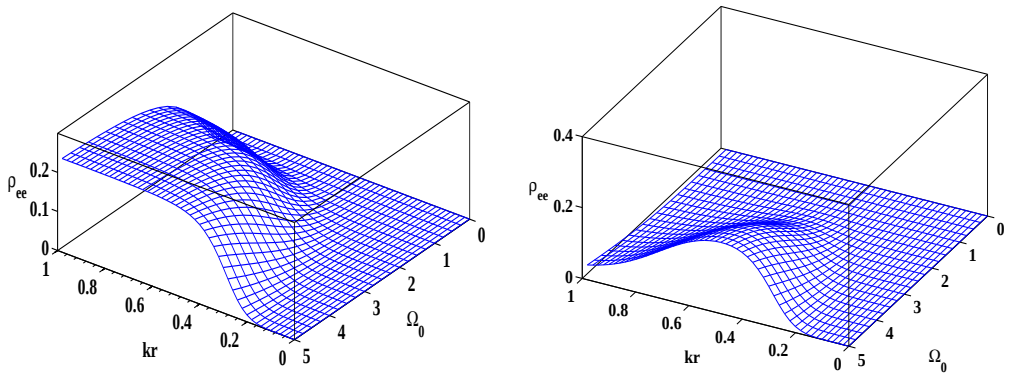

(a) (b)

Figure 2-13: *Steady State* ρ_{ee} *for the case of* (a) identical atoms (b) non-identical atoms

For all other values of kr, concurrence is minimum, and, in addition, is equal to zero whenever $\Omega_{12} < \frac{\Omega_0^2}{2}$. For non-identical atoms, the concurrence shows a more complex behaviour as is clear from figure 2-14(b).

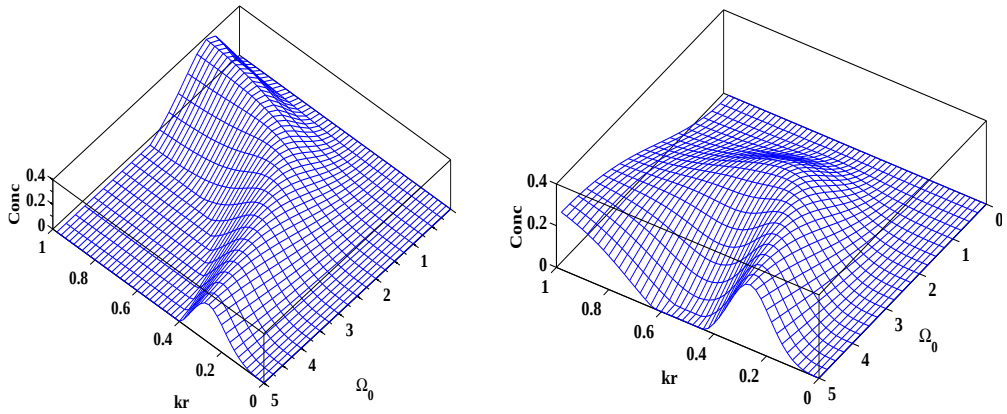

(a) (b)

Figure 2-14: *Steady State concurrence for the case of* (a) identical atoms (b) non-identical atoms

For moderate values of Ω_0, as kr is increased from 0 to 1, concurrence gradually increases. For higher values of Ω_0 (4 and above), there is a region of kr in which the concurrence goes to zero and remains zero, which can be

interpreted as entanglement sudden death (ESD). Further increase of kr for the same range of Ω_0 exhibits non zero concurrence, which on the same token can be understood as entanglement re-birth (ERB).

In summary, a careful inspection of figures 2-13 and 2-14 clearly shows that the parameter zones where dipole-blockade is maximized, which is same as decrease in the line-center population ρ_{ee}, are the same regions where concurrence is maximum. This is understandable because presence of dipole blockade is also an indicator of entanglement. From the results of figure 2-13, we can infer that the two-atom excitation depends upon two parameters, the Rabi coupling strength Ω_0 and the D-D interaction Ω_{12}. There is a competing effect with respect to how these two parameters affect simultaneous excitation of both atoms. The eigenvalue evolution with respect to Ω_{12} is linear in case of identical atoms and non-linear in case of non-identical atoms [cf: figure 2-11]. This appears surprising at first since for this particular case, we assume the same Ω_0 for both atoms even when they are non-identical. But the fact is that resonant two-atom excitation happens at $\Delta = 0 = \Delta_1 + \Delta_2$. This implies that effective coupling ratio Ω_0/Δ_1 for one atom differs from the Ω_0/Δ_2 for the other, which leads to different couplings. This strongly suggests that each atom has a set of values for Ω_0, Ω_{12} and Δ at which the probability of excitation is maximum. However, this is different from the value at which probability for both atoms getting excited together is maximum.

The study presented here quantifies the relationship between dipole blockade and entanglement. These quantitative connections between different atomic properties, presented here from a detailed analysis of the entanglement characteristics of the system, provide a possible estimate of the combinations of parameters where the system can be exploited.

2.6 Conclusion

In summary, we have explored the behaviour of two two-level atoms, both identical and non-identical in the context of interactions between atoms and the electromagnetic field. We have studied the effect of D-D coupling on level populations and various coherences both in transient and steady state case. The D-D coupling introduces modifications in the populations of single atom excited states as well as two-atom excited state. This modification is different depending on whether the atoms are identical or otherwise. With an increase in the dipole coupling strength, the frequency of oscillations of each of the populations shows an increase, which can be attributed to the change in the photon exchange rate resulting due to the stronger dipolar coupling. Increase in dipole coupling strength is resulting in a decrease in the excited state populations, thus suggesting that D-D coupling is inducing both the atoms to be trapped in the ground state. This is a clear manifestation of dipole blockade, which is nothing but inhibition of simultaneous excitation of two atoms due to increased dipolar coupling. The two photon resonance, which appears in the presence of the dipole coupling strength shows an increase upto certain values of the coupling strength and beyond this critical value, it decreases, thus exhibiting an anomalous behaviour, only for the case of non-identical atoms. However, this anomalous behaviour is observed in the coherence ρ_{eg} both for identical as well as non-identical atoms. This feature can be explained in a simple sense, as being due to different set of parameters Ω_0, Ω_{12} and Δ at which each atom individually has maximum excitation probability, which in turn is different from the probability for simultaneous excitation. Varying any of the parameter will traverse over the probability curve showing a non-monotonic

behaviour. From a detailed analysis of the two-atom excited state population and the concurrence, a qualitative connection between the dipole-blockade and the entanglement is made. To summarise, an attempt has been made, from an extensive analysis of the behaviour of the system, to provide a range of parameter values within which the properties of the atomic system can be manipulated/tuned for applications in say, quantum information processing.

References

[1] W. E. Lamb and R. C. Retherford, Phys. Rev. **72**, 339 (1947).

[2] E. T. Jaynes and F. W. Cummings, Proc. IEEE **51**, 89 (1963).

[3] L. Allen and J.H. Eberly, *Optical Resonance and Two-Level Atoms*, Dover Verlag (1987).

[4] C. Hettich, C. Schmitt, J. Zitzmann, S. Kuhn, I. Gerhardt and V. Sandogdar, Science **298**, 385 (2002); Z. Ficek and S. Swain, *Quantum Interference and Coherence: Theory and Experiments*, Springer series in optical sciences, ISSN 0342-4111 (2004); Z. Ficek and R. Tanás, Phys. Rep. **372**, 369 (2002).

[5] D. F. V. James, Phys. Rev. A **47**, 1336 (1993).

[6] H. T. Dung and K. Ujihara, Phys. Rev. Lett. **84**, 254 (2000); H. Zhao and K. Ujihara, J. Mod. Opt. **53**, 835 (2006).

[7] Z. C. Wang, Q. Wang, Y. S. Zhang and G. C. Guo, Chin.Phys. **14**, 0137 (2005); V. E. Lembessis, A. A. Rsheed, O. M. Aldossary and Z. Ficek, Phys. Rev. A **88**, 053814 (2013); V. E. Lembessis, A. Lyras, A. A. Rsheed, O. M. Aldossary and Z. Ficek, Phys. Rev. A **92**, 023850 (2015).

[8] D. Jaksch, J. I. Cirac, P. Zoller, S. L. Rolston, R. Côté and M. D. Lukin, Phys. Rev. Lett. **85**, 2208 (2000); R. Tanas, Phys. Scr. **T153**, 014059 (2013); Y. Yang, J. Hu and H. Yu, Phys. Rev. A **94**, 032337 (2016).

[9] I. E. Protsenko, G. Reymond, N. Schlosser and P. Grangier, Phys. Rev. A **65**, 052301 (2002); V. Vedral, M. B. Plenio, M. A. Rippin and P. L. Knight, Phys. Rev. Lett. 78, 2275 (1997).

[10] M. Saffman and T. G. Walker, Phys. Rev. A **66**, 065403 (2002); D. Mϕller, L. B. Madsen and K. Mϕlmer, Phys. Rev. Lett. **100**, 170504 (2008); M. Saffman and K. Mϕlmer, Phys. Rev. Lett. **102**, 240502 (2009).

[11] I. I. Ryabtsev, I. I. Beterov, D. B. Tretyakov, V. M. Entin and E. A. Yakshina, Phys. Usp. **59**, 196 (2016); A. Browaeys, D. Barredo and T. Lahaye, J. Phys. B **49**, 152001 (2016).

[12] G. V. Varada and G. S. Agarwal , Phys. Rev. A **45**, 6721 (1992); J. R. R. Leite and C. B. de Araujo, Chem. Phys. Lett. **73**, 71 (1980).

[13] T. Wilk, A. G$\ddot{a}$etan, C. Evellin, J. Wolters, Y. Miroshnychenko, P. Grangier and A. Browaeys, Phys. Rev. Lett. **104**, 010502 (2010).

[14] M. Saffman, T. G. Walker and K. Mlmer, Rev. Mod. Phys. **82**, 2313 (2010); L. Isenhower, E. Urban, X. L. Zhang, A. T. Gill, T. Henage, T. A. Johnson, T. G. Walker and M. Saffman, Phys. Rev. Lett. **104**, 010503 (2010).

[15] S. G. Clark and A. S. Parkins, Phys. Rev. Lett. **90**, 047905 (90).

[16] G. X. Li, K. Allaart and D. Lenstra, Phys. Rev. A **69**, 055802 (2004).

[17] S. Nicolosi, A. Napoli, A. Messina and F. Petruccione, Phys. Rev. A **70**, 022511(2004).

[18] $\ddot{O}$. Cakir, A. A. Klyachko and A. S. Shumovsky, Phys. Rev. A **71**, 034303 (2005).

[19] G. S. Agarwal, L. M. Narducci and E. Apostolidis, Opt. Comm. **36**, 285 (1981).

[20] Z. Ficek, R. Tanas and S. Kielich, Opt. Commun. **36**, 121 (1981).

[21] G. S. Agarwal, *Quantum Optics, Springer Tracts in Modern physics*, Vol 70, sec 6 ed G. Höhler et al, New York: Springer-Verlag (1974).

[22] M. D. Lukin, M. Fleischhauer, R. Cote, L. M. Duan, D. Jaksch, J. I. Cirac and P. Zoller, Phys. Rev. Lett. **87**, 037901 (2001).

[23] R. Horodecki, P. Horodecki, M. Horodecki and K. Horodecki,*Quantum entanglement*, Rev. Mod. Phys. **81**, 865 (2009).

[24] M. A. Nielsen and I. L. Chuang, *Quantum Computation and Quantum Information* (Cambridge University Press), 2000.

[25] A. Ekert, Phys. Rev. Lett. **67**, 661 (1991).

[26] A. Bareno, Contemp. Phys. **37**, 375 (1996).

[27] K. A. Valiev, A. A. Kokin, *Quantum computers: hopes and reality*, Research Center Regular and Chaotic Dynamics, Moscow and Izhevsk (2002).

[28] K. A. Valiev, *Quantum computers and quantum computations*. Phys. Usp. **48**(1), 1 (2005).

[29] L. Amico, R. Fazio, A. Osterloh and V. Vedral, *Entanglement in many-body systems*, Rev. Mod. Phys. **80**, 517 (2008).

[30] T. D. Ladd, F. Jelezko, R. Laflamme, Y. Nakamura, C. Monroe and J. L. ÓBrien, *Quantum computers*, Nature (London) **464**, 45 (2010).

[31] G. W. Gardiner and P. Zoller, Quantum Noise, 2nd ed (Springer-Verlag), (2000).

[32] C. H. Bennett, D. P. DiVincenzo, J. A. Smolin and W. K. Wootters, Phys. Rev. A **54**, 3824 (1996).

[33] V. Vedral and M. B. Plenio, Phys. Rev. A **57**, 1619 (1998).

[34] G. Vidal and R. F. Werner, Phys. Rev. A **65**, 032314 (2002).

[35] S. Hill and W. K. Wootters, Phys. Rev. Lett. **78**, 5022 (1997).

[36] W. K. Wootters, Phys. Rev. Lett. **80**, 2245 (1998).

Chapter 3

Studies on a system of three two-level atoms interacting with a single mode radiation field

In the previous chapter we have studied the effect of D-D interaction on a pair of two-level atoms interacting with a laser field. In the present chapter, we extend our study to a set of three two-level atoms interacting through D-D coupling. When there are more than two atoms, wherein some of them are excited while the others are in their ground states, the D-D interaction acts between the nearest ground-excited atom pairs. Many of the cooperative phenomena that are exhibited by a collection of atoms are manifestations of a coherent sum of these interactions. As a three-body problem, this leads to various effects such as formation of Effimov states [1–3] and/or correlation between those atoms that are not directly interacting with each other mediated by the intermediate atom are some of the phenomena that make the study of these systems worthwhile. Some of the recent works involve trapping of three atoms in microscopic optical tweezers [4–6] and the study of three atoms

in a cavity [7, 8], and of three fermionic atoms which form bipartite Cooper pairs [9]. Results of collisional interaction between three atoms are also experimentally studied [10]. This provides motivation to extend these interactions to many-atom systems.

In recent years, entanglement in multi-atom systems has been studied extensively from the perspective of quantum information processing as well as quantum communication [2, 12]. Two-level atoms, essentially equivalent to qubits or spin-1/2 particles, are ideal candidates for quantum computing and information storage. For the purpose of teleportation [23] and other quantum protocols, maximally entangled three qubit states such as the W-states and the GHZ-states are found to provide information transfer with very high fidelity. This necessitates a detailed study to characterize and quantify the entanglement of a given system or state [14].

In the current work, three coupled two-level atoms, all interacting with the same field, are considered. Inclusion of a third atom opens up multiple ways of arranging them. But we consider two of the simplest and important configurations - a linear chain where all the three atoms are on a single line and a closed configuration, where all three are on the vertices of an equilateral triangle [15]. Any other arrangement would be a simple variation of these two. In the linear (open loop) arrangement, the interaction between two farthest atoms can be neglected whereas in the closed loop arrangement, all three atoms interact with each other with equal strength. Because the atom-atom coupling manifests in different ways in both these configurations, the results for the two configurations are different as discussed in sections 3.3.1 and 3.3.2. We have also investigated the effects of D-D interaction and Rabi field strength on entanglement characteristics of the tripartite system in section 3.4.

3.1 The model

We consider a system of three identical two-level atoms (A, B, C) interacting through bipartite D-D interactions. We will assume in our calculations that these three atoms are coupled to a single mode of the driving field and experience the same phase. There are two configurations in which the three atoms may be arranged. In the first case, the atoms are arranged in a linear array, in which case D-D interactions exist between atoms A and B (Ω_{AB}), between atoms B and C (Ω_{BC}), but no interaction exists between atoms C and A (Ω_{CA}). The second arrangement is in the form of a closed loop, where each of the three atoms interacts with its neighbours. The behaviour of the open-loop (line configuration) case is different from that of the closed loop. The two configurations are shown in figure 3-1(a).

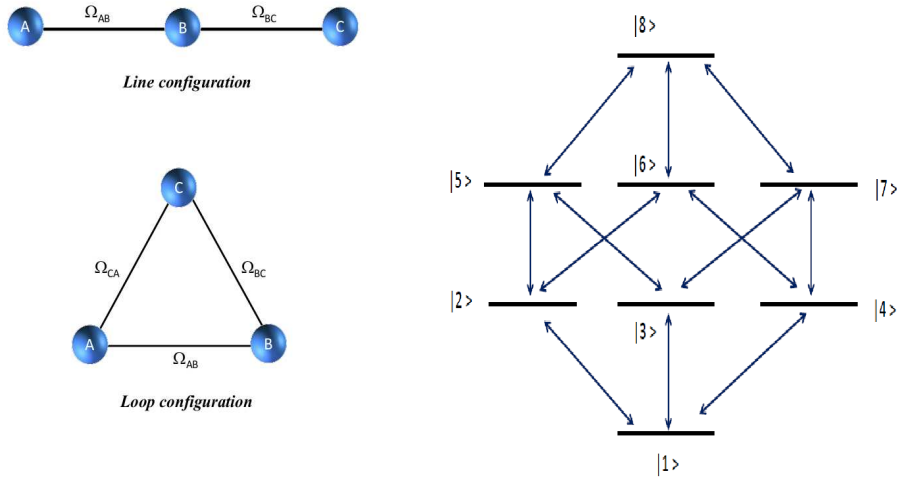

(a) (b)

Figure 3-1: (a) Schematic representation of Line and Loop configurations for three two-level atoms coupled via D-D interaction. (b) The eight energy levels in the combined space. See text for definition of levels $|1\rangle$ - $|8\rangle$.

The energies in the combined space will form a system of eight energy

levels, as shown in figure 3-1(b). Energy level labelled $|1\rangle$ corresponds to $|ggg\rangle$ where all three atoms are in ground state. The three levels wherein any one of the three atoms are excited are $|egg\rangle$, $|geg\rangle$ and $|gge\rangle$, which are all degenerate and are denoted respectively as $|2\rangle, |3\rangle$ and $|4\rangle$. The three levels with two atoms in excited state and one in ground state are $|eeg\rangle$, $|ege\rangle$ and $|gee\rangle$ and are denoted $|5\rangle$, $|6\rangle$ and $|7\rangle$. Finally the state with all three atoms excited is $|eee\rangle$ is denoted $|8\rangle$. Figure 3-1(b) also indicates the relevant laser couplings (blue arrows online) between the levels. This energy level scheme is same for both line (open loop) and closed loop arrangements, except that for the line configuration $\Omega_{CA} = 0$, indicating that there is no dipole dipole interaction between atom C and atom A.

3.2 Formulation

In the dipole approximation, the Hamiltonian for three identical atoms ($\Delta_1 = \Delta_2 = \Delta_3 = \Delta$), including both laser coupling Ω_0 as well as the D-D coupling between different levels is given by

$$H = \begin{bmatrix} -\frac{3\Delta}{2} & -\Omega_0 & -\Omega_0 & -\Omega_0 & 0 & 0 & 0 & 0 \\ -\Omega_0 & -\frac{\Delta}{2} & \Omega_{AB} & \Omega_{CA} & -\Omega_0 & -\Omega_0 & 0 & 0 \\ -\Omega_0 & \Omega_{AB} & -\frac{\Delta}{2} & \Omega_{BC} & -\Omega_0 & 0 & -\Omega_0 & 0 \\ -\Omega_0 & \Omega_{CA} & \Omega_{BC} & -\frac{\Delta}{2} & 0 & -\Omega_0 & -\Omega_0 & 0 \\ 0 & -\Omega_0 & -\Omega_0 & 0 & \frac{\Delta}{2} & \Omega_{BC} & \Omega_{CA} & -\Omega_0 \\ 0 & -\Omega_0 & 0 & -\Omega_0 & \Omega_{BC} & \frac{\Delta}{2} & \Omega_{AB} & -\Omega_0 \\ 0 & 0 & -\Omega_0 & -\Omega_0 & \Omega_{CA} & \Omega_{AB} & \frac{\Delta}{2} & -\Omega_0 \\ 0 & 0 & 0 & 0 & -\Omega_0 & -\Omega_0 & -\Omega_0 & \frac{3\Delta}{2} \end{bmatrix} \tag{3.1}$$

in units of $\hbar$, with the usual notations. For the line (open-loop) configuration, the dipole coupling parameter $\Omega_{CA} = 0$ and for the closed loop configuration,

all the Ω_{ij}s are non zero, where i, j= A, B, C. As a simplest case scenario, all the non zero D-D coupling factors Ω_{ij} and atom-field coupling strength Ω_0, both for the line and closed loop configurations are taken to be equal for computing the dynamics of the system. The master equation for the density operator (2.8), governing the dynamics of the tri-atom system, will give rise to sixty four coupled first order differential equations. As is the usual practice, introducing the completeness condition $\sum_{i=1}^{8} \rho_{ii} = 1$ and eliminating one of the populations, say ρ_{88} in this study, results in a set of sixty three coupled equations, which are solved in steady state, using same idea as outlined in the two-atom case.

Intuitively, it can be noticed that the D-D interaction in case of closed loop configuration is identical among all the atom pairs ($\Omega_{AB} = \Omega_{BC} = \Omega_{CA} = \Omega$). Whereas, in the line configuration, the atom in the middle (atom B) is interacting with two neighbours (A and C) whereas atoms A and C are interacting with only one neighbour(atom B). This lack of equivalence introduces difference in the behaviour of this system as compared to the closed loop system. The results presented in the next section are clearly indicative of this behaviour.

3.3 Numerical Results

3.3.1 Closed Loop configuration

The figure 3-2 shows the steady state populations ρ_{11} to ρ_{88} for the case of three identical atoms arranged in a loop configuration, as a function of total detuning. From this figure, it is observed that the level populations of the three atom system exhibit three peaked structure, with the peaks located at

$\Delta \equiv 0, -(\Omega_{AB} + \Omega_{BC} + \Omega_{CA}), -2(\Omega_{AB} + \Omega_{BC} + \Omega_{CA})$.

When $\Omega = 0$, ρ_{11} shows a single dip at $\Delta = 0$. However, the single excited atom case $\rho_{22} = \rho_{33} = \rho_{44}$ show two small peaks, instead of a single corresponding peak. The dip at the center can not be attributed to dipole blockade since at this point $\Omega = 0$. Instead, it has to be attributed to a loss of population to higher states, where more than one atom is excited. This is evident by the single peak structure seen in the populations $\rho_{55} = \rho_{66} = \rho_{88}$. Unlike the two atom case, it can be noticed that the system of three identical atoms shows different behaviour. Individual probabilities for getting any one of the atoms in the excited state (i.e., $\rho_{22} = \rho_{33} = \rho_{44}$) is equal to 0.14, which adds up to nearly a half of the probability for the three one-atom excited states. On the other hand, the case of any two of the atoms excited is much lower, adding upto 0.24 for all the three states $\rho_{55} = \rho_{66} = \rho_{77}$ combined together. Probability for having all three atoms excited together is even smaller, which is about 0.08 approximately.

Presence of Ω affects the above situation in an interesting way. The dip for ρ_{11} splits into two, with both the lobes shifted to red side of the resonance. This indicates that Ω causes a mixing of the energy levels in such a way as to create two super positions, both shifted closer to each other. The two lobes also have asymmetric widths, with the extreme one becoming broader and stronger as Ω increases. This behaviour is exactly mirrored by the two peaks for one-atom excited state $\rho_{22} = \rho_{33} = \rho_{44}$.

On the other hand, the two-atoms excited state does not exhibit a clear two-lobed structure. It shows a dominant single peak, which is matched at the resonance to the narrower peak of the one-atom excited case. For moderate Ω's, a small bump can be seen at $\Delta = 0$. This is most likely the population

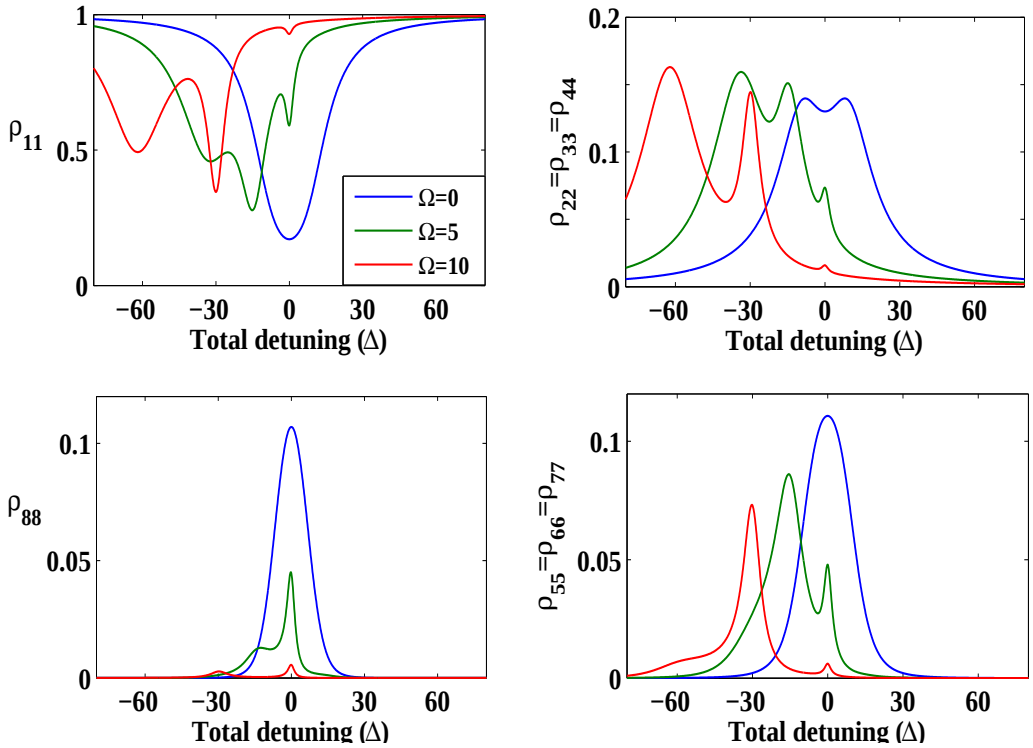

Figure 3-2: Populations for levels $|1\rangle$ to $|8\rangle$ for the loop configuration, for values of $\Omega = 0$ (blue curve), $\Omega = 5$ (green curve) and $\Omega = 10$ (red curve). All curves for Rabi frequency $\Omega_0 = 2$

that has decayed from level $|8\rangle$, which has a peak at $\Delta = 0$. Level $|8\rangle$, which corresponds to all three atoms in excited state has only a sharp peak at the center, with no side bands. The central peak too decreases drastically in height with increasing Ω. This can be interpreted as the presence of dipole blockade in the case of three atoms, wherein the excited atoms prevent other atoms from getting excited. Presence of the third atom indicates that the two-atom dipole blockade is not very effective: one of the atoms is excited once at least. Intuitively, one can then explain the two peaks of ρ_{22}, ρ_{33} and ρ_{44}, and a single side band of ρ_{55}, ρ_{66} and ρ_{77} as follows - the energy shift due to Ω causes two resonances for atomic excitation leading to any one of the three atoms to reach their respective excited states. Once excited, the atom prevents one of

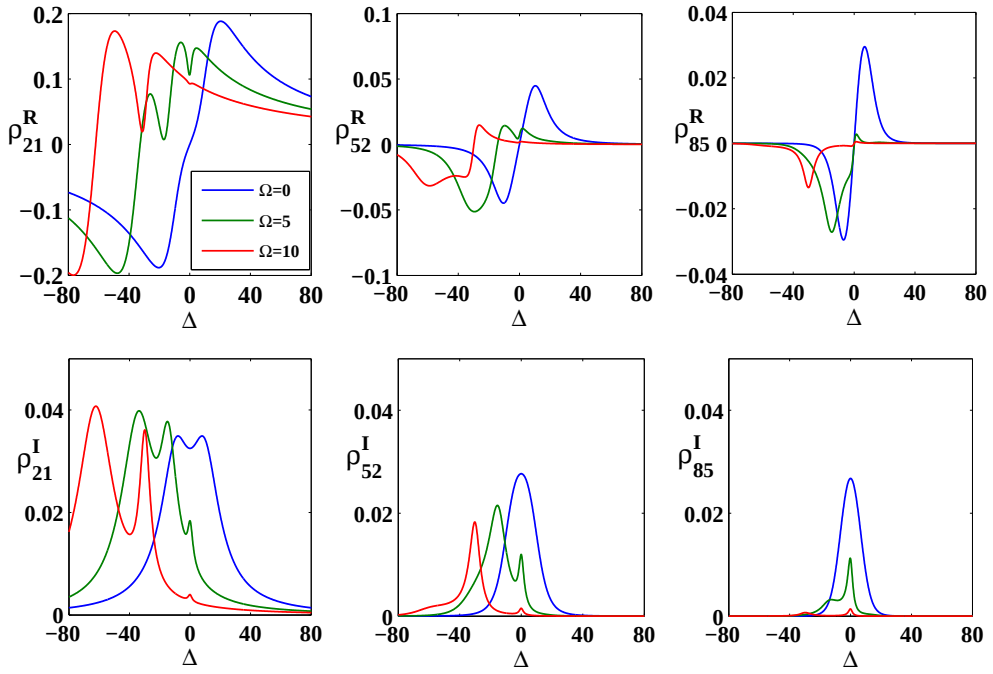

Figure 3-3: Real (row above) and imaginary (row below) part of coherences ρ_{21}, ρ_{52} and ρ_{85} as labelled. For the loop configuration, $\rho_{21} = \rho_{31} = \rho_{41}$. Coherence $\rho_{52} = \rho_{62} = \rho_{53} = \rho_{73} = \rho_{64} = \rho_{74}$ and $\rho_{85} = \rho_{86} = \rho_{87}$.

its neighbours from getting excited, which can be attributed to the absence of broad peak in populations. However, the third atom is not affected drastically by this blockade and gets excited. In other words, the standard dipole blockade prevents only one of the two atoms from getting excited, resulting in two atoms which can get excited.

Imaginary part of coherences, for case of dipole coupled transition, indicate absorption of light. Figure 3-3 shows these coherences for ρ_{21}, ρ_{52} and ρ_{85}. The coherence ρ_{21}, which is also same as ρ_{31} and ρ_{41} for the loop configuration case shows absorption of one photon by one of the atoms to get excited. The populations ρ_{22}, ρ_{33} and ρ_{44} mirror this absorption profile exactly. Similarly, population of two-atom excited states $\rho_{55} - \rho_{77}$ and coherences ρ_{52} (which is also equal to ρ_{53}, ρ_{62}, ρ_{64}, ρ_{73} and ρ_{74}) mirror each other perfectly. Similarly,

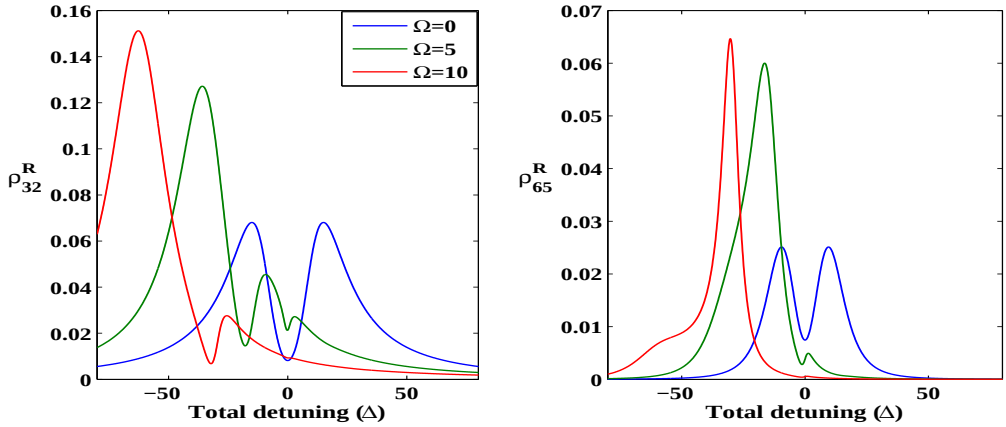

Figure 3-4: Real part of coherences : $\rho_{32} = \rho_{43} = \rho_{42}$ and $\rho_{65} = \rho_{76} = \rho_{75}$ for loop configuration

ρ_{85} (=$\rho_{86} = \rho_{87}$) and the population term ρ_{88} mirror each other. Real parts of coherences ρ_{32} and ρ_{65} are shown in figure 3-4.

3.3.2 Line (Open Loop) Configuration

Line configuration (figure 3-1(a)), shows drastically different results. In this configuration, we label the state which corresponds to the middle, as $|3\rangle$. This means that the D-D interaction couples states $|2\rangle$ to $|3\rangle$ and $|3\rangle$ and $|4\rangle$, but there is no coupling between $|2\rangle$ and $|4\rangle$. Similarly, there is no D-D interaction between states $|5\rangle$ and $|7\rangle$. Obviously, one expects that the populations ρ_{22} and ρ_{44}, which are both coupled to the state $|3\rangle$ through the dipole interaction, show identical behaviour while that of ρ_{33} differs from these two. For similar reasons one expects that ρ_{55} and ρ_{77} would be identical with each other, but different from that of ρ_{66}. The graphs shown in figure 3-5 and 3-6 clearly indicate this expected behaviour.

There are four resonance peaks in one atom excitation, as opposed to two that were present in the loop configuration. A small bump at the line centre

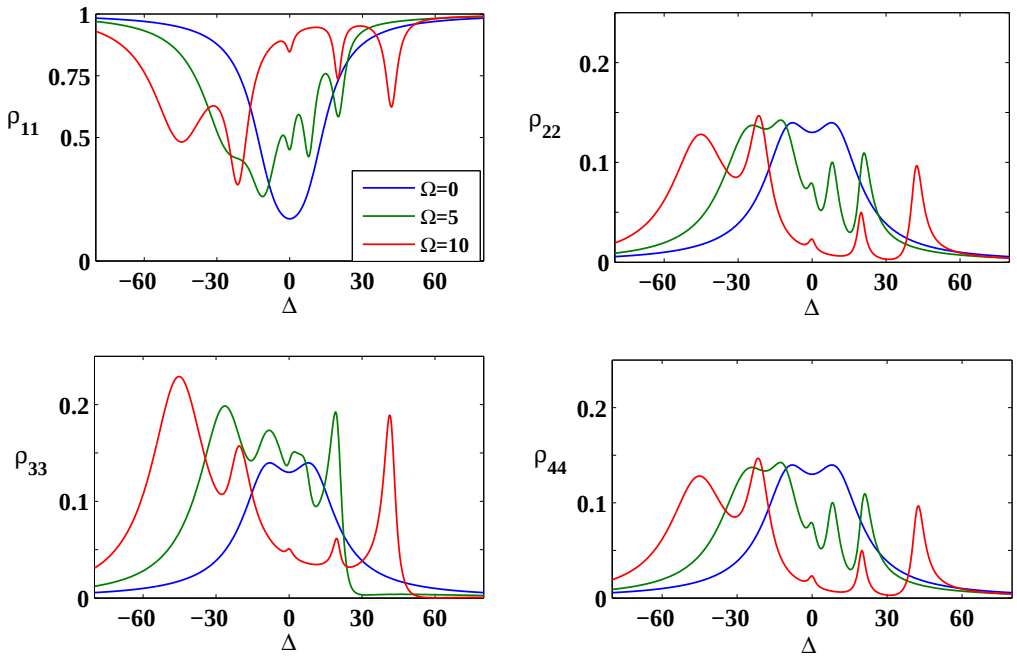

Figure 3-5: Populations for levels $|1\rangle$ to $|4\rangle$ for the line configuration

($\Delta = 0$) can be noticed in all the populations, indicating a three photon resonance. The population ρ_{88}, on the other hand, starts with a single peak for $\Omega = 0$, which splits into three as Ω is increased. The absorption is also strongly suppressed, indicating the presence of dipole blockade. From the above figure, it is observed that the sidebands are located symmetrically on either side of the central line ($\Delta = 0$), the locations of which are given by $\Delta \equiv \pm(\Omega_{AB} + \Omega_{BC}), \pm 2(\Omega_{AB} + \Omega_{BC})$. Figures 3-7, and 3-9 show the corresponding coherences.

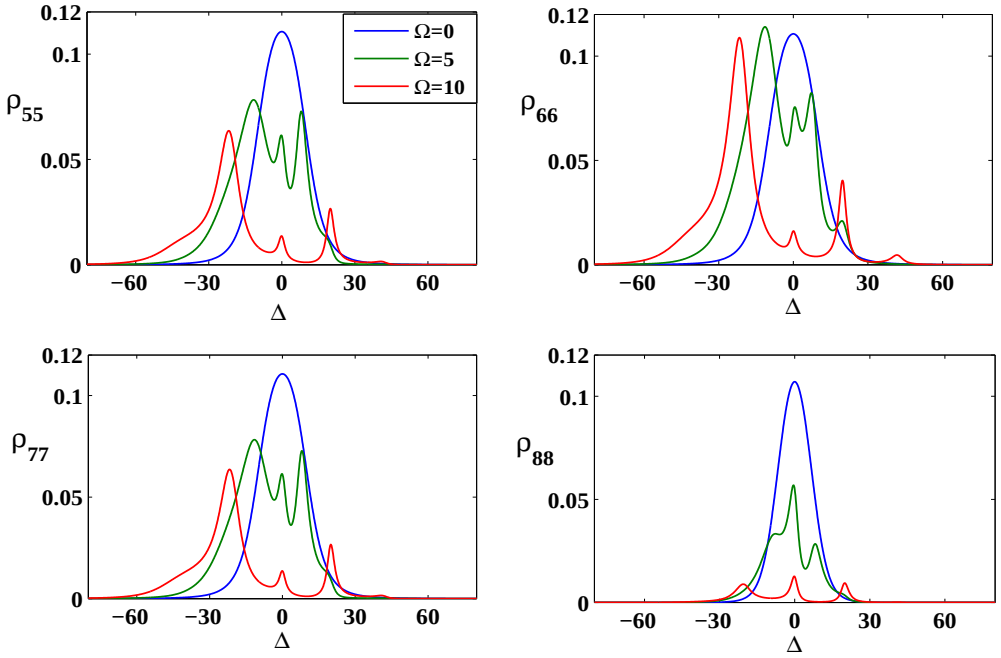

Figure 3-6: Populations for levels $|5\rangle$ to $|8\rangle$ for the line configuration

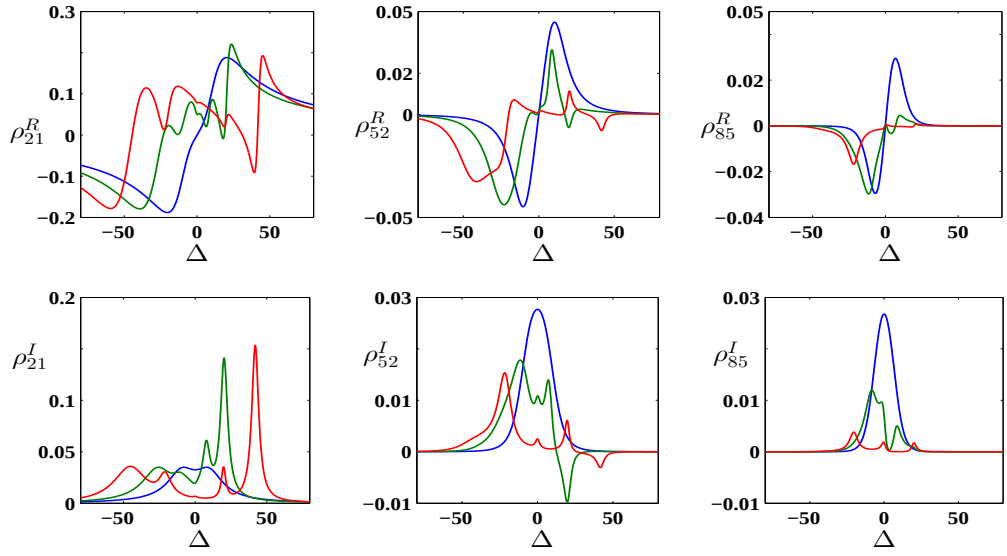

Figure 3-8: The atomic coherences : ρ_{21}, ρ_{52} and ρ_{85} for the line configuration

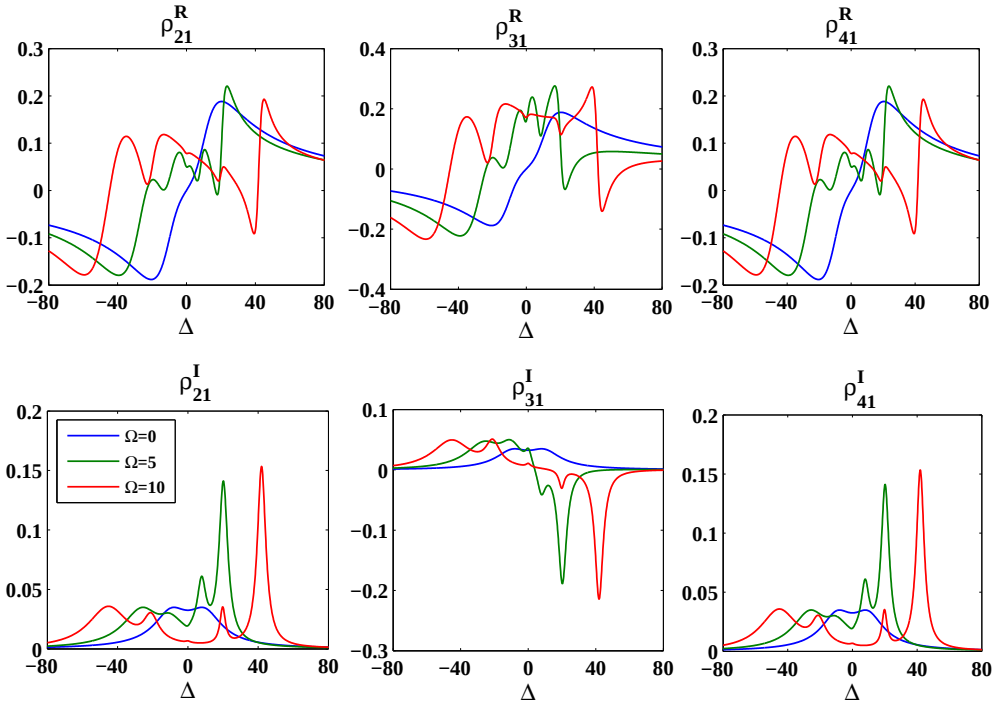

Figure 3-7: One-atom excited state coherences : ρ_{21}, ρ_{31} and ρ_{41} for the line configuration

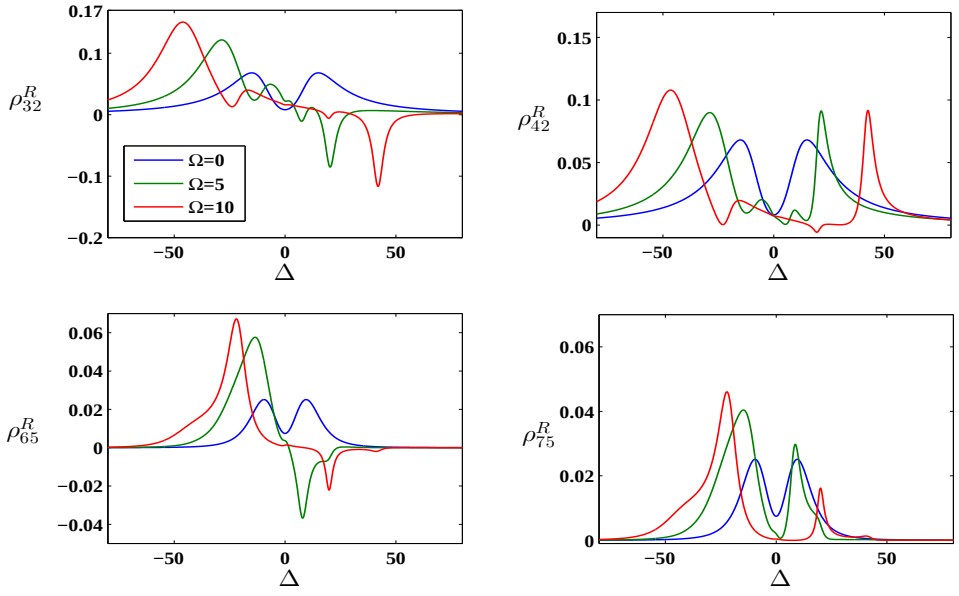

Figure 3-9: Real parts of atomic coherences between one atom excited states $\rho_{32} = \rho_{43}$, ρ_{42} (above) and two atom excited states $\rho_{65} = \rho_{76}$, ρ_{75}.

3.4 Entanglement characteristics of three atoms

In this section, we begin our discussion by considering pure tri-partite states. One can divide the separability/entanglement criterion into three categories, namely fully separable, biseparable or genuine entangled. For instance, a pure state $|\psi\rangle$ is said to be fully separable if it can be written as a tensor product of three pure states, $|\psi\rangle = |\phi_A\rangle \otimes |\phi_B\rangle \otimes |\phi_C\rangle$, biseparable if it is not fully separable but can be written as $|\psi\rangle = |\phi_A\rangle \otimes |\phi_{BC}\rangle$ with $|\phi_{BC}\rangle$ entangled (the index 'A' can denote any of the three subsystems), and fully inseparable (genuine entangled) otherwise.

For the case of mixed states, the classification criterion for separability/entanglement is same as that stated above for the pure tri-partite states. Any three-qubit mixed state ρ is fully separable if it is a convex combination of fully separable pure states. However, biseparable states have three different kinds of bipartite entanglements depending on the partitions. For a system of three qubits, the density operator ρ is separable under partition, of first qubit (say A) from the remaining two qubits (B and C), then it has the form $\rho = |A\rangle \otimes |BC\rangle$, with $|BC\rangle$, an entangled state of the second (B) and the third (C) qubits. This form of biseparable state is denoted as $A|BC$ separable state. Other possible biseparable states are $B|AC$ and $AB|C$. This enables one to define a general biseparable stsate. To summarize this classification criterion, a general biseparable state ρ is also a convex combinations of separable mixed states. On the other, ρ is genuine entangled if it is neither fully separable nor biseparable.

In this study, we investigate steady state entanglement characteristics of three two-level atoms interacting with a single mode radiation field. For this

purpose, we explore a valid measure of tripartite entanglement for a mixed state ρ through a study of negativity [16, 17] defined as

$$N_{ABC}(\rho) = (N_{A-BC} N_{B-AC} N_{C-AB})^{1/3}. \tag{3.2}$$

The tripartite negativity N_{ABC} is the geometric mean of the bipartite negativities, where the bipartite negativities [18–20] are defined as $N_{I-JK} = -2\sum_i \lambda_i(\rho^{T_I})$. Here $\lambda_i(\rho^{T_I})$ are the negative eigenvalues of partially transposed density matrix ρ with respect to subsystem I, denoted by ρ^{T_I}. The relation between elements of ρ^{T_I} and ρ is given by $\langle i_I, j_{JK}|\rho^{T_I}|k_I, l_{JK}\rangle = \langle k_I, j_{JK}|\rho|i_I, l_{JK}\rangle$ with $I = A, B, C$ and $JK = BC, CA, AB$ respectively. Here, N_{A-BC} represents the entanglement between the subsystems B and C and are product with respect to subsystem A. Note that the value $N_{ABC} = 0$ corresponds to separable states and $N_{ABC} = 1$ corresponds to maximally entangled states.

Numerical Results

In this section, we start with a discussion of the results of the entanglement properties of three atoms arranged in a line, as a function of Rabi field strength. In figure 3-10, results are presented for bipartite negativities N_{A-BC}, N_{B-AC} for three different values of D-D coupling strength Ω = 1, 5 and 10. From the figure, it is clearly evident that $N_{A-BC}(= N_{C-AB}) > N_{B-AC}$ and these negativities increase as the dipole coupling strength Ω is increased. Here, one observes that N_{B-AC} (where A and C are the atoms arranged at the two ends of the linear chain), is non zero which implies that quantum entanglement between the end atoms A and C is still present even though they are not

coupled by the dipole interaction. As the strength of the Rabi field increases, the magnitude of $N_{A-BC}(N_{B-AC})$ increases upto its maximum value (less than 0.25) and then starts decreasing and drops to zero, which is referred to as entanglement sudden death (ESD). Thus, there is an optimal value of the Rabi field strength for obtaining maximum bipartite entanglement for a given D-D coupling Ω and this optimal value of the field strength is seen to increase with an increase in Ω.

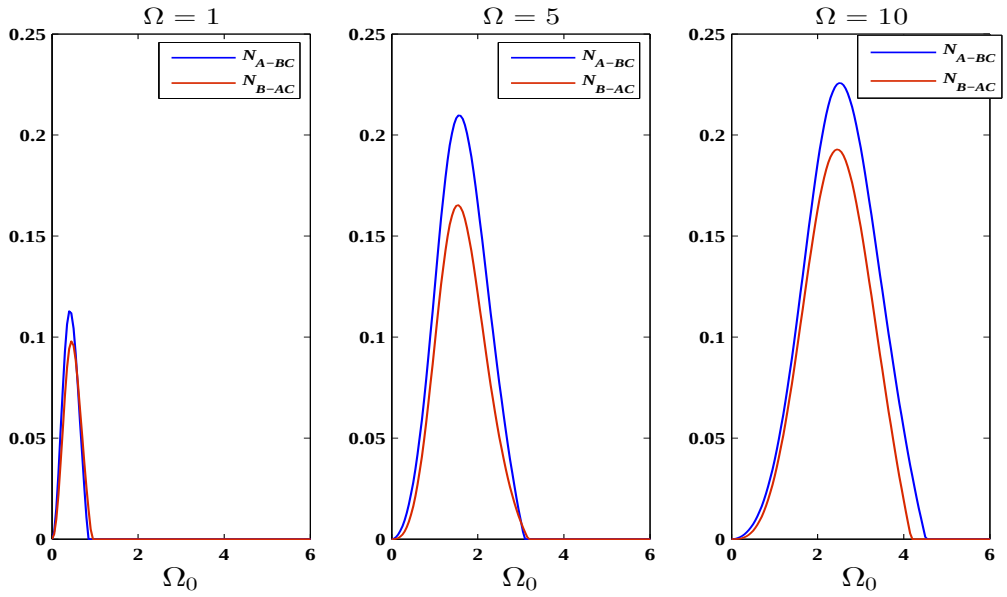

Figure 3-10: Bi-separable negativities for line configuration $N_{A-BC}(= N_{C-AB})$ and N_{B-AC} as a function of applied Rabi field strength Ω_0 for different values of Ω.

For the case of atoms arranged in loop configuration, the overall behaviour of bipartite entanglement, namely the variation as a function of the Rabi field strength for a range of values of the dipole coupling strength, is similar to that observed in the line configuration. Figure 3-11 shows the bipartite negativities for the same parameters as in figure 3-10. It can be observed from figure 3-11 that the bipartite negativity $N_{A-BC}(= N_{B-AC} = N_{C-AB})$ is zero at $\Omega_0 = 0$

and builds up as Ω_0 increases and then decreases to zero showing entanglement sudden death. In addition, with the increase of D-D coupling Ω the bipartite negativity$N_{A-BC}(N_{B-AC})$ shows an increase as a function of the applied field strength.

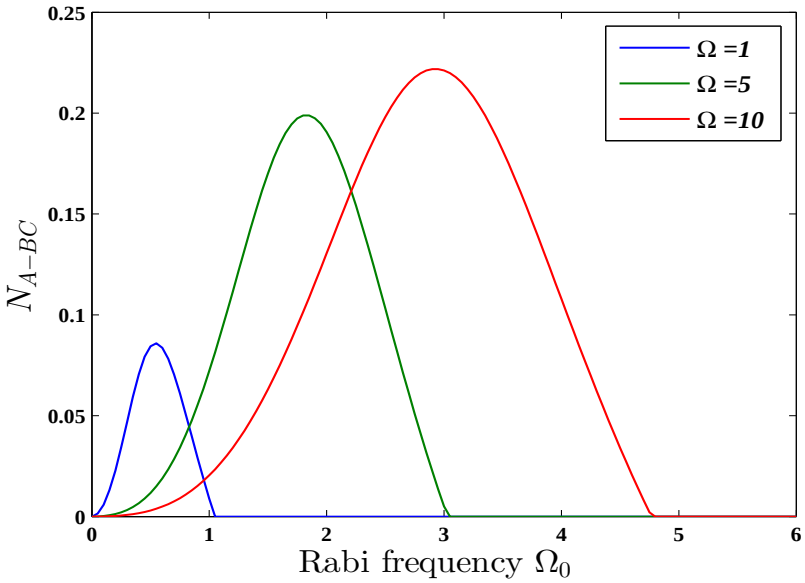

Figure 3-11: Bi-separable negativity for loop configuration $N_{A-BC}(= N_{C-AB} = N_{B-AC})$ as a function of applied Rabi field strength Ω_0 for different values of Ω.

Next, we compare the total entanglement of the system both for line and loop configurations in figures 3-12 and 3-13. As shown in the figure 3-12, the tripartite entanglement N_{ABC} as a function of Rabi field strength for three different values of $\Omega = 1$, 5 and 10 are presented. For weak dipole coupling strength $\Omega = 1$, N_{ABC} for line configuration is more when compared to its counterpart for the loop configuration, while for strong D-D coupling N_{ABC} for the loop configuration is slightly larger than that of the line configuration.

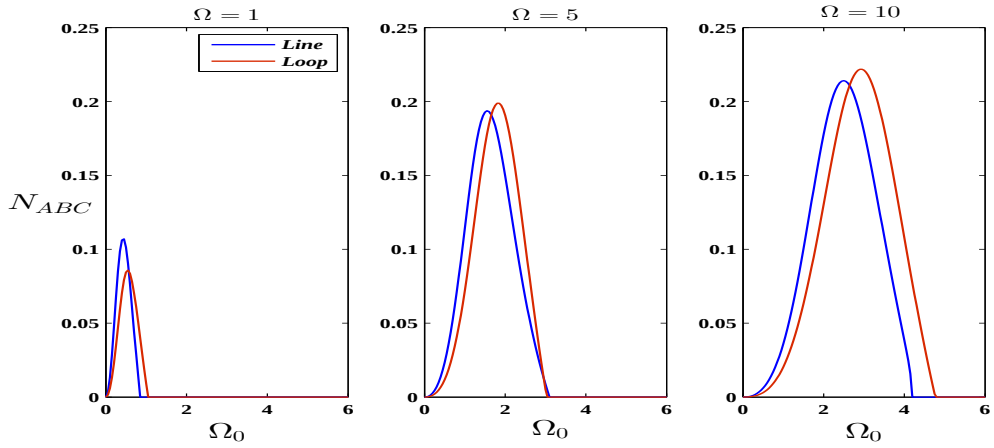

Figure 3-12: Tripartite negativity N_{ABC} as a function of applied Rabi field strength Ω_0 for different values of Ω.

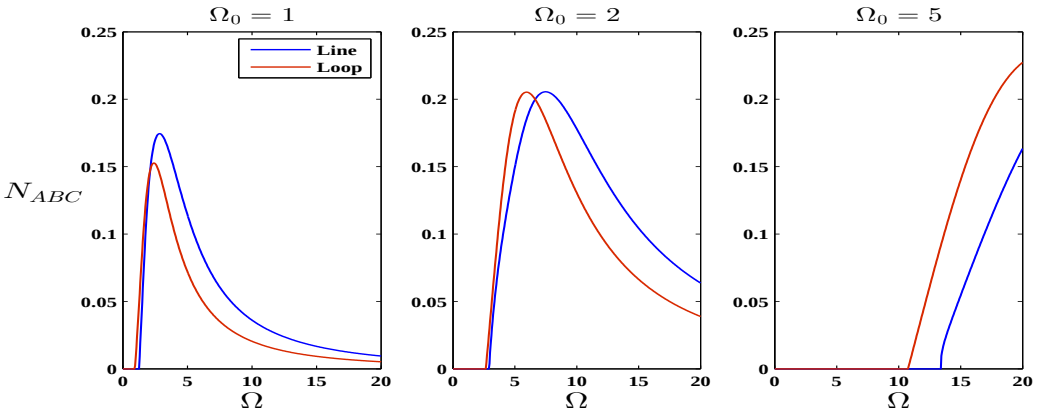

Figure 3-13: Tripartite negativity N_{ABC} as a function of Ω for different values of applied Rabi field strength Ω_0.

Finally in fig 3-13, we compare tripartite negativity for both the line and loop configurations as a function of Ω. It is observed that entanglement birth is delayed for both line and loop configurations. That is, upto a certain value of the dipole coupling strength, the tripartite negativity remains zero and it suddenly attains a non zero value which rises sharply and this phenomenon

also is known by the name entanglement sudden birth. It is clearly seen that the tripartite negativity N_{ABC} can be enhanced by increasing the Rabi frequency and this enhancement is slightly more in case of the loop configuration. A remarkable feature that is observed is that the tripartite negativity N_{ABC} completely vanishes only in the asymptotic limit of large D-D coupling strength.

3.5 Conclusion

In this chapter, we have presented our results for the steady state characteristics of three identical atoms interacting with one another through D-D coupling under an external electromagnetic field. The D-D interaction is represented by a coupling factor Ω between an excited atom and an atom in the ground state. Considering only the nearest-neighbour interaction, we found that the interaction suppresses one of the neighbouring atoms from getting excited but not both. We have studied two possible scenarios in which the three atoms can be present and the results for both these scenarios show different behaviour. Attempts have been made to explain the differences in behaviour of the system under the two cases. Our results on level populations of the three atoms system, both in line and closed loop configurations, are in good agreement with the experimental findings of Barredo et al. [4].

We have also studied the entanglement characteristics of the system both in line and loop configurations. In particular, the bipartite and tripartite negativities as a function of Ω and Ω_0 are discussed. We observe that there is an optimal value of Ω_0 for which the tripartite negativity is maximum and this optimal value increases as a function of the dipole coupling strength. En-

tanglement sudden death is observed both in line and loop configurations. It is shown that the entanglement between the end atoms is still present even though they are not connected directly. For weak interaction strength, tripartite negativity in line configuration is slightly more when compared with loop configuration. But for strong interaction strength, tripartite negativity in loop configuration is slightly higher as compared to line configuration. This study throws light on the entanglement behaviour of the coupled three atom system but further insight can be obtained by refining the study.

References

[1] V. Efimov, Phys. Lett. B **33**, 563 (1970).

[2] V. Efimov, Nuclear Physics A **210**, 157 (1973).

[3] E. Braaten and H. W. Hammer, Annals of Physics **322**, 120 (2007).

[4] D. Barredo, S. Ravets, H. Labuhn, L. Bėguin, A. Vernier, F. Nogrette, T. Lahaye and A. Browaeys, Phys. Rev. Lett. **112**, 183002 (2014); D. Barredo, H. Labuhn, S. Ravets, T. Lahaye and A. Browaeys, Phys. Rev. Lett. **114**, 113002 (2015).

[5] T. Pohl and P. R. Berman, Phys. Rev. Lett. **102**, 013004 (2009).

[6] M. Kiffner, M. Huo, W. Li and D. Jaksch, Phys. Rev. A **89**, 052717 (2014).

[7] G. S. Jin, S. S. Li, S. L. Feng and H. Z. Zheng, Phys. Rev. A **71**, 034307 (2005).

[8] M. Lu, Y. Xia, J. Song and H. Song, J. Phys. B: At. Mol. Opt. Phys. **46**, 015502 (2013).

[9] K. Inaba and S. Suga, Phys. Rev. A **80**, 041602 (2009).

[10] S. A. Abdullah, M. Allegrini, S. Gozini and L. Moi, Nuovo Cimento D **9**, 1467 (1987).

[11] S. Bose, Phys. Rev. Lett **91**, 207901 (2003); S. Khan and M. Jan, Int. J. Theor. Phys. **55**, 1515 (2016); L. Zhai and Y. Zheng, J. Chem. Phys. **144**, 234308 (2016).

[12] A. Streltsov, S. Lee and G. Adesso, Phys. Rev. Lett. **115**, 030505 (2015); A. M. Lance, T. Symul, W. P. Bowen, B. C. Sanders and P. K. Lam, Phys. Rev. Lett. **92**, 177903 (2004).

[13] W. D*ü*r, G. Vidal and J. I. Cirac, Phys. Rev. A **62**, 062314 (2000).

[14] D. D. B. Rao, S. Ghosh and P. K. Panigrahi, Phys. Rev. A **78**, 042328 (2008).

[15] M. Kiffner, W. Li and D. Jaksch, Phys. Rev. Lett. **111**, 233003 (2013); M. Kiffner, M. Huo, W. Li and D. Jaksch, Phys. Rev. A **89**, 052717 (2014).

[16] C. Sab́in and G. Garcia Alcaíne, Eur. Phys. J. D **48**, 435 (2008).

[17] F. Buscemi and P. Bordone, Phys. Rev. A **87**, 042310 (2013).

[18] A. Peres, Phys. Rev. Lett. **77**, 1413 (1996).

[19] P. Horodecki, Phys. Lett. A **232**, 333 (1997).

[20] H. T. Lim, Y. S. Kim, Y. S. Ra, J. Bae and Y. H. Kim, Phys. Rev. Lett. **107**, 160401 (2011).

Chapter 4

Temperature dependent quantum correlations in three two-level atoms

In this chapter, we study the effects of temperature and D-D coupling strength on the entanglement characteristics and quantum correlations of three coupled two-level atoms. It is well known that a knowledge of different measures of entanglement and its distribution over each of the constituent atoms is crucial for tasks such as quantum teleportation [1] and super dense coding [2–4]. Here, the entanglement property of the system is characterized by concurrence [5,6] and the quantum correlations are characterized by quantum discord [7–10]. We investigate the entanglement characteristics of three atoms, considering the two configurations that were proposed in chapter 3, namely in the line as well as loop configurations. It is observed that the entanglement measures exhibit an unexpected, qualitative change when the atoms are arranged in loop configuration, which feature is markedly absent in the line configuration. In particular, we observe an interesting result that any one of

the qubits is indeed entangled with the other two qubits in the system, which are not mutually entangled, for arbitrary values of dipole coupling strengths. We also show that the quantum correlations may be enhanced, upon decreasing the temperature and increasing the dipole coupling strength, both in line and loop configurations.

4.1 Formulation

The Hamiltonian for the system of three atoms (A, B, C) coupled through dipole-dipole interaction is given by

$$H = \omega \sum_{i=A,B,C} S_i^z + \sum_{i \neq j = A,B,C} \Omega_{ij}(S_i^+ S_j^- + H.C)$$

The first term describes the unperturbed energy of the system while the second term represents the dipole-dipole interaction between the atoms, where Ω_{ij}, the dipole dipole interaction strength, is a function of the inter-atomic separation 'd'. In the above, ω is the atomic transition frequency, $S_i^+ = |1\rangle_i\langle 0|$ and $S_i^- = |0\rangle_i\langle 1|$ are the raising and lowering operators of the i^{th} atom. Here, we assume that all the three atoms are identical, i.e., $\omega_A = \omega_B = \omega_C = \omega$ and D-D strength $\Omega_{ij} = \Omega$ for $i \neq j = A, B, C$. For the three atom system, in thermal equilibrium at temperature T, the density matrix can be expressed as

$$\rho_{ABC} = \frac{1}{Z} \sum_{i=1}^{8} |\psi_i\rangle\langle\psi_i| e^{-\beta\epsilon_i}, \tag{4.1}$$

where $Z = \mathrm{Tr}(e^{-\beta\epsilon_i})$ is the partition function and $\beta = \frac{1}{k_B T}$ (k_B is Boltzmann constant). Given how crucial the measure of entanglement and its distribution

over different atoms is, for tasks such as quantum teleportation [1] and super dense coding [2–4], in this work we investigate the entanglement properties of the three atoms system.

The focus here is on the pairwise entanglement associated with any two atoms in terms of concurrence $C(\rho_{ij})$ and quantum discord $D(\rho_{ij})$. For pairwise thermal entanglement, one can obtain the reduced density matrices ρ_{ij} by taking partial transpose of ρ_{ijk} with respect to k, given by

$$\rho_{ij} = \mathrm{Tr}_k(\rho_{ijk}) \tag{4.2}$$

where $i, j, k = A, B, C$. A detailed description of concurrence is already provided in chapter 2. In the following, we give a brief description of the quantum discord.

4.2 Quantum discord

Entanglement, well-known for many decades [11, 12], is an important feature of quantum mechanics and also plays a very important part in the context of quantum information science where the quantum mechanical features of the states of the system are exploited [13–15]. This is also largely dependent on the initial state of the system and has a sensitive dependence on the interaction between the system and its surrounding environment. A composite system is defined as being separable, if it is not entangled. However, this statement has to be taken with caution as certain classically separable composite systems may contain different types of correlations, which are referred to as nonclassical correlations. Among such nonclassical correlations, one of

the well investigated measure is the "quantum discord". The quantum discord was first introduced and studied by Zurek et al. [7–10].

This measure of nonclassical correlation, the quantum discord, for two correlated subsystems A and B, is given by the difference between the total correlation and the corresponding classical correlation, and is expressed as $D = I - Q$. In a bipartite quantum system, designated by ρ_{AB}, the quantum mutual information I [16, 17] quantifies the total correlation between its two subsystems A and B. The relation for this quantum mutual information is given as

$$I(\rho_{AB}) = S(\rho_A) + S(\rho_B) - S(\rho_{AB}). \tag{4.3}$$

In the above, the subsystems A and B are denoted by their respective reduced density matrices ρ_A and ρ_B. The von Neumann entropy denoted by $S(\rho)$ is defined by the relation

$$S(\rho) = -\mathrm{Tr}\rho \log \rho. \tag{4.4}$$

It is to be noted that $I_{\rho_{AB}} = 0$ is a necessary and sufficient condition for the factorizability of ρ_{AB}, namely $\rho_{AB} = \rho_A \otimes \rho_B$, which implies the absolute non-correlativity of A and B in the product state. In view of the above, in quantum information theory, one considers the mutual information to quantify the total (both classical and quantum) correlations between the two subsystems of bipartite quantum system. On the other hand, measurements performed on one system, in general, influence the state of the other system, even if the two systems are far away from each other and do not directly interact [18]. Postulating that the total classical part of correlations is the maximal amount of information about one subsystem, say A, that can be extracted by performing

a measurement on the other subsystem B, Henderson and Vedral [9] suggested taking, as a measure of classical correlation, the quantity

$$C(\rho_{AB}) = max_{\{B_i\}}\{S(\rho_A) - \sum_i p_i S(\rho_A^i)\}. \tag{4.5}$$

Here $\{B_i\}$ is a complete set of measurements on the subsystem B and

$$\rho_A^i = \frac{\mathrm{Tr}_B(B_i \rho_{AB} B_i^\dagger)}{\mathrm{Tr}_{AB}(B_i \rho_{AB} B_i^+)} \tag{4.6}$$

is the remaining state of A after obtaining the outcome i on B, and

$$p_i = \mathrm{Tr}_{AB}(B_i \rho_{AB} B_i^\dagger) \tag{4.7}$$

is the probability to detect the result i. Now, we have two quantum analogs of the classical mutual information - the original quantum mutual information $I(\rho_{AB})$, and the measurement-induced quantum mutual information $C(\rho_{AB})$. The difference between these two quantities

$$D(\rho_{AB}) = I(\rho_{AB}) - C(\rho_{AB}), \tag{4.8}$$

is the so-called quantum discord, and is interpreted as a measure of quantum correlations by Olliver and Zurek [7]. In what follows, we present details of the quantum correlations in both line and loop configurations.

4.3 Quantum correlations in line configuration

At thermal equilibrium, the quantum state of a three atom system is a weighted superposition of all the eigenstates. By diagonalizing the Hamiltonian H (Eq.5.1), we can obtain all the eigenvalues ϵ_i and their corresponding eigenstates $|\psi_i\rangle$. The eigenvalues ϵ_i, in the line configuration, are

$$\begin{aligned}\epsilon_1 = \frac{-3\omega}{2};\ \epsilon_2 = -\sqrt{2}\Omega - \frac{\omega}{2};\ \epsilon_3 = -\frac{\omega}{2};\ \epsilon_4 = \sqrt{2}\Omega - \frac{\omega}{2}\\ \epsilon_5 = -\sqrt{2}\Omega + \frac{\omega}{2};\ \epsilon_6 = \frac{\omega}{2};\ \epsilon_7 = \sqrt{2}\Omega + \frac{\omega}{2};\ \epsilon_8 = \frac{3\omega}{2}\end{aligned} \tag{4.9}$$

and the corresponding eigenstates $|\psi_i\rangle$ of the system, are given by

$$\begin{aligned}&|\psi_1\rangle = |g_1g_2g_3\rangle; |\psi_2\rangle = \frac{1}{2}\Big[|e_1g_2g_3\rangle - \sqrt{2}|g_1e_2g_3\rangle + |g_1g_2e_3\rangle\Big]\\ &|\psi_3\rangle = \frac{1}{\sqrt{2}}\Big[|g_1g_2e_3\rangle - |e_1g_2g_3\rangle\Big]; |\psi_4\rangle = \frac{1}{2}\Big[|e_1g_2g_3\rangle + \sqrt{2}|g_1e_2g_3\rangle + |g_1g_2e_3\rangle\Big]\\ &|\psi_5\rangle = \frac{1}{2}\Big[|e_1e_2g_3\rangle - \sqrt{2}|e_1g_2e_3\rangle + |g_1e_2e_3\rangle\Big]; |\psi_6\rangle = \frac{1}{\sqrt{2}}\Big[|g_1e_2e_3\rangle - |e_1e_2g_3\rangle\Big]\\ &|\psi_7\rangle = \frac{1}{2}\Big[|e_1e_2g_3\rangle + \sqrt{2}|e_1g_2e_3\rangle + |g_1e_2e_3\rangle\Big]; |\psi_8\rangle = |e_1e_2e_3\rangle.\end{aligned} \tag{4.10}$$

Considering the standard basis $\{|g_1g_2g_3\rangle$, $|e_1g_2g_3\rangle$, $|g_1e_2g_3\rangle$, $|g_1g_2e_3\rangle$, $|e_1e_2g_3\rangle$, $|e_1g_2e_3\rangle$, $|e_1e_2g_3\rangle$, $|e_1e_2e_3\rangle\}$ of the system, one can obtain the thermal density

matrix of the form

$$\rho_{ABC}(T) = \frac{1}{Z}\begin{bmatrix} \rho_{11} & 0 & 0 & 0 & 0 & 0 & 0 & 0 \\ 0 & \rho_{22} & \rho_{23} & \rho_{24} & 0 & 0 & 0 & 0 \\ 0 & \rho_{32} & \rho_{33} & \rho_{34} & 0 & 0 & 0 & 0 \\ 0 & \rho_{42} & \rho_{43} & \rho_{44} & 0 & 0 & 0 & 0 \\ 0 & 0 & 0 & 0 & \rho_{55} & \rho_{56} & \rho_{57} & 0 \\ 0 & 0 & 0 & 0 & \rho_{65} & \rho_{66} & \rho_{67} & 0 \\ 0 & 0 & 0 & 0 & \rho_{75} & \rho_{76} & \rho_{77} & 0 \\ 0 & 0 & 0 & 0 & 0 & 0 & 0 & \rho_{88} \end{bmatrix} \tag{4.11}$$

where the partition function Z is given by

$$Z = e^{\frac{3\omega}{2k_BT}} + e^{\frac{-3\omega}{2k_BT}} + e^{\frac{(\frac{\omega}{2}-\sqrt{2}\Omega)}{k_BT}} + e^{-\frac{(\frac{\omega}{2}+\sqrt{2}\Omega)}{k_BT}} + e^{\frac{(\frac{\omega}{2}+\sqrt{2}\Omega)}{k_BT}} + e^{-\frac{(\frac{\omega}{2}-\sqrt{2}\Omega)}{k_BT}} + e^{\frac{\omega}{2k_BT}} + e^{\frac{-\omega}{2k_BT}}.$$

The non-vanishing density matrix elements of $\rho_{ABC}(T)$ are given by

$$\begin{aligned}
&\rho_{11} = e^{\frac{3\omega}{2k_BT}}; \quad \rho_{88} = e^{\frac{-3\omega}{2k_BT}} \\
&\rho_{22} = \rho_{44} = \frac{1}{4}\left[e^{\frac{(\frac{\omega}{2}-\sqrt{2}\Omega)}{k_BT}} + e^{\frac{(\frac{\omega}{2}+\sqrt{2}\Omega)}{k_BT}} + 2e^{\frac{\omega}{2k_BT}}\right]; \quad \rho_{33} = \frac{1}{2}\left[e^{\frac{(\frac{\omega}{2}-\sqrt{2}\Omega)}{k_BT}} + e^{\frac{(\frac{\omega}{2}+\sqrt{2}\Omega)}{k_BT}}\right] \\
&\rho_{55} = \rho_{77} = \frac{1}{4}\left[e^{-(\frac{\omega}{2}-\sqrt{2}\Omega)k_BT} + e^{-\frac{(\frac{\omega}{2}+\sqrt{2}\Omega)}{k_BT}} + 2e^{-\frac{\omega}{2k_BT}}\right]; \ \rho_{66} = \frac{1}{2}\left[e^{-\frac{(\frac{\omega}{2}-\sqrt{2}\Omega)}{k_BT}} + e^{-\frac{(\frac{\omega}{2}+\sqrt{2}\Omega)}{k_BT}}\right] \\
&\rho_{23} = \rho_{34} = \frac{1}{2\sqrt{2}}\left[e^{\frac{(\frac{\omega}{2}-\sqrt{2}\Omega)}{k_BT}} - e^{\frac{(\frac{\omega}{2}+\sqrt{2}\Omega)}{k_BT}}\right]; \quad \rho_{24} = \frac{1}{4}\left[e^{\frac{(\frac{\omega}{2}-\sqrt{2}\Omega)}{k_BT}} + e^{\frac{(\frac{\omega}{2}+\sqrt{2}\Omega)}{k_BT}} - 2e^{\frac{\omega}{2k_BT}}\right] \\
&\rho_{56} = \rho_{67} = \frac{1}{2\sqrt{2}}\left[e^{-\frac{(\frac{\omega}{2}+\sqrt{2}\Omega)}{k_BT}} - e^{-\frac{(\frac{\omega}{2}-\sqrt{2}\Omega)}{k_BT}}\right]; \ \rho_{57} = \frac{1}{4}\left[e^{-\frac{(\frac{\omega}{2}+\sqrt{2}\Omega)}{k_BT}} + e^{-\frac{(\frac{\omega}{2}-\sqrt{2}\Omega)}{k_BT}} - 2e^{-\frac{\omega}{2k_BT}}\right].
\end{aligned} \tag{4.12}$$

It is well known that a mixed state ρ is separable if it can be expressed as a convex sum of three pure states, $|\psi\rangle = |\phi_A\rangle \otimes |\phi_B\rangle \otimes |\phi_C\rangle$, otherwise it is called an entangled state. In this case, in the high temperature limit ($\beta \to 0$),

the density matrix ρ_{ABC} of the system simplifies to,

$$\rho = \frac{1}{8}\begin{bmatrix} 1 & 0 & 0 & 0 & 0 & 0 & 0 & 0 \\ 0 & 1 & 0 & 0 & 0 & 0 & 0 & 0 \\ 0 & 0 & 1 & 0 & 0 & 0 & 0 & 0 \\ 0 & 0 & 0 & 1 & 0 & 0 & 0 & 0 \\ 0 & 0 & 0 & 0 & 1 & 0 & 0 & 0 \\ 0 & 0 & 0 & 0 & 0 & 1 & 0 & 0 \\ 0 & 0 & 0 & 0 & 0 & 0 & 1 & 0 \\ 0 & 0 & 0 & 0 & 0 & 0 & 0 & 1 \end{bmatrix} \tag{4.13}$$

which can further be expressed as a convex combination of three pure states,

$$\rho = \frac{1}{8}\begin{pmatrix} 1 & 0 \\ 0 & 0 \end{pmatrix} \otimes \begin{pmatrix} 1 & 0 \\ 0 & 0 \end{pmatrix} \otimes \begin{pmatrix} 1 & 0 \\ 0 & 0 \end{pmatrix} + ... + \frac{1}{8}\begin{pmatrix} 0 & 0 \\ 0 & 1 \end{pmatrix} \otimes \begin{pmatrix} 0 & 0 \\ 0 & 1 \end{pmatrix} \otimes \begin{pmatrix} 0 & 0 \\ 0 & 1 \end{pmatrix}. \tag{4.14}$$

From the above description, one observes that the system at high temperature is perfectly separable. However, for intermediate temperatures, the system is in a mixed state and we investigate the entanglement properties of such a system, from a study of its pairwise concurrence $C(\rho_{ij})$ and quantum discord $D(\rho_{ij})$.

4.3.1 Numerical results

In this section, we study the pairwise concurrence $C(\rho_{ij})$ and discord $D(\rho_{ij})$ as functions of the ratio of D-D coupling strength Ω to atomic transition frequency. In addition, the influence of atomic transition frequency ω and the temperature k_BT, on the discord and concurrence of the system are also discussed.

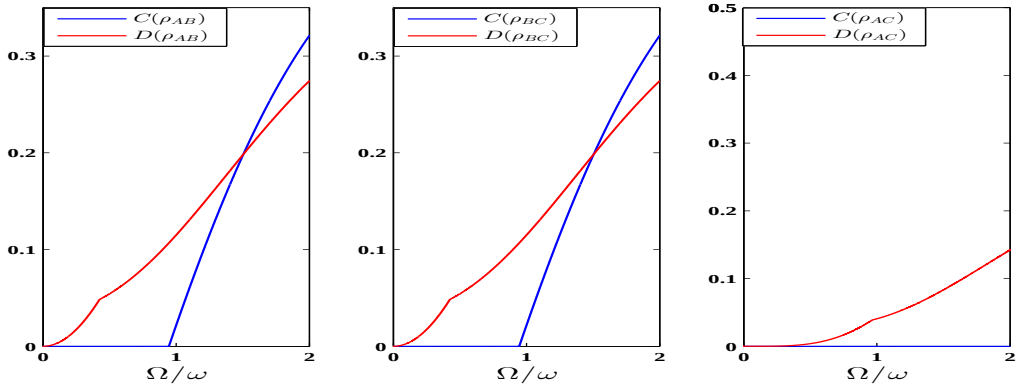

Figure 4-1: Line configuration: Pairwise $C(\rho_{ij})$ and $D(\rho_{ij})$ as a function of Ω/ω for $k_BT/\omega = 1$.

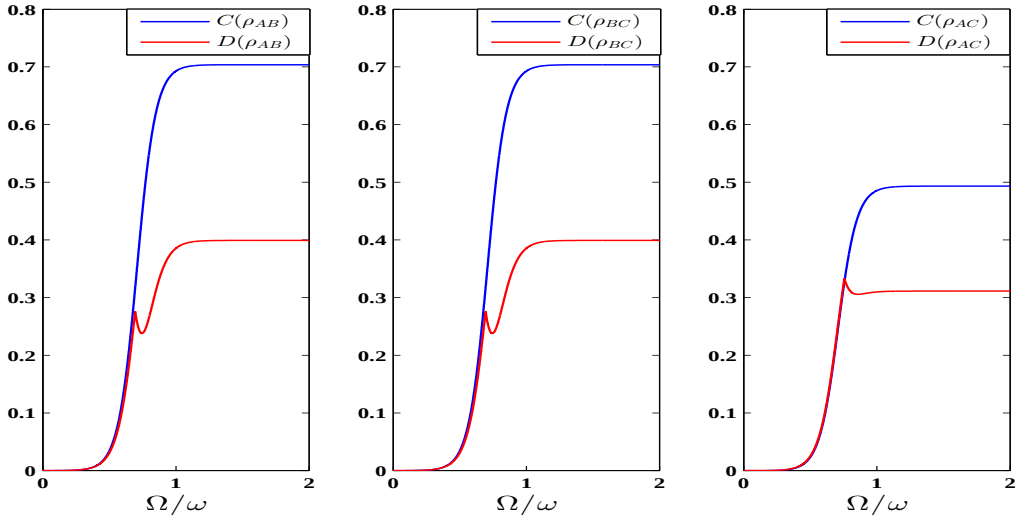

Figure 4-2: Line configuration: Pairwise $C(\rho_{ij})$ and $D(\rho_{ij})$ as a function of Ω/ω for $k_BT/\omega = 0.1$.

Figure 4-1 shows the variation of the pairwise concurrence $C(\rho_{ij})$ and discord $D(\rho_{ij})$ as a function of Ω/ω for the temperature $k_BT/\omega = 1$. From the figure, it is clearly seen that $C(\rho_{ij})$ and $D(\rho_{ij})$ are zero when there is no coupling

between the atoms. With increasing Ω/ω, it is observed that $C(\rho_{AB}) = C(\rho_{BC})$ and $D(\rho_{AB}) = D(\rho_{BC})$ where as $C(\rho_{AC}) = 0$. But $D(\rho_{AC})$ is non zero which implies that quantum correlations are still present even though end atoms A and C are not directly dipole coupled. We also note that the pairwise concurrence $C(\rho_{AB}), C(\rho_{BC})$ has non zero values only when $\Omega \geq k_B T$. In addition, it is observed that the quantum discord $D(\rho_{AB})(D(\rho_{BC}))$ dominates over the concurrence $C(\rho_{AB})(C(\rho_{BC}))$ when the condition $\Omega/\omega \leq 1.5$ is met. In the other regime, i.e., for $\Omega/\omega > 1.5$, concurrence dominates over the corresponding discord. This clearly shows that one can not write a simple relation between the concurrence and the discord for any subsystem comprising of one pair of qubits. This result is in agreement with that of [19], where they have considered a system of two qubits.

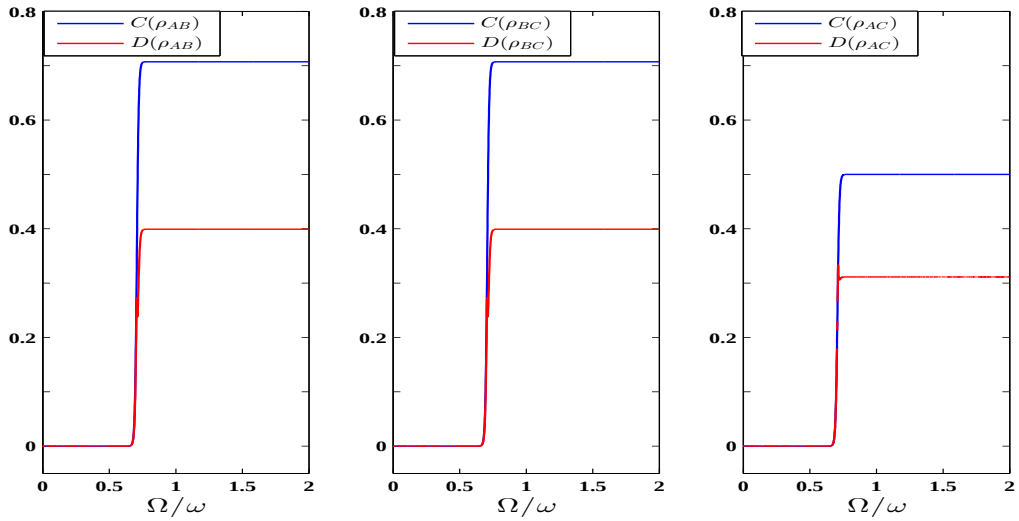

Figure 4-3: Line configuration: Pairwise $C(\rho_{ij})$ and $D(\rho_{ij})$ as a function of Ω/ω for $k_B T/\omega = 0.01$.

In the lower temperature regime, the concurrence $C(\rho_{ij})$ and the quantum

discord $D(\rho_{ij})$ are greatly enhanced as shown in figures 4-2 and 4-3. Here the figures 4-2 and 4-3 show the variation of $C(\rho_{ij})$ and $D(\rho_{ij})$ as a function of ω/Ω for $k_BT/\omega = 0.1$ and $k_BT/\omega = 0.01$, respectively. For $k_BT/\omega = 0.1$, it is observed that the pairwise concurrence $C(\rho_{AB}) = C(\rho_{BC})$ and $D(\rho_{AB}) = D(\rho_{BC})$ whereas $C(\rho_{AC})$ attains a non zero value. We can thus deduce from a careful inspection of Figs. 4-2 and 4-3 that the quantum correlations $D(\rho_{ij})$ and pairwise entanglement $C(\rho_{ij})$ tend to increase with increasing D-D coupling strength, and reach a maximum/saturation value. Further decrease in temperature shows a very interesting feature in both these quantities. It is clearly seen that with a decrease of temperature, the curves of $C(\rho_{ij})$ and $D(\rho_{ij})$ plotted as a function of Ω/ω attain sharper edges, with all the kinks removed, thus resembling the shape of a switch, which in this context is referred to as a correlation /quantum switch [20]. This behaviour is much better elucidated when the quantities $C(\rho_{ij})$ and $D(\rho_{ij})$ are plotted as functions of atomic transition frequency ω in the lower temperature regime ($k_BT = 0.01$), which are shown in figure 4-4. From the results presented here for different temperatures and dipole coupling strengths, it is clear that these quantum correlation switches can be constructed by properly tuning the temperature and dipole coupling strengths.

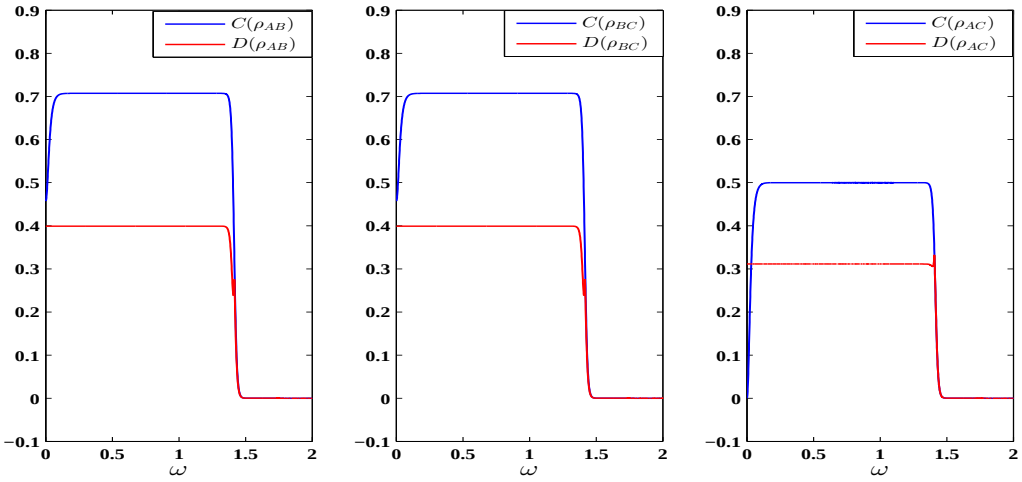

Figure 4-4: Line configuration: Pairwise $C(\rho_{ij})$ and $D(\rho_{ij})$ as a function of ω for $k_BT = 0.01$ and $\Omega = 1$.

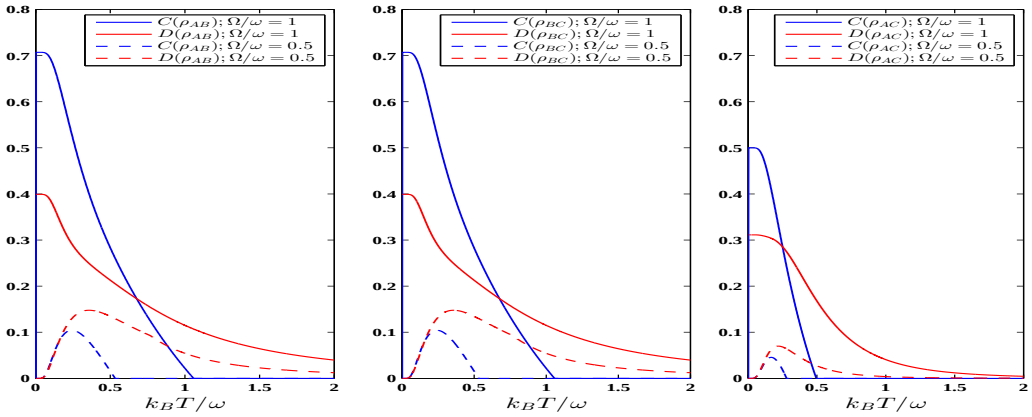

Figure 4-5: Line configuration: Pairwise $C(\rho_{ij})$ and $D(\rho_{ij})$ as a function of k_BT/ω for $\Omega/\omega = 1$ and 0.5.

In figure 4-5, we study the pairwise $C(\rho_{ij})$ and $D(\rho_{ij})$ as a function of k_BT/ω for different values of D-D coupling strength ($\Omega/\omega = 1, 0.5$). It is clearly seen that the pairwise quantum discord $D(\rho_{ij})$ has non zero values at $k_BT = 0$. This is in contrast to the property of pairwise entanglement $C(\rho_{ij})$.

The concurrence $C(\rho_{ij})$ vanishes at $k_BT = 0$, and then attains non-zero values as the temperature is raised and reaches a maximum value after which it falls to zero very rapidly at a specific temperature, namely when $k_BT = \Omega$. But the discord $D(\rho_{ij})$ continues to remain non-zero and vanishes at much higher temperatures. This indicates the robustness of quantum discord $D(\rho_{ij})$ against the concurrence, as the temperature is increased. For higher values of dipole coupling strengths (Ω/ω) also, similar features are observed. To conclude, quantum correlations may be enhanced by lowering the temperature and/or by increasing the dipole-dipole coupling strength, when the atoms are arranged on a line.

4.4 Quantum correlations in loop configuration

In this section, we investigate the thermal entanglement properties of a triangular system of dipole coupled two-level atoms, placed at the vertices of the triangle. The eigenvalues of the Hamiltonian are

$$\epsilon_1 = \frac{-3\omega}{2};\ \epsilon_2 = -\Omega - \frac{\omega}{2};\ \epsilon_3 = -\Omega - \frac{\omega}{2};\ \epsilon_4 = 2\Omega - \frac{\omega}{2}$$

$$\epsilon_5 = \frac{\omega}{2} - \Omega;\ \epsilon_6 = \frac{\omega}{2} - \Omega;\ \epsilon_7 = \frac{\omega}{2} + 2\Omega;\ \epsilon_8 = \frac{3\omega}{2}$$

and the corresponding eigenstates $|\phi_i\rangle$ of the system are given by

$$|\phi_1\rangle = |g_1g_2g_3\rangle; \quad |\phi_2\rangle = \frac{1}{\sqrt{2}}\Big[|g_1e_2g_3\rangle - |e_1g_2g_3\rangle\Big]$$
$$|\phi_3\rangle = \frac{1}{\sqrt{2}}\Big[|g_1g_2e_3\rangle - |e_1g_2g_3\rangle\Big]; \quad |\phi_4\rangle = \frac{1}{\sqrt{3}}\Big[|e_1g_2g_3\rangle + |g_1e_2g_3\rangle + |g_1g_2e_3\rangle\Big]$$
$$|\phi_5\rangle = \frac{1}{\sqrt{2}}\Big[|e_1g_2e_3\rangle - |e_1e_2g_3\rangle\Big]; \quad |\phi_6\rangle = \frac{1}{\sqrt{2}}\Big[|g_1e_2e_3\rangle - |e_1e_2g_3\rangle\Big]$$
$$|\phi_7\rangle = \frac{1}{\sqrt{3}}\Big[|e_1e_2g_3\rangle + |e_1g_2e_3\rangle + |g_1e_2e_3\rangle\Big]; \quad |\phi_8\rangle = |e_1e_2e_3\rangle.$$

By substituting the above eigenvalues and eigenvectors in Eq.(4.1), one can obtain the temperature dependent density matrix elements and the non-vanishing density matrix elements thus obtained are listed below.

$$\begin{aligned}
&\rho_{11} = e^{\frac{3\omega}{2k_BT}}; \quad \rho_{88} = e^{\frac{-3\omega}{2k_BT}} \\
&\rho_{22} = \frac{1}{3}e^{\frac{(\frac{\omega}{2}-2\Omega)}{k_BT}} + e^{\frac{(\frac{\omega}{2}+\Omega)}{k_BT}}; \quad \rho_{33} = \rho_{44} = \frac{1}{3}e^{\frac{(\frac{\omega}{2}-2\Omega)}{k_BT}} + \frac{1}{2}e^{\frac{(\frac{\omega}{2}+\Omega)}{k_BT}} \\
&\rho_{55} = \frac{1}{3}e^{-\frac{(\frac{\omega}{2}+2\Omega)}{k_BT}} + e^{-\frac{(\frac{\omega}{2}-\Omega)}{k_BT}}; \quad \rho_{66} = \rho_{77} = \frac{1}{3}e^{-\frac{(\frac{\omega}{2}+2\Omega)}{k_BT}} + \frac{1}{2}e^{-\frac{(\frac{\omega}{2}-\Omega)}{k_BT}} \\
&\rho_{23} = \rho_{24} = \frac{1}{3}e^{\frac{(\frac{\omega}{2}-2\Omega)}{k_BT}} - \frac{1}{2}e^{\frac{(\frac{\omega}{2}+\Omega)}{k_BT}}; \quad \rho_{34} = \frac{1}{3}e^{\frac{(\frac{\omega}{2}-2\Omega)}{k_BT}} \\
&\rho_{56} = \rho_{57} = \frac{1}{3}e^{-\frac{(\frac{\omega}{2}+2\Omega)}{k_BT}} - \frac{1}{2}e^{-\frac{(\frac{\omega}{2}-\Omega)}{k_BT}}; \quad \rho_{67} = \frac{1}{3}e^{-\frac{(\frac{\omega}{2}+2\Omega)}{k_BT}}
\end{aligned} \tag{4.15}$$

The partition function for this system is given by

$$Z = e^{\frac{3\omega}{2k_BT}} + e^{\frac{-3\omega}{2k_BT}} + e^{\frac{(\frac{\omega}{2}-2\Omega)}{k_BT}} + e^{-\frac{(\frac{\omega}{2}+2\Omega)}{k_BT}} + 2e^{\frac{(\frac{\omega}{2}+\Omega)}{k_BT}} + 2e^{\frac{-(\frac{\omega}{2}-\Omega)}{k_BT}}.$$

At high temperature, the density matrix reduces to a mixed state, which can not be written in terms of product states. For three atoms in loop configuration, certain interesting features are observed, which will be discussed in detail

in the next section. For instance, some simply bi-separable mixed states have shown no reduced entanglement, when the separable qubit is traced over. This is in confirmation with the earlier reports [21, 22] which state that generalized bi-separable states contain bipartite entanglement in more than one pair of qubits and that they have distributed bipartite entanglement.

For atoms in the loop configuration, the reduced density matrix ρ_{AB} for the two atoms A and B, obtained by tracing over atom C from the state $\rho_{ABC}(T)$, can be written as

$$\rho_{AB}(T) = \frac{1}{Z}\begin{bmatrix} \rho_{11}^{'} & 0 & 0 & 0 \\ 0 & \rho_{22}^{'} & \rho_{23}^{'} & 0 \\ 0 & \rho_{32}^{'} & \rho_{33}^{'} & 0 \\ 0 & 0 & 0 & \rho_{44}^{'} \end{bmatrix} \tag{4.16}$$

with

$$\begin{aligned} &\rho_{11}^{'} = e^{\frac{3\omega}{2k_BT}} + \frac{1}{2}e^{\frac{(\frac{\omega}{2}+\Omega)}{k_BT}} + \frac{1}{3}e^{\frac{(\frac{\omega}{2}-2\Omega)}{k_BT}};\quad \rho_{22}^{'} = e^{\frac{(\frac{\omega}{2}+\Omega)}{k_BT}} + \frac{1}{3}e^{\frac{(\frac{\omega}{2}-2\Omega)}{k_BT}} + \frac{1}{2}e^{\frac{-(\frac{\omega}{2}-\Omega)}{k_BT}} + \frac{1}{3}e^{\frac{-(\frac{\omega}{2}+2\Omega)}{k_BT}} \\ &\rho_{33}^{'} = \frac{1}{2}e^{\frac{(\frac{\omega}{2}+\Omega)}{k_BT}} + \frac{1}{3}e^{\frac{(\frac{\omega}{2}-2\Omega)}{k_BT}} + \frac{1}{2}e^{\frac{-(\frac{\omega}{2}-\Omega)}{k_BT}} + \frac{1}{3}e^{\frac{-(\frac{\omega}{2}+2\Omega)}{k_BT}};\ \rho_{44}^{'} = e^{\frac{-3\omega}{2k_BT}} + e^{\frac{-(\frac{\omega}{2}-\Omega)}{k_BT}} + \frac{1}{3}e^{\frac{-(\frac{\omega}{2}+2\Omega)}{k_BT}} \\ &\rho_{23}^{'} = \frac{1}{3}e^{\frac{(\frac{\omega}{2}-2\Omega)}{k_BT}} - \frac{1}{2}e^{\frac{(\frac{\omega}{2}+\Omega)}{k_BT}} + \frac{1}{3}e^{\frac{-(\frac{\omega}{2}+2\Omega)}{k_BT}};\quad \rho_{32}^{'} = (\rho_{23}^{'})^* \end{aligned} \tag{4.17}$$

Similarly, we can obtain the reduced density matrix ρ_{BC} for the two atoms B and C by tracing over atom A from the state $\rho_{ABC}(T)$. The corresponding

density matrix elements of ρ_{BC} are given by

$$\rho_{11}^{''} = e^{\frac{3\omega}{2k_BT}} + e^{\frac{(\frac{\omega}{2}+\Omega)}{k_BT}} + \frac{1}{3}e^{\frac{(\frac{\omega}{2}-2\Omega)}{k_BT}};\quad \rho_{22}^{''} = \frac{1}{2}e^{\frac{(\frac{\omega}{2}+\Omega)}{k_BT}} + \frac{1}{3}e^{\frac{(\frac{\omega}{2}-2\Omega)}{k_BT}} + e^{\frac{-(\frac{\omega}{2}-\Omega)}{k_BT}} + \frac{1}{3}e^{\frac{-(\frac{\omega}{2}+2\Omega)}{k_BT}}$$
$$\rho_{33}^{''} = \frac{1}{2}e^{\frac{(\frac{\omega}{2}+\Omega)}{k_BT}} + \frac{1}{3}e^{\frac{(\frac{\omega}{2}-2\Omega)}{k_BT}} + \frac{1}{2}e^{\frac{-(\frac{\omega}{2}-\Omega)}{k_BT}} + \frac{1}{3}e^{\frac{-(\frac{\omega}{2}+2\Omega)}{k_BT}};\ \rho_{44}^{''} = e^{\frac{-3\omega}{2k_BT}} + \frac{1}{2}e^{\frac{-(\frac{\omega}{2}-\Omega)}{k_BT}} + \frac{1}{3}e^{\frac{-(\frac{\omega}{2}+2\Omega)}{k_BT}}$$
$$\rho_{23}^{''} = \frac{1}{3}e^{\frac{(\frac{\omega}{2}-2\Omega)}{k_BT}} - \frac{1}{2}e^{-\frac{(\frac{\omega}{2}+\Omega)}{k_BT}} + \frac{1}{3}e^{\frac{-(\frac{\omega}{2}+2\Omega)}{k_BT}};\quad \rho_{32}^{''} = (\rho_{23}^{''})^* \tag{4.18}$$

We can also write the density matrix elements for the reduced density matrix $\rho_{AC}(T)$ as follows:

$$\rho_{11}^{'''} = e^{\frac{3\omega}{2k_BT}} + \frac{1}{2}e^{\frac{(\frac{\omega}{2}+\Omega)}{k_BT}} + \frac{1}{3}e^{\frac{(\frac{\omega}{2}-2\Omega)}{k_BT}};\quad \rho_{22}^{'''} = e^{\frac{(\frac{\omega}{2}+\Omega)}{k_BT}} + \frac{1}{3}e^{\frac{(\frac{\omega}{2}-2\Omega)}{k_BT}} + e^{\frac{-(\frac{\omega}{2}-\Omega)}{k_BT}} + \frac{1}{3}e^{\frac{-(\frac{\omega}{2}+2\Omega)}{k_BT}}$$
$$\rho_{33}^{'''} = \frac{1}{2}e^{\frac{(\frac{\omega}{2}+\Omega)}{k_BT}} + \frac{1}{3}e^{\frac{(\frac{\omega}{2}-2\Omega)}{k_BT}} + \frac{1}{2}e^{\frac{-(\frac{\omega}{2}-\Omega)}{k_BT}} + \frac{1}{3}e^{\frac{-(\frac{\omega}{2}+2\Omega)}{k_BT}};\ \rho_{44}^{'''} = e^{\frac{-3\omega}{2k_BT}} + \frac{1}{2}e^{\frac{-(\frac{\omega}{2}-\Omega)}{k_BT}} + \frac{1}{3}e^{\frac{-(\frac{\omega}{2}+2\Omega)}{k_BT}}$$
$$\rho_{23}^{'''} = \frac{1}{3}e^{\frac{(\frac{\omega}{2}-2\Omega)}{k_BT}} - \frac{1}{2}e^{\frac{(\frac{\omega}{2}+\Omega)}{k_BT}} - \frac{1}{2}e^{\frac{-(\frac{\omega}{2}-\Omega)}{k_BT}} + \frac{1}{3}e^{\frac{-(\frac{\omega}{2}+2\Omega)}{k_BT}};\quad \rho_{32}^{'''} = (\rho_{23}^{'''})^* \tag{4.19}$$

Due to the structure symmetry of the equilateral triangle and the exchange invariability of the three dipoles A, B and C, which comes from the assumption that all atoms are assumed to be identical, it seems to be a trivial observation that the three reduced density matrices ρ_{AB}, ρ_{BC}, and ρ_{AC} have the identical X state form. However, a careful inspection of different density matrix elements, on which the different entanglement measures depend, suggests that their entanglement properties might be different. As numerical results will provide more insight into this feature, the same are presented for a range of parameter values in the next section.

4.4.1 Numerical results

In this section, we present a discussion on the results that are obtained on the thermal entanglement properties of three atoms arranged in a loop configuration. In this case, we observe that the reduced density matrices ρ_{AB}, ρ_{BC} and ρ_{AC} have different entanglement characteristics, though all of them have identical X-state form.

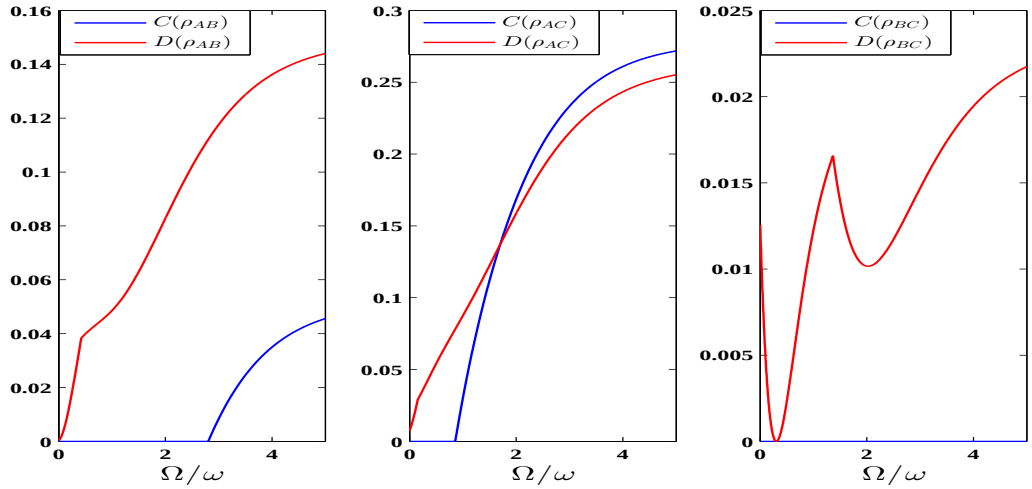

Figure 4-6: Loop configuration: Pairwise $C(\rho_{ij})$ and $D(\rho_{ij})$ as a function of Ω/ω for $k_BT/\omega = 1$.

A comparison between the quantum discord $D(\rho_{ij})$ and the concurrence $C(\rho_{ij})$ for $k_BT/\omega = 1.0$ is displayed in figure4-6. From the figure, it is clearly seen that reduced density matrix ρ_{BC} is separable and contains zero entanglement for all values of D-D coupling Ω, whereas the other reduced density matrices ($C(\rho_{AB}) \neq C(\rho_{AC})$) have non-zero entanglement. This surprising yet remarkable feature has been discussed in the literature [21, 22] for certain pure states. Similarly, one notes that the quantum correlations $D(\rho_{AB}) \neq D(\rho_{AC}) \neq D(\rho_{BC})$.

The same quantities as shown in figure 4-6, for lower temperatures, viz., $k_BT/\omega = 0.1$ and $k_BT/\omega = 0.01$ are illustrated in figures 4-7 and 4-8 respectively. As the temperature is lowered from $k_BT/\omega = 1$ to 0.1 and 0.01, there is a significant increase in the quantum discord $D(\rho_{AB})$, $D(\rho_{AC})$ as well as the concurrence $C(\rho_{AB})$, $C(\rho_{AC})$. However, the discord $D(\rho_{BC})$, which had a non-zero value at a higher temperature shows a monotonic decrease with lowered temperatures and further, when the temperature is sufficiently lowered, it approaches zero.

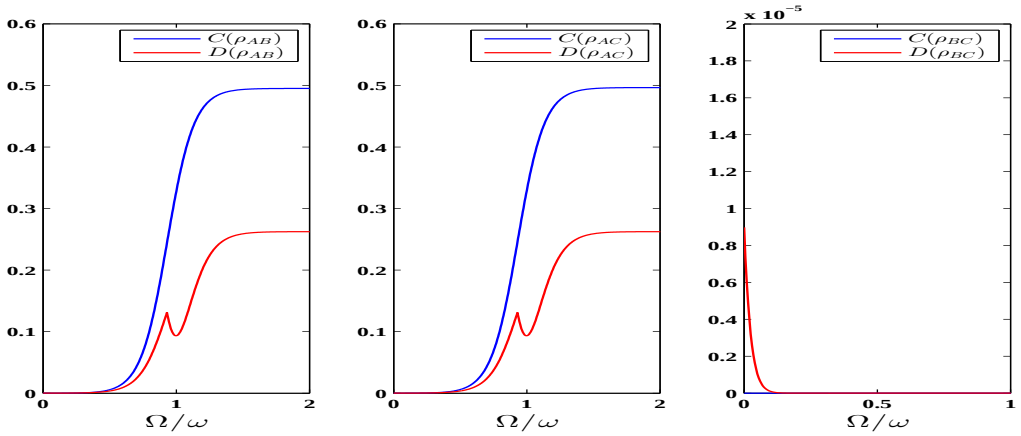

Figure 4-7: Loop configuration: Pairwise $C(\rho_{ij})$ and $D(\rho_{ij})$ as a function of Ω/ω for $k_BT/\omega = 0.1$.

The interesting feature of switch-like behaviour at lower temperatures, exhibited by the atoms arranged in line configuration is also seen when they are arranged in a loop [cf fig.4-9]. However, unlike in the line configuration, in the case of the loop configuration, only two of the correlations corresponding to ρ_{AB} and ρ_{AC}, show this switch-type feature, while the third correlation (involving ρ_{BC}) is nearly zero, with only the discord having a small nonzero value at very small values of ω, and quickly becoming zero with further increase in ω, with clear absence of the 'switch' feature. It is believed that these

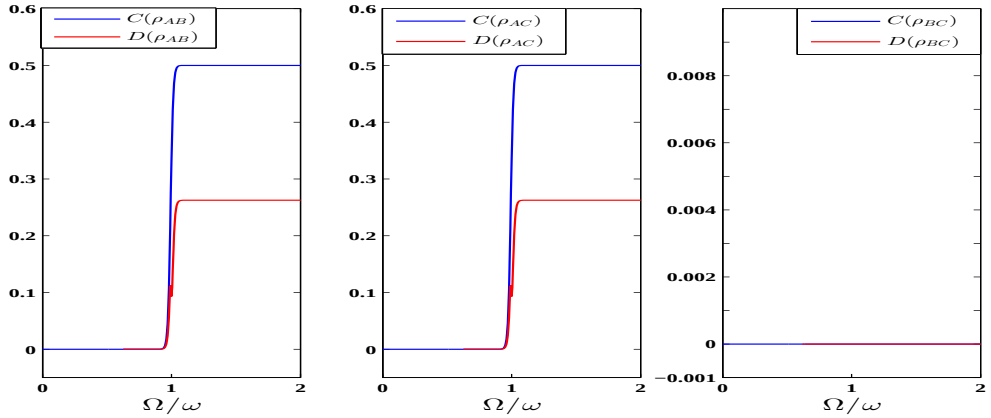

Figure 4-8: Loop configuration: Pairwise $C(\rho_{ij})$ and $D(\rho_{ij})$ as a function of Ω/ω for $k_BT/\omega = 0.01$.

quantum switches have important consequences in quantum computing, in the implementation of quantum gates.

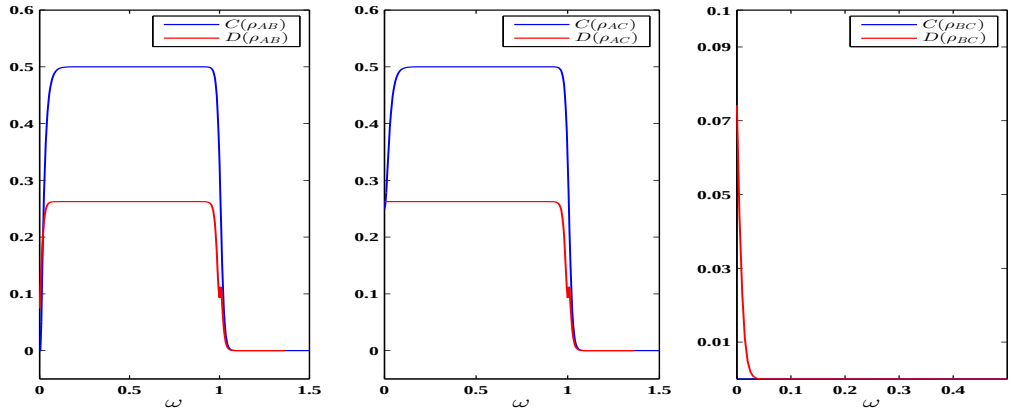

Figure 4-9: Loop configuration: for Pairwise $C(\rho_{ij})$ and $D(\rho_{ij})$ as a function of ω for $k_BT = 0.01$ and $\Omega = 1$.

In figure 4-10, all the pairs of quantum correlations are plotted for typical values of dipole coupling strength Ω as a function of the ratio of temperature to atomic transition frequency. As seen from figure 4-10, the two concurrences

$C(\rho_{AB})$ and $C(\rho_{AC})$ start from 0 at zero temperature, attain a maximum value at certain temperature and then decrease to zero with further increase in the temperature, while the corresponding discords $D(\rho_{AB})$ and $D(\rho_{AC})$ both peak at zero temperature and decrease as the temperature is increased, for all values of the coupling strength Ω that are considered here. Further, the concurrences are observed to rapidly diminish while the quantum discords persist longer, with a much slower decay. In general, both types of quantum correlations are seen to decay with increase in temperature due to thermal relaxation effects. To summarize, it is seen that the quantum correlations increase with increase in the dipole coupling strength associated with a corresponding decrease as the temperature is increased. As has already been discussed, this feature is attributed to have resulted from the thermal relaxation effects.

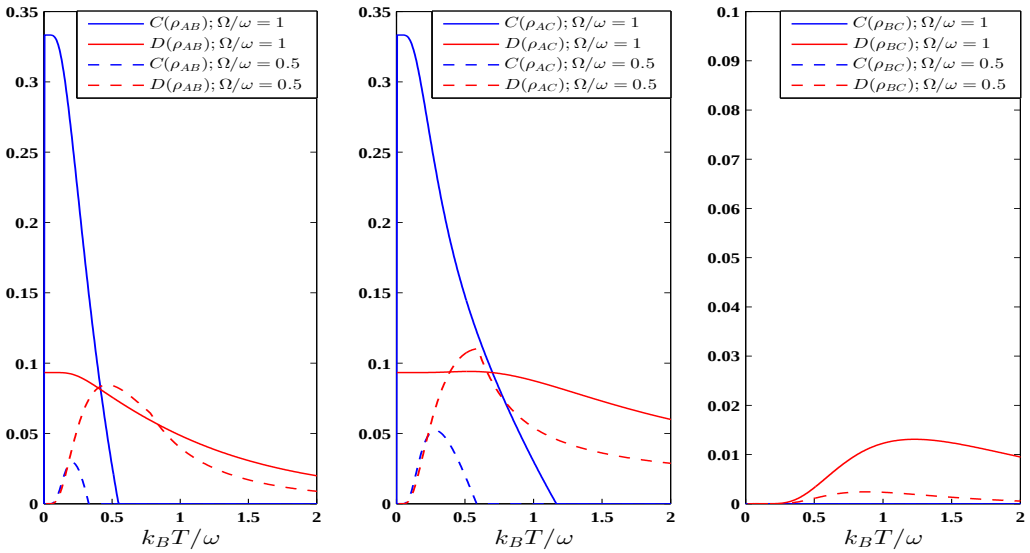

Figure 4-10: Loop configuration: Pairwise $C(\rho_{ij})$ and $D(\rho_{ij})$ as a function of k_BT/ω for different values of $\Omega/\omega = 1, 0.5$.

4.5 Conclusion

The temperature dependent behaviour of two quantum correlations, concurrence and discord, for all possible bipartite subsystems of the three coupled atoms in both line and loop configuration is studied in detail. In both the line and loop configurations, it is seen that the quantum correlations increase with increase in the ratio of dipole coupling strength to atomic transition frequency and decrease as the ratio of temperature to atomic transition frequency is increased, the latter of which is attributed to thermal relaxation. In particular when the atoms are in loop configuration, certain interesting features are observed which are in agreement with the earlier reported studies on similar systems. It is worth mentioning here that D*ür* [23] has shown that the entanglement properties of a qubit with its neighbours are not simply determined by the mere number of its entangled neighbours but also by the properties of these entangled neighbours. In other words, the presence of entanglement or classical correlations on certain pairs of qubits may imply correlations on other pairs, if these are in any way connected to the qubits. These features very well substantiate our results on the entanglement properties, inferred from a study of the quantum correlations, of atoms arranged in a loop configuration.

References

[1] C. H. Bennett, G. Brassard, C. Crepeau, R. Jozsa, A. Peres and W. K. Wootters, Phys. Rev. Lett. **70**, 1895 (1993).

[2] S. Bose, V. Vedral and P. L. Knight, Phys. Rev. A **57**, 822 (1998).

[3] M. Ban, J. Opt. B: Quant. Semiclass. Opt. **1**, L9 (1999).

[4] A. K. Pati, P. Parashar and P. Agrawal, Phys. Rev. A **72**, 012329 (2005).

[5] S. Hill and W. K. Wootters, Phys. Rev. Lett. **78**, 5022 (1997).

[6] W. K. Wootters, Phys. Rev. Lett. **80**, 2245 (1998).

[7] H. Ollivier and W. H. Zurek, Phys. Rev. Lett. **88**, 017901 (2001).

[8] H. Zurek, Ann. Phys. (Berlin) **9**, 855 (2000).

[9] L. Henderson and V. Vedral, J. Phys. A **34**, 6899 (2001).

[10] V. Vedral, Phys. Rev. Lett. **90**, 050401 (2003).

[11] A. Einstein, B. Podolsky and N. Rosen, Phys. Rev. **47**, 777 (1935).

[12] E. Schrödinger, Naturwissenschaften 23, 807; ibid 823; ibid 844 (1935).

[13] D. Bouwmeester, J. W. Pan, K. Mattle, M. Eibl, H. Weinfurter and A. Zeilinger, Nature (London) **390**, 575 (1997).

[14] A. Ekert, Phys. Rev. Lett. **67**, 661 (1991).

[15] C. H. Bennett and S. J. Wiesner, Phys. Rev. Lett. **69**, 2881 (1992).

[16] V. Vedral, Rev. Mod. Phys. **74**, 197 (2002).

[17] B. Groisman, S. Popescu and A. Winter, Phys. Rev. A **72**, 032317 (2005).

[18] A. S. Holevo, *Probability and Statistical Aspects of Quantum Theory*, MT-sNMO, Moscow (2003).

[19] S. Luo, Phys. Rev. A **77**, 042303 (2008).

[20] Q. Wei, S. Kais and Y. P. Chen, J. Chem. Phys. **132**, 121104 (2010).

[21] C. Sab́in and G. García-Alcaine, Eur. Phys. J. D **48**, 435 (2008).

[22] M. Plesch and V. Bužek, Phys. Rev. A **67**, 012322 (2003).

[23] W. D*ür*, Phys. Rev. A **63**, 020303 (2001).

Chapter 5

Intensity and radiation statistics of three two-level atoms

Superradiance, is the coherent spontaneous emission of radiation generated due to the cooperative effects among atoms [1], whereas spontaneous emission is a random process, in which the emitted radiation obeys an exponential law, with the natural radiative lifetime $1/\gamma$. In 1954, Dicke [2] theoretically predicted that when the number of atoms N, in a given volume, becomes sufficiently large, the collection of atoms starts to radiate spontaneously much faster, with decay time proportional to $1/N\gamma$, with an emission stronger than that arising from N independent atoms. Further, the enhanced mean radiated intensity is scattered anisotropically, i. e., radiation is emitted in a well defined direction. Depending upon the geometry of the sample, the emission could be proportional to the square of the number of atoms (N^2) in the ensemble, instead of N, as is the case for independent atoms. The emission from a system is defined to be superradiant if its radiative decay rate is greater than the single atom decay rate and it is said to be subradiant if it is the other way round.

Superradiance has been extensively studied in the literature, with the identification of a phase transition, separating the coherent phase of radiation from the incoherent part [3–5]. It has attracted significant interest due to its wide range of possible applications, ranging from generation of X-ray lasers with high powers [6], short pulse generation [7] and self-phasing in a system of classical oscillators [8], to name a few. It has also been studied experimentally in many physical systems [9–11]. It can provide insight into various applications of the entangled atomic ensembles and generated quantum states of light for quantum memories [12, 13], quantum communication [14], quantum cryptography [15, 16] and quantum information [17]. In the context of quantum information, it is of particular interest to explore how the super radiant behaviour gets affected for a collection of atoms, when the states are entangled in different ways. This will allow optical probing of entangled states and may also provide insight into the nature of entanglement.

In this chapter, we examine the characteristics of the emission from a system of three two-level atoms, in its two possible configurations (line and closed loop) as described in chapter 3. For each of these configurations, one can generate two different types of entangled states which exhibit different quantum correlations, known as the W-state and the Greenberger-Horne-Zeilinger (GHZ) state respectively. One can generate two distinct types of W-states, which carry a nonzero bipartite entanglement, formed from linear combinations of the three atom product states. The first type corresponds to the combination where one atom is in the excited state and the remaining two atoms are in the ground state and the second type is constructed from states where two atoms are excited and the third atom is in ground state. Likewise, one can also realize the GHZ-state under suitable parametric conditions. Unlike the W-state, the

GHZ-state does not show bipartite entanglement, but has a nonzero tripartite entanglement. The specific superpositions underlying these different tripartite states are responsible for their different entanglement properties, which will influence the resulting radiation pattern. Therefore, a systematic investigation of the emitted radiation characteristics is expected to carry signature of the nature of entanglement. In the following, we carry out such a systematic study of the emitted radiation field in the far field zone and specifically investigate its super and subradiant properties, in different parameter regimes.

5.1 Formulation

Let us consider a system of three dipolar coupled identical atoms, where the excited state $|e_i\rangle$ and the ground state $|g_i\rangle$ (i=1, 2, 3) are separated by an energy interval $\hbar\omega$. The corresponding Hamiltonian for the system is given by

$$H = \omega \sum_{i=1}^{3} S_i^z + \sum_{i \neq j=1}^{3} \Omega_{ij} (S_i^+ S_j^- + H.C), \tag{5.1}$$

As the atom-atom couplings are in different in both line and loop configurations, the results for field intensities and radiation statistics for the two configurations are found to be markedly different. In the absence of applied radiation field, the Hamiltonian (5.1) can be expanded in the standard basis, $|ijk\rangle$, with $i, j, k = 0, 1$. The presence of dipole coupling Ω between the atoms causes a mixing of the energy levels leading to creation of entangled states. Depending on the number of atoms that are in the excited state, two different type of entangled states manifest. In the first case, only one atom is in the excited state and in the second, two atoms are in the excited state generating

different types of W-states. The GHZ - state is also generated in both the configurations.

5.2 The intensity characteristics of light emitted by three atoms in a line configuration

As mentioned earlier, in the line configuration, we consider a system of three identical dipole coupled two-level atoms placed symmetrically along a line. The positions of these atoms are given by R_1, R_2 and R_3, and further we consider the case where interatomic spacing d between each adjacent pair is taken to be equal as depicted in Fig. 5-1, with $\Omega_{12} = \Omega_{23}$.

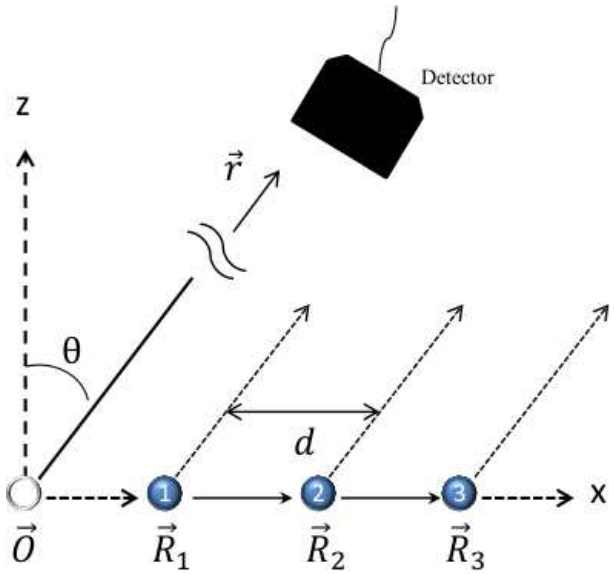

Figure 5-1: Schematic diagram of the system of 3 two-level atoms located at positions $\vec{R}_1$ to $\vec{R}_3$ with the detector placed at position $\vec{r}$, recording photons in the far field regime.

In this section, the intensity emitted by this three atom system in the far field zone is investigated. For this purpose, we consider a detector placed at

position $\vec{r}$ and the positive frequency component of the electric-field operator [37] is considered,

$$\hat{E}^{(+)} = -\frac{e^{ikr}}{r}\sum_j \vec{n}\times(\vec{n}\times\vec{p}_{ge})e^{-i\phi_j}\hat{S}_j^- \tag{5.2}$$

where the unit vector $\vec{n} = \frac{\vec{r}}{r}$ and $\vec{p}_{ge}$ is the dipole moment of the transition $|e\rangle \leftrightarrow |g\rangle$. Here ϕ_j is the relative phase of the emitted photon at position $\vec{R}_j$ and detected at $\vec{r}$

$$\phi_j(\vec{r}) \equiv \phi_j = k\vec{n}.\vec{R}_j = jkd\sin\theta. \tag{5.3}$$

Here, the dipole moment $\vec{p}_{ge}$ is assumed to be oriented along y direction and the unit normal $\vec{n}$ in the x-z plane, resulting in a vanishing $\vec{p}_{ge}.\vec{n}$. These assumptions give rise to dimensionless expressions for the amplitudes and hence intensities, resulting in the following expression for the radiated intensity at $\vec{r}$:

$$\begin{aligned} I(\vec{r}) &= \sum_{i,j}\langle\hat{S}_i^+\hat{S}_j^-\rangle e^{i(\phi_i-\phi_j)} \\ &= \sum_i\langle\hat{S}_i^+\hat{S}_i^-\rangle + \left(\sum_{i\neq j}\langle\hat{S}_i^+\rangle\langle\hat{S}_j^-\rangle + \sum_{i\neq j}(\langle\hat{S}_i^+\hat{S}_j^-\rangle - \langle\hat{S}_i^+\rangle\langle\hat{S}_j^-\rangle)\right)e^{i(\phi_i-\phi_j)} \end{aligned} \tag{5.4}$$

The characteristics of the intensity would depend on the incoherent terms $\langle\hat{S}_i^+\hat{S}_i^-\rangle$, the non-vanishing of the dipole moments $\langle\hat{S}_i^+\rangle$ and the quantum correlations like $\langle\hat{S}_i^+\hat{S}_j^-\rangle - \langle\hat{S}_i^+\rangle\langle\hat{S}_j^-\rangle$.

It has been observed earlier, the presence of dipole coupling between the atoms causes a mixing of the energy levels and creates different entangled W states. The one-atom excited states give rise to one class of W states while the two-atom excited states lead to a second class of W states. One of the

possible W state for the two-atom excitation is given by,

$$|W_{2,1}\rangle = \frac{1}{2}\left[|110\rangle + |011\rangle + \sqrt{2}|101\rangle\right], \quad \lambda_1 = \sqrt{2}g + \frac{\omega}{2} \tag{5.5}$$

where λ_1 is the corresponding eigenvalue. The resulting intensity pattern can be exactly calculated:

$$I_{|W_{2,1}\rangle} = 2 + \frac{1}{2}\left[\cos(\phi_1 - \phi_3) + \sqrt{2}\{\cos(\phi_1 - \phi_2) + \cos(\phi_2 - \phi_3)\}\right] \tag{5.6}$$

From the above equation, it is clearly seen that the radiation intensity $I_{|W_{2,1}\rangle}$ can be greater or less than 2. Note that for three uncorrelated atoms with two atoms in excited state, the total radiation intensity is equal to 2. However, the intensity $I_{|W_{2,1}\rangle} > 2$ can be regarded as a signature for superradiance where as $I_{|W_{2,1}\rangle} < 2$ represents subradiance for the three correlated atoms. Moreover, the intensity $I_{|W_{2,1}\rangle}$, depicted in fig 5-2, shows angular dependence and exhibits a maximum value,

$$[I_{|W_{2,1}\rangle}]^{Max} = 3.914,$$

for $\theta = 0, \pi$. The maximum intensity is higher than the corresponding intensity of the separable state, arising from the non-zero quantum correlations in case of W-state. Comparing with the results of [35, 38–40], the presence of dipole coupling does not have appreciable effect on the maxima and minima of the intensity. However, the behaviour in the regions between the maxima and minima has significant difference in the presence and absence of the interaction, as is evident from fig 5-2.

Another type of anti-symmetric W state for the two atom in the excited

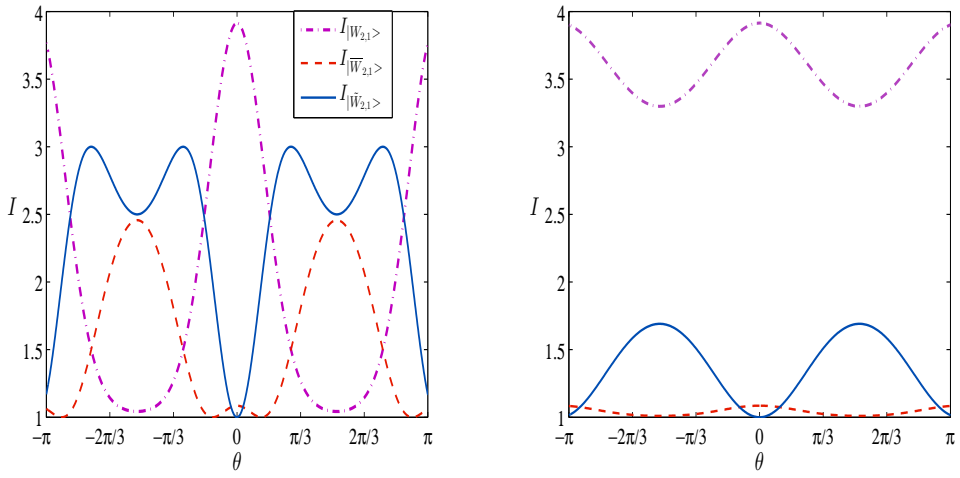

(a) (b)

Figure 5-2: Line configuration: Intensity of the initial state $|W_{2,1}\rangle$(dot-dashed line), anti-symmetric state $|\overline{W}_{2,1}\rangle$ (dashed line) and GHZ state $|\tilde{W}_{2,1}\rangle$(solid line) as a function of the observation angle θ for (a) weak D-D interaction strength ($\Omega_{12} = \Omega_{23} = 0.29\gamma$, for $d = \frac{\lambda}{3}$) and (b) strong D-D interaction strength ($\Omega_{12} = \Omega_{23} = 2.6\gamma$, for $d = \frac{\lambda}{10}$).

state is obtained as,

$$|\overline{W}_{2,1}\rangle = \frac{1}{2}\Big[|110\rangle + |011\rangle - \sqrt{2}|101\rangle\Big], \quad \lambda_2 = \frac{\omega}{2} - \sqrt{2}g, \tag{5.7}$$

and the corresponding intensity is given by

$$I_{|\overline{W}_{2,1}\rangle} = 2 + \frac{1}{2}\Big[\cos(\phi_1 - \phi_3) - \sqrt{2}\{\cos(\phi_1 - \phi_2) + \cos(\phi_2 - \phi_3)\}\Big] \tag{5.8}$$

The intensity minima occurs at

$$[I_{|\overline{W}_{2,1}\rangle}]^{Min} = 1.086,$$

when $\theta = 0, \pi$.

A second type of anti-symmetric state, of the GHZ type, with two atoms

in excited state,

$$|\tilde{W}_{2,1}\rangle = \frac{1}{\sqrt{2}}\left[|011\rangle - |110\rangle\right] \tag{5.9}$$

with $\lambda_3 = \dfrac{\omega}{2}$, has the intensity form,

$$|I_{|\tilde{W}_{2,1}\rangle} = 2 - \cos(\phi_1 - \phi_3). \tag{5.10}$$

As is evident from figure 5-2, the angular intensity distribution of different W states for increase in the dipole-dipole coupling strengths show distinctly different behaviour. Similarly, the intensities from each member of the states

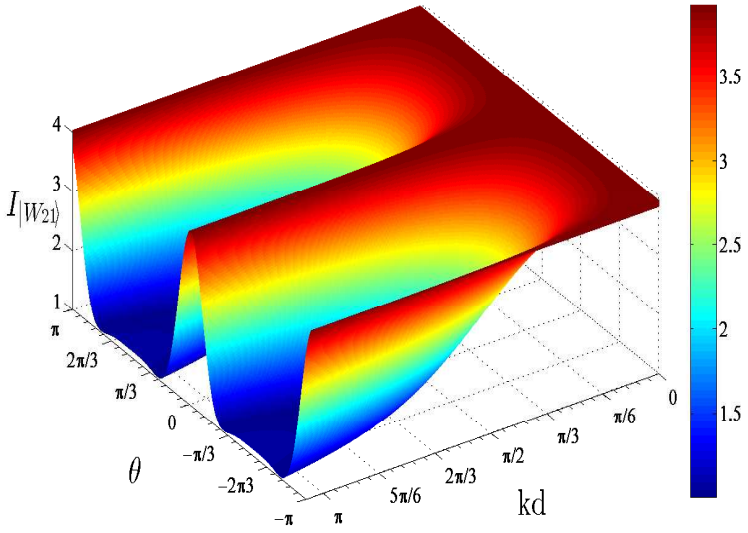

Figure 5-3: (Color online) Line configuration: Surface plot of intensity $I_{|W_{2,1}\rangle}$ as a function of observation angle θ and inter atomic distance kd

($|W_{21}>, |\overline{W}_{2,1}\rangle$ and $|\tilde{W}_{2,1}\rangle$) are markedly different from one other. The intensities from the anti-symmetric $|\overline{W}_{2,1}\rangle$ state and the GHZ-state $|\tilde{W}_{2,1}\rangle$ are showing a clear complementary behaviour at certain observation angles, for example at $\theta = 0, \pm\pi\ /2$. It is worth noting that inclusion of the dipole-dipole interaction leads to significantly different behaviour from that of ref [**?**].

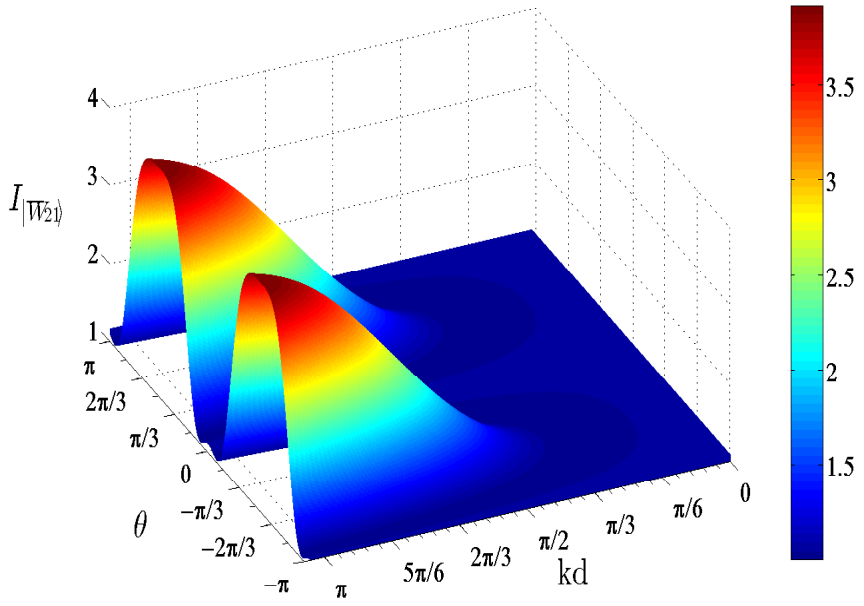

Figure 5-4: Line configuration: Surface plot of intensity $I_{|\overline{W}_{2,1}\rangle}$ as a function of observation angle θ and inter atomic distance kd

For a clearer visual understanding of this feature, three-dimensional plots of the intensities for both the state $|W_{2,1}\rangle$ as well as the anti - symmetric state $|\overline{W}_{2,1}\rangle$ are presented in figures 5-3 and 5-4, for a range of inter atomic distances and as a function of the observation angle. The three - dimensional view clearly shows the separated subradiant (blue) and superradiant (red) regions. We also observe that, as the inter atomic distance is decreased, the superradiant behaviour becomes more pronounced for the state $|W_{2,1}\rangle$, where as, the subradiant behaviour becomes stronger for the anti - symmetric state $|\overline{W}_{2,1}\rangle$. In addition, one clearly sees the complementary behaviour of the intensities for these two states.

5.2.1 Photon Statistics

In addition to the intensities, study of photon statistics, inferred from the second order intensity - intensity correlation function, enables one to gain insight into the characteristics of the emitted radiation field. In this section, such a study for the emitted photons is carried out. In particular, we concentrate on the super/subradiant behaviour of the emitted radiation. The second-order

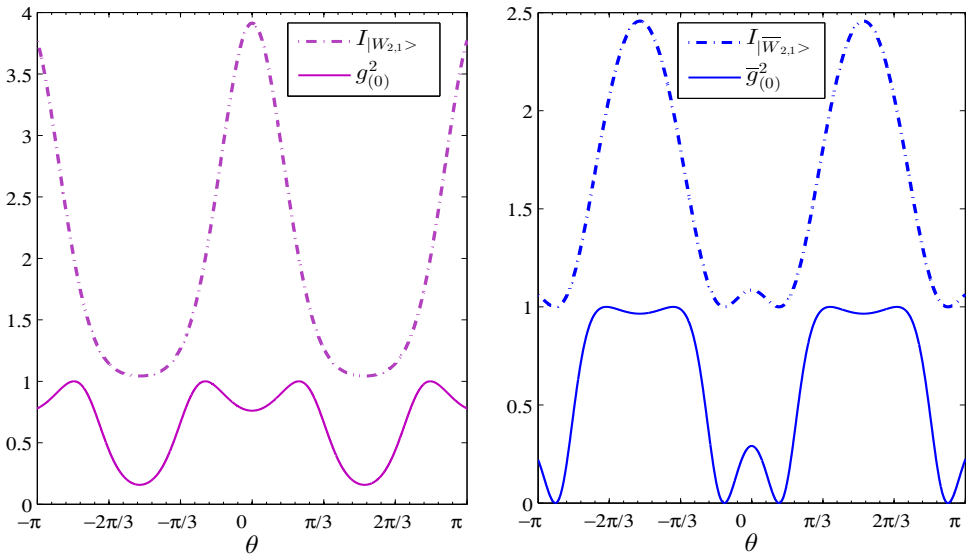

Figure 5-5: Line configuration: The intensity (dot-dashed line) and the second order correlation function of radiation field (solid line), emitted by two atoms which are initially in (a) the $|W_{2,1}\rangle$ state and (b)$|\overline{W}_{2,1}\rangle$ as a function of observation angle θ, for $kd = \dfrac{2\pi}{10}$.

(intensity-intensity) correlation function of the radiation field, with zero time lag, is defined as,

$$g^{(2)}(0) = \frac{\langle E^- E^- E^+ E^+ \rangle}{\langle E^- E^+ \rangle \langle E^- E^+ \rangle} \tag{5.11}$$

Violation of classical inequalities of this second-order correlation function points to non-classical character. In particular, $g^{(2)}(0) < 1$, a non-classical sig-

nature, refers to the sub-Poissonian photon statistics of the radiation field, while $g^{(2)}(0) > 1$ corresponds to the super-Poissonian. The reference value of $g^{(2)}(0) = 1$ is a characteristic of the Poissonian photon statistics, as exhibited by the laser field. After a lengthy calculation, the second-order correlation function of the radiation field, emitted from the $|W_{21}>$ state is obtained as

$$g^{(2)}(0) = \frac{4 + 2[\cos(\phi_3 - \phi_1) + \sqrt{2}(\cos(\phi_1 - \phi_2) + \cos(\phi_2 - \phi_3))]}{\left[2 + \frac{1}{2}\{\cos(\phi_3 - \phi_1) + \sqrt{2}[\cos(\phi_1 - \phi_2) + \cos(\phi_2 - \phi_3)]\}\right]^2} \quad (5.12)$$

The corresponding expression for the intensity correlation, when the two atoms are initially in $|\overline{W}_{2,1}\rangle$, denoted here by $\bar{g}^{(2)}(0)$, is given as,

$$\bar{g}^{(2)}(0) = \frac{4 + 2[\cos(\phi_3 - \phi_1) - \sqrt{2}(\cos(\phi_1 - \phi_2) + \cos(\phi_2 - \phi_3))]}{\left[2 + \frac{1}{2}\{\cos(\phi_3 - \phi_1) - \sqrt{2}(\cos(\phi_1 - \phi_2) + \cos(\phi_2 - \phi_3))\}\right]^2} \quad (5.13)$$

In figure 5-5, the results corresponding to the intensity, as well as the second order correlation function are presented for the $|W_{2,1}\rangle$ and the anti - symmetric $|\overline{W}_{2,1}\rangle$ states, for an inter-atomic distance $kd = \frac{2\pi}{10}$. It is observed that for both the states, the correlation function exhibits non classical nature for most of the angular region, except at four different observation angles in each case. In this case it attains the value of 1 pointing to the Poissonian character. For the range of observation angles, corresponding to relatively smaller values of the correlation functions, one finds stronger non classical character and the corresponding intensity shows subradiant behaviour. Whereas for the range of observation angles for relatively larger values of the correlation function, which can be interpreted as weak nonclassicality, the intensity is super-radiant.

Similar association between the strong/weak non-classicality and sub/super radiant intensity is seen for the anti-symmetric $|\overline{W}_{2,1}\rangle$ states. In figure 5-5, a careful examination of (a) and (b) shows that, wherever the intensity of one of the W - states is subradiant, that of the other state is superradiant and vice-versa. In summary, both the W - states reveal strong non-classicality, with their intensities showing complementary behaviour.

5.3 The intensity characteristics of light emitted by three atoms in a loop configuration

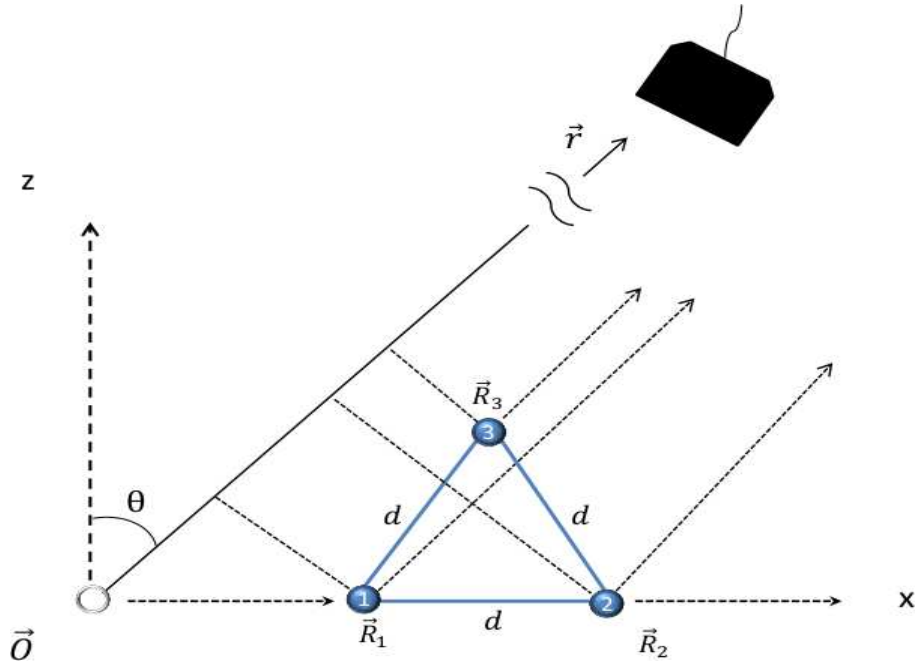

Figure 5-6: Schematic diagram of the system: where three identical and equidistant two-level atoms are localized at the vertices of an equilateral triangle. A detector at position $\bar{r}$ records the photon scattered by the atoms, in the far field regime.

The far-field intensities from different GHZ-states and the symmetric W-

state $|W_{2,1}\rangle$, corresponding to the loop configuration shows entirely different behaviour from that of the line-configuration. In the loop configuration, the schematic of which is shown in Fig. 5-6, the relative optical phase accumulated by a photon emitted at $\vec{R}_j$ and detected at $\vec{r}$ is given by

$$\phi_1(\vec{r}) \equiv \phi_1 = k\vec{n}.\vec{R}_1 = kd\sin\theta \tag{5.14}$$

$$\phi_2(\vec{r}) \equiv \phi_2 = k\vec{n}.\vec{R}_2 = 2kd\sin\theta \tag{5.15}$$

$$\phi_3(\vec{r}) \equiv \phi_3 = k\vec{n}.\vec{R}_3 = \frac{3kd\sin\theta + \sqrt{3}kd\cos\theta}{2} \tag{5.16}$$

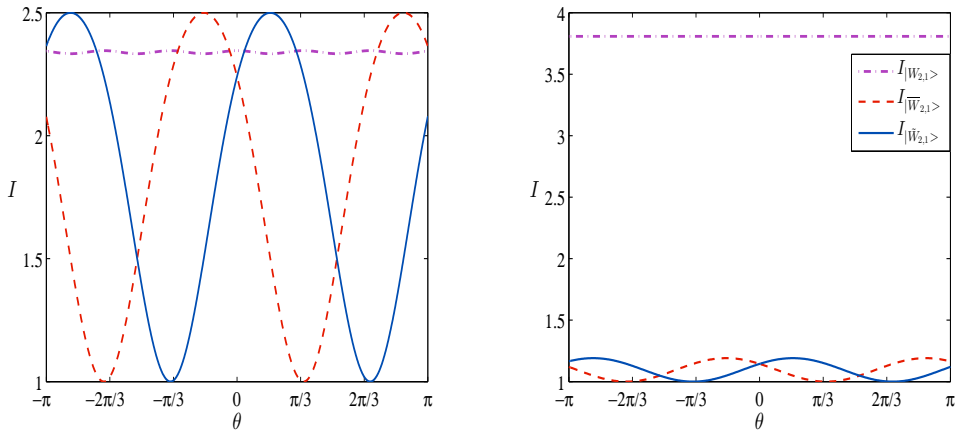

(a) (b)

Figure 5-7: Loop configuration: Intensity of the initial symmetric state $|W_{2,1}\rangle$ (dot-dashed line), GHZ state$|\overline{GHZ}_{2,1}\rangle$ (dashed line) and second type GHZ state $|\widetilde{GHZ}_{2,1}\rangle$ (solid line) as a function of the observation angle θ for the inter atomic distance (a) $d = \frac{\lambda}{3}$ (corresponding $\Omega_{12} = \Omega_{23} = 0.29\gamma$) and (b) $d = \frac{\lambda}{10}$ ($\Omega_{12} = \Omega_{23} = 2.6\gamma$).

For this configuration, the resulting symmetric W - state is given by

$$|W_{2,1}\rangle = \frac{1}{\sqrt{3}}\left[|110\rangle + |011\rangle + |101\rangle\right], \quad \lambda_4 = 2\Omega + \frac{\omega}{2} \tag{5.17}$$

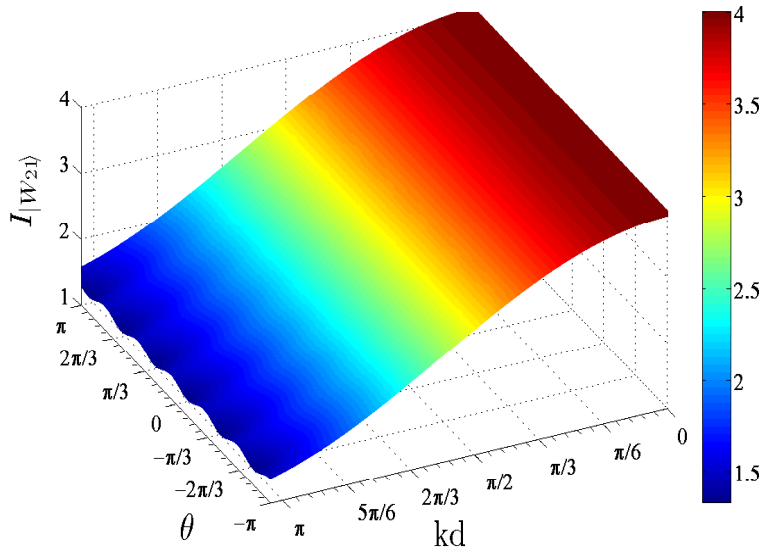

Figure 5-8: Surface plot of $I_{|W_{2,1}\rangle}$ as a function of θ and kd

and the corresponding intensity is found to be,

$$I_{|W_{2,1}\rangle} = 2 + \frac{2}{3}\left[\cos(\phi_1 - \phi_3) + \cos(\phi_1 - \phi_2) + \cos(\phi_2 - \phi_3)\right]. \tag{5.18}$$

Similarly, one can construct two types of GHZ states, when two atoms are present in the excited state:

$$|\overline{GHZ}_{2,1}\rangle = \frac{1}{\sqrt{2}}\left[|101\rangle - |110\rangle\right], \quad \lambda_5 = \frac{\omega}{2} - \Omega, \tag{5.19}$$

with the intensity,

$$I_{|\overline{GHZ}_{2,1}\rangle} = 2 - \cos(\phi_2 - \phi_3), \tag{5.20}$$

and

$$|\widetilde{GHZ}_{2,1}\rangle = \frac{1}{\sqrt{2}}\left[|011\rangle - |110\rangle\right], \quad \lambda_6 = \frac{\omega}{2} - \Omega, \tag{5.21}$$

with the intensity,

$$I_{|\widetilde{GHZ}_{2,1}\rangle} = 2 - \cos(\phi_1 - \phi_3). \tag{5.22}$$

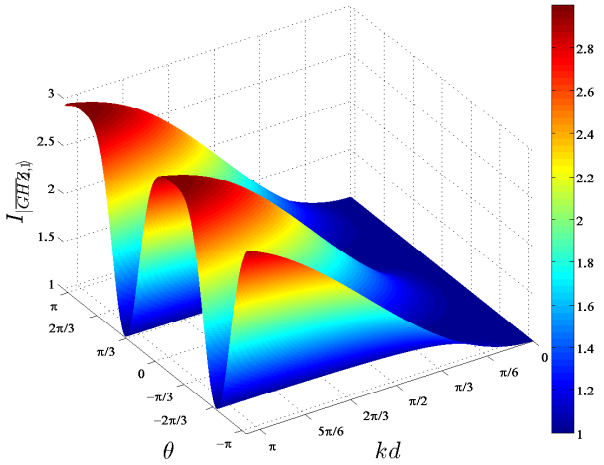

Figure 5-9: Loop configuration: Surface plot of $I_{|\overline{GHZ}_{2,1}\rangle}$, as a function of observation angle θ and inter atomic distance kd.

The intensity profiles of these different GHZ-states $|\overline{GHZ}_{2,1}\rangle$, $|\widetilde{GHZ}_{2,1}\rangle$ and the symmetric W-state $|W_{2,1}\rangle$ as defined above, for the loop configuration, are shown in Fig.5-7 for two different values of the dipole coupling strength. The intensity in case of the symmetric $|W_{2,1}\rangle$ state is super-radiant for the chosen dipole coupling strength and nearly independent of the observation angle, indicating that the emitted radiation is nearly isotropic. Another interesting feature about the behaviour of the radiation from this $|W_{2,1}\rangle$ state is that for stronger dipole coupling strength, which results in stronger superradiant character, the small fluctuations about a base-line value, in the emitted radiation disappear and the emitted radiation is indeed isotropic. As for the two GHZ-states, that we have defined for the case of two atoms initially in the excited states, the intensity is periodically varying from superradiant to subradiant

values, as the observation angle is changed for a relatively larger inter atomic distance ($kd = \frac{2\pi}{3}$). For a smaller inter atomic distance ($kd = \frac{2\pi}{10}$), the intensity remains subradiant for all observation angles. In addition, the radiation from these two states is out of phase, the phase difference being a function of the inter atomic distance, as is clearly be seen from parts (a) and (b) of Fig.5-7. Three dimensional plots of the radiated intensity of the symmetric $|W_{2,1}\rangle$ state and the $|\overline{GHZ}_{2,1}\rangle$ state of Fig. reffig:Loop 2 are shown in Fig. 5-8 and Fig. 5-9 respectively. In case of the W-state, one can clearly see how the intensity changes from subradiant to superradiant, with gradual decrease in the inter atomic distance. The vanishing of the fluctuations of the intensity is also clearly visible. Comparing the figures 5-8 and 5-9, one can observe the sensitive dependence of the intensity pattern of the GHZ-state on both the observation angle, as well as the inter atomic distance and near-absence of the same for the W - state. One further observes that the intensity can be tuned by changing the inter atomic distances, which in turn results in the change of the dipole coupling strengths. This suggests the exciting possibility of optical probing of the entanglement characteristics.

5.3.1 Photon statistics

In this section, numerical results of the photon statistics of the radiation field, when two of the three atoms in the loop configuration are in the excited state, are presented . The second-order equal-time correlation function, when the system is initially in the $|W_{21} >$ state is given by,

$$g^{(2)}(0) = \frac{4 + \frac{8}{3}\left[\cos(\phi_1 - \phi_2) + \cos(\phi_2 - \phi_3) + \cos(\phi_3 - \phi_1)\right]}{\left[2 + \frac{2}{3}\{\cos(\phi_1 - \phi_2) + \cos(\phi_2 - \phi_3) + \cos(\phi_3 - \phi_1)\}\right]^2}. \qquad (5.23)$$

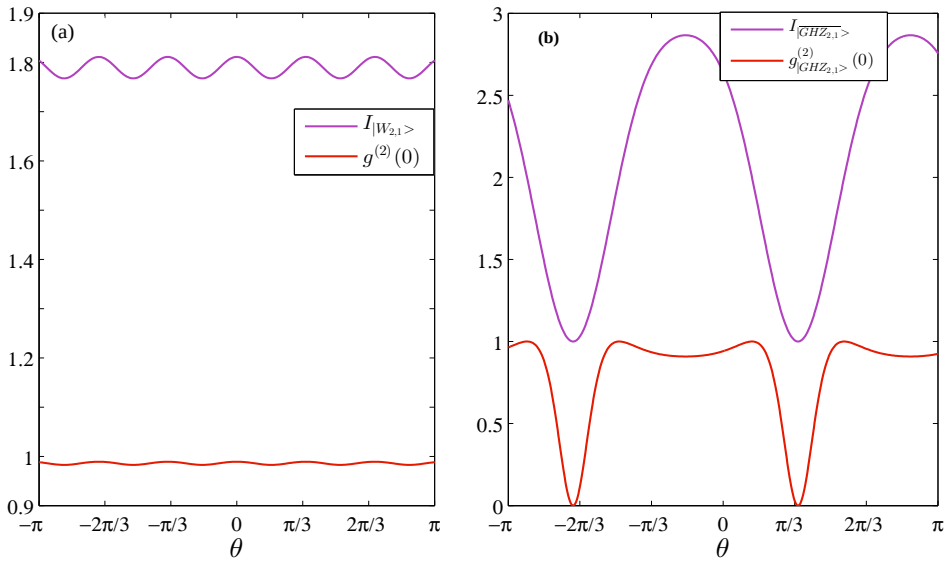

Figure 5-10: Loop configuration: The intensity (magenta line) and the second order correlation function (red line) of radiation field for (a) the symmetric $|W_{21}>$ state and (b) $|\overline{GHZ}_{2,1}\rangle$ state, as a function of observation angle θ for $kd = \dfrac{5\pi}{6}$.

In case of the symmetric $|W_{21}>$ state, a careful observation of Fig.5-10(a) and Fig.5-11 (a) shows that the photon statistics remains sub-Poissonian for both the weak and strong coupling strengths, whereas the intensity changes from subradiant to super radiant. In the GHZ-state (Fig.5-10(b) and Fig.5-11(b)), it is however quite different in the sense that for weak coupling strengths, the radiation emitted is showing periodic variations between subradiant and super radiant regimes and with increased coupling strength these oscillations are confined to subradiant regime alone. The corresponding photon statistics is similar to that of the W - state, viz., the non-classicality as seen from the behaviour of correlation function, is getting stronger with increase in coupling strength.

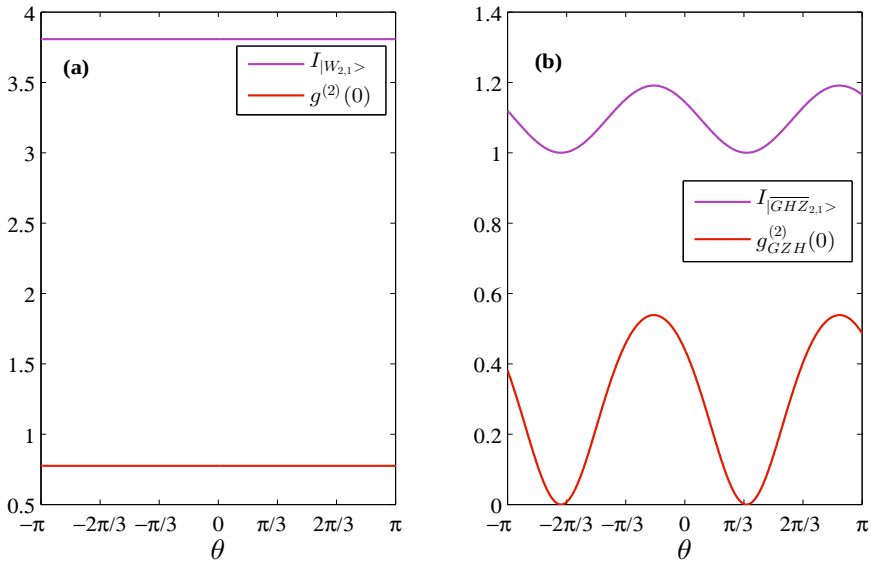

Figure 5-11: Loop configuration: The intensity (magenta line) and the second order correlation function (red line) of radiation field for (a) the symmetric $|W_{21}>$ state and (b) $|\overline{GHZ}_{2,1}\rangle$ state, as a function of observation angle θ for $kd = \dfrac{2\pi}{10}$.

In summary, for the case of GHZ - state, the photon statistics is varying from sub-Poissonian to Poissonian with clear dependence on the angle of observation, whereas in the case of $|W_{21}>$ state, it is remaining sub-Poissonian throughout and is essentially independent of the observation angle. Hence, the entanglement property of the three atom dipolar coupled system is found to yield characteristically distinct far-field radiation pattern, as also the photon statistics, in different configurations. It is also observed, this behaviour can be tuned by appropriate change of the atomic distances as also the dipolar couplings.

5.4 Conclusion

In this work, we have investigated intensity and radiation characteristics of three correlated atoms arranged in both line and loop configurations. We have observed that the nature of initial entangled states influences its radiative characteristics leading to superradiant/subradiant emission of photons. The effect of dipole-dipole coupling and the angular distribution of the emission of photons by entangled atoms from different entangled states is examined. For the case of loop configuration, it is interesting to note that the intensity emitted from the symmetric $|W_{2,1}\rangle$ state exhibits non classical nature for the chosen dipole coupling strength and nearly independent of the observation angle, meaning thereby that the emitted radiation is nearly isotropic. In conclusion, the fact that entanglement arises due to superposition of states, with the degree of entanglement being controlled by the nature of superposition, offers the possibility of its signature on the radiation pattern. It is interesting to note that distinct entangled configurations, in a tripartite system studied here, indeed revealed distinct radiation pattern as also intensity-intensity correlation. This opens a way for optical probing of the entanglement characteristics.

References

[1] M. Gross and S. Haroche, Phys. Rep. **93**, 301 (1982).

[2] R. H. Dicke, Phys. Rev. **93**, 99 (1954).

[3] N. Skribanowitz, I. P. Herman, J. C. MacGillivray and M. S. Feld, Phys. Rev. Lett. **30**, 309 (1973).

[4] M. O. Scully, E. S. Fry, C. H. R. Ooi and K. Wodkiewicz, Phys. Rev. Lett **96**, 010501 (2006).

[5] E. A. Sete, A. A. Svidzinsky, H. Eleuch, Z. Yang, R. D. Neels and M. O. Scully, J. Mod. Opt. **57**, 1311 (2010).

[6] R. Bonifacio, N. Piovella and B. W. J. McNeil, Phys. Rev. A **44**, R3441(1991).

[7] E. Prat, L. Florian and S. Reiche, Phys. Rev. ST Accel. Beams **18**, 100701 (2015).

[8] P. Sprangle and T. Coffey, Phys. Today **37**, No. 3, 44 (1984).

[9] M. Scheibner, T. Schmidt, L. Worschech, A. Forchel, G. Bacher, T. Passow and D. Hommel, Nat. Phys. **3**, 106 (2007).

[10] M. Gross, C. Fabre, P. Pillet and S. Haroche, Phys. Rev. Lett. **36**, 1035 (1976).

[11] A. Goban, C. L. Hung, J. D. Hood, S. P. Yu, J. A. Muniz, O. Painter and H. J. Kimble, Phys. Rev. Lett. **115**, 063601 (2015).

[12] B. Casabone, K. Friebe, B. Brandstatter, K. Schuppert, R. Blatt and T. E. Northup, Phys. Rev. Lett. **114**, 023602 (2015).

[13] R. Reimann, W. Alt, T. Kampschulte, T. Macha, L. Ratschbacher, N. Thau, S. Yoon and D. Meschede, Phys. Rev. Lett. **114**, 023601 (2015).

[14] M. D. Eisaman, A. Andre, F. Massou, M. Fleischhauer, A. S. Zibrov and M. D. Lukin, Nature (London) **438**, 837 (2005).

[15] A. Kalachev and S. Kroll, Phys. Rev. A **74**, 023814 (2006).

[16] A. Kalachev, Phys. Rev. A **76**, 043812 (2007).

[17] D. Porras and J. I. Cirac, Phys. Rev. A **78**, 053816 (2008).

[18] A. Biswas and G. S. Agarwal, J. Mod. Opt. **51**, 1627 (2004).

[19] D. M. Greenberger, M. A. Horne and A. Zeilinger, *Quantum theory and conceptions of the Universe* (Springer, Netherlands), 69 (1989).

[20] W. D*ü*r, G. Vidal and J. I. Cirac, Phys. Rev. A **62**, 062314 (2000).

[21] J. Joo, Y. J. Park, S. Oh and J. Kim, New J. Phys. **5**, 136 (2003).

[22] M. Bourennane, M. Eibl, C. Kurtsiefer, S. Gaertner, H. Weinfurter, O. G*ü*hne, P. Hyllus, D. Bru, M. Lewenstein and A. Sanpera, Phys. Rev. Lett. **92**, 087902 (2004).

[23] H. H*ä*ffner, W. H*ä*nsel, C. F. Roos, J. Benhelm, D. Chek-al-kar, M. Chwalla, T. K*ö*rber, U. D. Rapol, M. Riebe, P. O. Schmidt, C. Becher, O. G*ü*hne, W. D*ü*r and R. Blatt, Nature **438**, 643 (2005).

[24] A. Rauschenbeutel, C. Nogues, S. Osnaghi, P. Bertet, M. Brune, J. M. Raimond and S. Haroche, Science **288**, 2024 (2000).

[25] S. Zheng, Eur. Phys. Journal. D **54**, 719 (2009).

[26] C. S. Yu, X. X. Yi, H. S. Song and D. Mei, Phys. Rev. A **75**, 044301 (2007).

[27] C. H. Bennett, G. Brassard, C. Crepeau, R. Jozsa, A. Peres and W. K. Wootters, Phys. Rev. Lett. **70**, 1895 (1993).

[28] D. D. Bhaktavatsala Rao, S. Ghosh and P. K. Panigrahi, Phys. Rev. A **78**, 042328 (2008).

[29] A. Karlsson and M. Bourennane, Phys. Rev. A **58**, 4394 (1998).

[30] M. Eibl, N. Kiesel, M. Bourennane, C. Kurtsiefer and H. Weinfurter, Phys. Rev. Lett. **92**, 077901 (2004).

[31] D. Bouwmeester, J. W. Pan, M. Daniell, H. Weinfurter and A. Zeilinger, Phys. Rev. Lett. **82**, 1345 (1999).

[32] A. Rauschenbeutel, G. Nogues, S. Osnaghi, P. Bertet, M. Brune, J. M. Raimond and S. Haroche, Science **288**, 2024 (2000).

[33] C. F. Roos, M. Riebe, H. Häffner, W. Hänsel, J. Benhelm, G. P. T. Lancaster, C. Becher, F. Schmidt-Kaler and R. Blatt, Science **304**, 1478 (2004).

[34] K. Rama Koteswara Rao and Anil Kumar, Int. J. Quantum Info. **10**, 1250039 (2012).

[35] R. Wiegner, J. von Zanthier and G. S. Agarwal, Phy. Rev. A **84**, 023805 (2011).

[36] Z. J. Deng, M. Feng and K. L. Gao , Phys. Rev. A **73**, 014302 (2006).

[37] G. S. Agarwal, *Quantum Optics* (Cambridge University Press, Cambridge, UK), (2013).

[38] M. O. Scully, Phys. Rev. Lett. **115**, 243602 (2015) .

[39] A. A. Svidzinsky, X. Zhang and M. O. Scully, Phys. Rev. A **92**, 013801 (2015).

[40] N. Ten Brinke and R. Schtzhold, Phys. Rev. A **92**, 013617 (2015).

Chapter 6

Conclusions and outlook

This thesis focuses on the role played by the dipole-dipole (D-D) interaction on a collection of two-level atoms. For example, the D-D interaction modifies the behaviour of the system resulting in creation of entangled states, enhanced multi photon absorption, suppression of excitation probabilities and a host of other interesting features. We narrow down our study to analyse, in particular, the effect of D-D coupling on the entanglement characteristics of two and three atom systems, which offer attractive possibilities for quantum information processing. The first chapter of this thesis provides an introduction and overview of previous work and the justification for carrying out the work presented in this dissertation.

In chapter 2, the influence of the dipole interaction on a system of two two-level atoms, interacting with a single mode radiation field, is investigated, in order to understand the various manifestations of the dipole coupling, viz., the role of dipole blockade, the modifications in the two photon absorption, level populations and other effects. In this chapter, some of the previous results are reproduced in order to maintain continuity of discussion and some of the new results that are obtained in our current study are discussed. The transient

(cf. section 2.3) and steady state (cf. section 2.4) solutions of different level populations and atomic coherences are presented for a wide range of parameters to gain insight into the role played by different competing interactions that can influence the behaviour of the system. In the time dependent study of level populations, the number of oscillations, which arise due to the photon exchange interaction, is seen to increase as the dipole coupling strength Ω is increased, for all the populations. This is indicative of the fact that the rate of photon exchange increases with increase in the dipole coupling strength. Increase in dipole coupling strength also gives rise to a decrease in the excited state populations, showing that D-D coupling enhances the probability for both the atoms to be trapped in the ground state. In the steady state, results for an extensive range of parameters are presented, with particular emphasis on highlighting the competing effects of D-D coupling vs. the Rabi field strength (Ω_0). It is observed that, for the case of two identical atoms, the simultaneous excitation of both the atoms (which corresponds to the central peak in ρ_{44}) decreases with increasing dipole coupling strength, which is known popularly as the dipole blockade. Moreover, the dipole blockade in the laser excitation, which offers attractive possibilities for quantum engineering, is seen to be optimized for the case of non-identical atoms. This study on two two-level atoms is continued further with an investigation of the role of D-D interaction on concurrence, which is one of the measures of entanglement, in section 2.5. The effect of Rabi field strength Ω_0 on the sudden death and sudden birth of entanglement is studied. From a detailed analysis of the two-atom excited state population and the concurrence, a qualitative connection between the dipole blockade and the entanglement is made.

In chapter 3, the study is extended to a set of three dipole-coupled two-level

atoms arranged in two different configurations: in a line with nearest neighbour coupling and in a closed loop with each atom interacting with both its neighbours. When the system of three atoms is irradiated with a single mode radiation field, it is observed that the interaction suppresses one of the neighbouring atoms from getting excited but not both. This can be attributed to the role played by the dipole blockade in the case of three atoms, wherein the excited atoms prevent other atoms from reaching their excited states. Presence of the third atom indicates that the two-atom dipole blockade is not very effective, meaning thereby that one of the atoms is excited once at least. In other words, the standard dipole blockade prevents only one of the remaining two atoms from getting excited, resulting in possibility of simultaneous excitation of two atoms. We have also explored the entanglement properties of the system both in line and loop configurations, from a study of the negativity. In particular, the bipartite and tripartite negativities as a function of the D-D coupling and the Rabi field strength are discussed. We observe that there is an optimal value of Ω_0 for which the tripartite negativity is maximum and this optimal value increases as the dipole coupling strength is increased. Entanglement sudden death is also observed both in line and loop configurations. It is shown that the entanglement between the end atoms is still present even though they are not coupled directly. For weak interaction strength, tripartite negativity in line configuration is slightly more when compared to its counterpart in the loop configuration. However, as the interaction strength is increased, tripartite negativity in loop configuration is slightly higher as compared to that in the line configuration. This study throws light on the entanglement behaviour of the coupled three atom system but further insight can be obtained by refining the study. A further study of the other entanglement measures of this system

in different environment is presented in the next chapter.

In chapter 4, we have investigated the effect of D-D coupling on the entanglement characteristics of three atoms system under a dissipative environment. We studied the entanglement characteristics of three atoms (cf. sections 4.2 and 4.3) and show that they undergo an unexpected, qualitative change when the atoms are arranged in loop configuration. In particular, we observe an interesting result that any one of the qubits is indeed entangled with the other qubits in the system, for arbitrary values of D-D coupling strength, eventhough the other qubits are not mutually entangled. We also demonstrated that the quantum correlations may be enhanced as the temperature is lowered and that they are also increased by increasing the D-D coupling strength both in line and loop configurations.

Finally, in chapter 5, we have investigated the super and sub-radiance characteristics of the radiation emitted from a system of three two-level atoms, in the GHZ-and W-states. We have observed that the nature of initial entangled states influences its radiative characteristics leading to superradiant/subradiant emission of photons. The effect of D-D coupling and the angular distribution of the photon emission process by entangled atoms, from different possible entangled states is examined. For the case of loop configuration, it is interesting to note that the intensity emitted from the symmetric $|W_{2,1}>$ state exhibits non classical nature for the chosen dipole coupling strength and nearly independent of the observation angle, meaning thereby that the emitted radiation is nearly isotropic. In conclusion, the fact that entanglement arises due to superposition of states, with the degree of entanglement being controlled by the nature of superposition, offers the possibility of its signature on the radiation pattern in the present case of coupled dipolar

system. It is interesting to note that distinct entangled configurations, in a tripartite system studied here, indeed revealed distinct radiation pattern as also intensity-intensity correlation. This study shows that by studying the emitted radiation characteristics, one can gain insight into the nature of entanglement that is present in the states from which it has originated. This opens a way for optical probing of the entanglement characteristics.

Outlook

There exist a lot of studies on real physical systems which exhibit features that have been observed from our theoretical analysis of the two and three atoms systems, under different environments. A deeper understanding is required to connect the dots and make a correspondence between these two in order to be able to apply our results to real physical systems. In particular, even though the investigations of the intensity correlation measurements presented in this thesis provide an insight into the physics of multi-photon interferences, there remain a number of open questions. An extensive study of various atomic properties in different parameter regimes is required, for exploring the suitability of this system for storage of quantum information. Recently there has been a report on the modification in the performance of the photonic Carnot engine powered by a quantum spin-star network which, we strongly believe, is connected to the work presented in Chapter 4 on thermal entanglement characteristics. A more careful and deeper understanding would certainly provide the clear connection between our theoretical analysis and the experimental reports.

So far, all investigations of intensity, intensity-intensity correlation func-

tions, various measures of entanglement, that are discussed in this dissertation, have been limited to three identical atoms. Extending the study from two to three atoms itself has opened up a host of exciting newer possibilities, as demonstrated in this thesis. It would be exciting to explore further extension of this analysis to include other interactions, say, spin-spin interaction, that could lead to variations in the behaviour of this system to bring it closer to the real physical systems.

List of Publications

Shaik Ahmed, Ashoka Vudayagiri, P. Anantha Lakshmi "*Competition effects in presence of dipole-dipole interaction in two atom systems:A steady state analysis* "Physical Science International Journal vol **4**, issue 4, 591 (2014).

P. Anantha Lakshmi, Ashoka Vudayagiri, **Shaik Ahmed** " *Effect of pairwise dipole - dipole interaction among three atoms Systems* "Pramana - J. Phys. **83**, issue 2, 167 (2014).

Shaik Ahmed, Preeti N. Wasnik, Suneel Singh and P. Anantha Lakshmi " *Intensity correlations and anticorrelations in a three level cascade system* "Pramana - J. Phys. **87**, issue 85, 1 (2016).

Shaik Ahmed, Prasanta K. Panigrahi and P. Anantha Lakshmi "*Intensity and radiation statistics of correlated dipoles in GHZ and W-states* ", is under review at Physical Review A, arXiv: 1610.09128v1, 2016.

Shaik Ahmed "*Temperature dependent quantum correlations in three dipolar coupled two-level atoms* ", is under review Physical Review A, arXiv:1611.07063v1, 2016.

International/national conference proceedings

Shaik Ahmed, Ashoka Vudayagiri, P. Anantha Lakshmi "*Effect of dipole-dipole interaction on quantum correlations in two two-level atoms* "International conference on 'Nano, Bio and Material Sciences (ICONBMS-2014) ', 8-10 January 2014, organized by Nizam College, Osmania University, Hyderabad.

Shaik Ahmed, Ashoka Vudayagiri, P. Anantha Lakshmi "*Manifestations of the competing effects of Rabi field strength vs. dipole-dipole coupling*"National Laser Symposium (NLS-21), 6-9 February 2013, organized by BARC-Mumbai, Mumbai.

Shaik Ahmed, V S Ashoka, P. Anantha Lakshmi "*Competition effects in presence of dipole-dipole interaction in two atom systems* "AMOP-2012, December 2012, organized by IISER-Kolkata, Kolkata.

Shaik Ahmed, V S Ashoka, P. Anantha Lakshmi "*Competition between field strength and d-d interaction in two two-level atoms* "Frontiers in Optics and Photonics (FOP-11), 3-5 December 2011, organized by IIT-Delhi, Delhi.

Shaik Ahmed, V S Ashoka, P. Anantha Lakshmi "*Cooperative effect in two atom system: d-d coupling* "Frontiers in Physics, 28-29 October 2011, organized by University of Hyderabad, Hyderabad.

THESIS

ORIGINALITY REPORT

%32	%21	%23	%1
SIMILARITY INDEX	INTERNET SOURCES	PUBLICATIONS	STUDENT PAPERS

PRIMARY SOURCES

1	www.researchgate.net Internet Source	%10
2	www.ias.ac.in Internet Source	%7
3	R. Wiegner. "Quantum-interference-initiated superradiant and subradiant emission from entangled atoms", Physical Review A, 08/2011 Publication	%1
4	Khulud Almutairi. "Generating two-photon entangled states in a driven two-atom system", Physical Review A, 07/2011 Publication	<%1
5	T. G. Rudolph. "Two-atom resonance fluorescence in running- and standing-wave laser fields", Physical Review A, 07/1995 Publication	<%1
6	Kuznetsova, E. I., and M. A. Yurischev. "Quantum discord in spin systems with dipole–dipole interaction", Quantum Information Processing, 2013.	<%1

School of Physics
University of Hyderabad
Hyderabad 500 046, INDIA

Dr. P. Anantha Lakshmi
Professor

phone: +91 40 23134334
FAX :+91 40 23010227

DECLARATION

Out of the 32% similarity index identified by the Turnitin Software, 18% is from the candidate's own publications related to this thesis.

P. Anantha Lakshmi
Thesis Supervisor of Shaik Ahmed, Roll No. 08PHPH09

30 December, 2016

P. Anantha Lakshmi
Phone: +91-40-23134334
School of Physics
FAX: +91-40-23010227